ULTRASONIC WAVE REFLECTION MEASUREMENTS ON SELF-COMPACTING PASTES AND CONCRETES

BY

PRANNOY SURANENI

THESIS

Submitted in partial fulfillment of the requirements
for the degree of Master of Science in Civil Engineering
in the Graduate College of the
University of Illinois at Urbana-Champaign, 2011

Urbana, Illinois

Advisers:

Professor Leslie J. Struble
Associate Professor John S. Popovics

ABSTRACT

The objective of this study was to extend the use of combined longitudinal (P-wave) and shear (S-wave) ultrasonic wave reflection (UWR) to monitor the setting and stiffening of self-compacting pastes and concretes. An additional objective was to interpret the UWR responses of various modified cement pastes. A polymeric buffer with acoustic impedance close to that of cement paste, high impact polystyrene, was chosen to obtain sensitive results from the early hydration period. Criteria for initial and final set developed by our group in a prior study were used to compute setting times by UWR. UWR results were compared with standard penetration measurements. Stiffening behavior and setting times for normal cement pastes, pastes modified with mineral and chemical admixtures, self-compacting pastes, and concretes were explored using penetration resistance, S-wave and P-wave reflection. All three methods showed that set times of pastes varied linearly with w/c, that superplasticizer and fly ash delayed the set times of pastes, and that differences in w/cm, sp/cm, and fa/cm could be detected. Final set times determined from UWR correlated well with those from penetration resistance. Initial set times from S-wave reflection did not correlate very well with those from penetration resistance. Final set times from P-wave and S-wave reflection were roughly the same. Pastes with different chemical admixtures were tested, and the effects of these admixtures on stiffening were determined using UWR. Self-compacting concretes were studied using UWR, and their response and setting times were largely similar to that of corresponding self-compacting pastes. The P-wave reflection response was explored in detail, and the phenomenon of partial debonding and the factors affecting it were explained. Partial debonding is probably caused by autogenous shrinkage at final set, and was controlled and limited by water. The extent of partial debonding was higher with the transducers placed on the side as opposed to the bottom, and the S-wave

transducer seemed to promote debonding in the P-wave reflection, whereas the P-wave transducer seemed to reduce debonding in the S-wave reflection. Simultaneous formwork pressure testing and UWR were performed; however, no clear correlation was seen between the two properties.

Keywords: ultrasonic wave reflection, shear wave, longitudinal wave, setting time, self-compacting concrete, partial debonding.

ACKNOWLEDGEMENTS

"What a long, strange trip it's been." – The Grateful Dead, 1970.

Starting the acknowledgements section with a quotation is surely clichéd, but the above quote so aptly describes the last three years of my life that I cannot deny its rightful place. This work has taken up the better part of those three years, and it has been a great learning experience for me. Several people have been a part of this trip along with me, and I take the opportunity here to thank them for that.

I would like to thank Prof. Leslie J. Struble for her guidance in this project. Her experience, knowledge, and brilliance has helped me a lot (and hopefully rubbed off on me a bit). The Cement Center work that I did for Prof. Struble gave me an all round knowledge of construction materials, and I am thankful to Prof. Struble for giving me that opportunity. I also thank her for letting me be the teaching assistant for CEE501, and for her financial support through the project.

I would also like to thank Prof. John S. Popovics. His knowledge of non-destructive testing has come in particularly handy whenever we have had issues with the project. I am also particularly thankful for his suggestions, many of which have helped guide me in the right direction.

I would also like to thank Prof. David Lange for his insights on formwork pressure and underpressure. I appreciate the financial support provided by Prof. Lange. I would also like to thank Prof. Popovics, Prof. Struble, and Prof. Paramita Mondal for allowing me to be the teaching assistant for CEE300.

I would like to thank Prof. Ravindra Gettu and Prof. Manu Santhanam at the Indian Institute of Technology Madras. I would never have been interested in construction materials if

not for their beautiful presentation of the topic. I thoroughly enjoyed working for them during my undergraduate years.

I also have to thank my colleague Dr. Chul-woo Chung, whose project this is an extension of. Chul-woo was a mentor to me. Without him, I doubt I would have managed to get anything done at all. I would also like to thank Dr. Andres Salas for help with equipment and guidance in general. I wish to thank Ashna Chopra, Sravanthi Puligilla, and Eric Kim for many productive hours spent discussing research, and for their support, and encouragement. Thanks are also due to Paul Mockus, Jeffery Zhang, and Jorge Avalos who helped me in the lab. I also wish to thank my colleagues in the Civil Engineering Department for their suggestions and their friendship. Special thanks are due to the teaching assistants of CEE300, who made the job so much fun.

I wish to thank my friends for being around when I needed them. I cannot imagine what I would have done without you guys. Thank you, Abhishek, Adi, Ani, Ashna, Jayanthi, Laavi, Rannesh, Rimpa, Sneha, Sravanthi, and Swati.

Lastly I wish to thank my parents for everything. Mom, Dad, thanks for always being there, I do hope I have made you proud.

TABLE OF CONTENTS

1. INTRODUCTION

Hydration and setting of cement paste have been widely researched and studied topics. Classically, penetration resistance tests have been used to determine the setting time of concretes. However, limited information is obtained from these tests, and they are laborious and time consuming. Additionally, they are not actually done on concrete, but on mortar extracted from concrete. Newer non-destructive testing methods have been developed to study stiffening of cement pastes, including electrical and acoustic methods. Much work on cement setting has been done with ultrasonic waves. Transmitted and reflected ultrasonic waves have both been studied, with reflected waves having the advantage of not needing two-sided access. Most of the work using reflected ultrasonic waves has focused on strength development; relatively little work has been done on setting and stiffening.

Ultrasonic wave reflection (UWR) involves measuring the reflected wave energy at the interface of a buffer and a hydrating cementitious material. When the cementitious material is fluid, most of the incident energy is reflected back; whereas relatively more energy is transmitted with the material hardens. Changes in this reflected energy are monitored and plotted as a function of time. Shear and longitudinal waves have been used for this purpose, though rarely have they both been used in the same study.

This work is a continuation of the Ph. D. work done by Chung at the University of Illinois [1]. Chung used combined shear and longitudinal (S- and P-wave) UWR with a low impedance buffer material, high impact polystyrene (HIPS), to obtain sensitive information about early age hydration of cement pastes. Both S- and P-wave UWR reflection data were collected, analyzed, and the wave responses were interpreted for normal cement pastes. Criteria

for initial and final set using UWR were developed. The partial debonding response observed with P-waves was broadly explained.

The main objective of this study is to extend the application of combined shear and longitudinal UWR to self-compacting pastes and concretes. An additional objective is to understand the responses of various cementitious pastes using UWR. Pastes modified with mineral and chemical admixtures, fly ash-water pastes, geopolymers, and bacteria modified pastes were tested with UWR and their responses interpreted. The P-wave response is explained in detail, and instrumentation effects on the response are elaborated on. Setting times from UWR are compared with penetration resistance setting times. Combined UWR and formwork pressure tests are done in order to explore the relationship between UWR and formwork pressure.

The thesis is divided into the following chapters, which have content as described. Chapter 2 is a survey of existing literature on cement hydration, self-compacting concretes, penetration resistance, wave reflection, and formwork pressure. In Chapter 3, experimental details are provided, along with information about materials and mixing. The results from the testing are presented in Chapters 4 – 8. Penetration resistance results, S-wave results, and P-wave results are presented in Chapter 4, Chapter 5, and Chapter 6, respectively. The above results are presented for normal cement pastes, modified pastes, and self-compacting mixtures. Instrumentation effects are detailed in Chapter 7 and Chapter 8 gives the results of formwork pressure testing. Conclusions are presented in Chapter 9 and references in Chapter 10.

2. LITERATURE REVIEW

2.1. Stiffening of cement paste

Hydration of cement begins immediately after the cement and water are mixed. As hydration progresses, the initially fluid paste gradually hardens. This hardening or stiffening is due to the formation and interaction of hydration products. Cement hydration is complex, but it resembles the hydration reaction of alite, which has been well studied. There are five stages in the reaction [2, pp. 159-161], the heat curve of which is presented in Figure 2.1. Stage 1 is rapid evolution of heat, which occurs right after mixing alite with water. This is due to dissolution of Ca^{+2} ions, which in this case is an exothermic reaction. Stage 2 is an "induction period" in which there is no heat evolution, and seemingly no reaction. This induction period lasts around a couple of hours. There are many proposed reasons for the induction period [2, pp. 162-164], with the most accepted one being a formation of thin layer of hydration product around the cement particles which drastically slows down further dissolution of Ca^{+2} ions. However, dissolution still continues at a very slow rate, and when the Ca^{+2} ion concentration reaches a critical saturation level, nucleation of Ca^{+2} occurs, and CH and C-S-H are formed, which causes further reaction, and the end of the induction period. Initial set occurs roughly near this point, and the paste starts to become solid and is no longer easily deformable. This is the beginning of Stage 3 of the reaction, and reaction proceeds rapidly with much heat. This heat evolution reaches a maximum and then slows down, and the reaction changes from dissolution control to diffusion control, where ions must diffuse through the layer of hydration products for further reaction. A roughly solid framework is formed at this point, and the paste can carry load, and this is final set. This is Stage 4 of the reaction. Rate of reaction reduces further until it approaches a steady state, Stage 5 [2, pp. 159-161]. Heat curves of cement pastes are roughly similar to those of alite, and

therefore, in normal cement pastes, initial and final set are due to the same mechanisms as for alite.

The hydration reactions of the aluminate phases are very different in the presence or absence of gypsum [2, pp. 193-194]. When there is no gypsum, C_3A reacts extremely rapidly with water with much heat evolution, causing instant stiffening in the paste. This is known as flash set. This is due to the formation of C_4AH_{13} and C_2AH_8, which form interlocking layers, causing rapid stiffening [2, pp. 193-194]. In the presence of gypsum, this reaction is avoided, and ettringite and monosulfate are formed instead [2, pp. 194-195]. The hydration reactions of ferrite are similar to that of aluminate but much slower and thus are not discussed here [2, pp. 196].

Hydration products are formed on the surface of cement particles and as hydration proceeds, they grow outward into the pore space. At the same time, they bond with and grow into each other. Hydration also leads to an increase in the volume fraction of the solids present. Both of these cause an interconnected solid layer to be formed, and hence the paste stiffens with time after water is added.

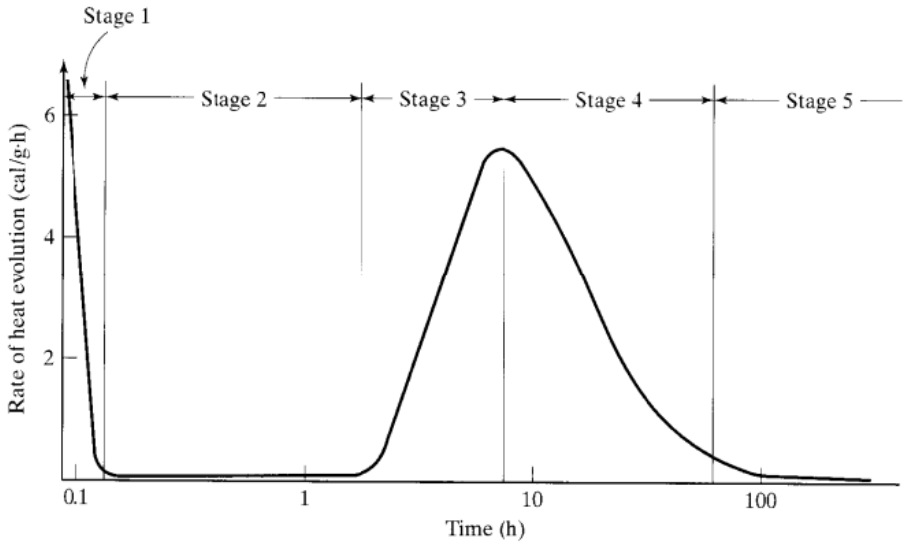

Figure 2.1. Heat evolution curve of alite [3].

2.2. Self-compacting concretes and pastes

Self-compacting concrete flows under the action of its own weight and does not require additional compaction to flow. Self-compacting concrete must have high flowability, passing ability, and segregation resistance. High flowability ensures adequate spread and flow of concrete in the mold, passing ability is required so the concrete passes through narrow gaps, and segregation resistance is needed for reducing shrinkage and creep [4]. Self-compacting concretes are usually made by adding mineral admixtures and superplasticizers to normal concrete mixes. Aggregate content, especially coarse aggregate, is reduced, and low water-cementitious materials ratios are used. Viscosity modifying agents may also be used in self-compacting concretes. The mineral and chemical admixtures used in self-compacting concrete make it set much later than normal concrete. Also, the superplasticizer causes the cement particles to be initially in a dispersed state, as opposed to a flocculated state in normal cement pastes.

2.3. Penetration resistance

The standard tests for setting of cementitious materials are penetration resistance tests, in which the resistance to penetration of the materials by probes is monitored with time. The penetration method is well understood, simple, inexpensive, and easy to use. However, it is also laborious, time consuming, and does not give a continuous data output. There are primarily two penetration resistance tests done on cementitious materials: ASTM C191, the Vicat test [5], and ASTM C403, the Proctor test [6]. The Vicat test uses only one needle for penetration, and is typically used for very stiff cement pastes. The Vicat test does not provide information on the evolution of stiffening with time. The Proctor test uses needles of various sizes to measure the penetration resistance of mortar extracted from concrete. According to the standard, initial set of the concrete occurs at a penetration resistance of 3.5 MPa and final set of concrete at a

penetration resistance of 27.3 MPa. It is to be noted that these values are arbitrary, and no specific change occurs in the concrete at this point. Penetration resistance testing on concretes with fly ash [7] and superplasticizers [8] shows that both fly ash and superplasticizer retard the setting of concrete, with increasing dosages of each causing further retardation. Penetration resistance of self-compacting concretes show that such concretes display delayed set [7].

In a previous study in our laboratory [9], the Proctor test was adapted for use on cement pastes. Initial penetration resistance values are very low, and then increase in an exponential manner. By comparing pastes and corresponding concretes, initial set was assigned to be at a penetration resistance of 2 MPa and final set at a penetration resistance of 14 MPa. Penetration resistance on cement pastes with all variables controlled gave reproducible results, and the test could easily distinguish between pastes of differing w/c [1].

2.4. Ultrasonic wave reflection theory

When a normal wave encounters a boundary between two different materials, the wave is partly transmitted through the boundary and partly reflected at the boundary. The relative amounts of wave energy transmitted and reflected at the boundary depend on the relative acoustic impedances of the two materials. The amount of reflected and transmitted wave energies are given by the reflection coefficient, R, and the transmission coefficient, T, which are given as

$$R = \left|\frac{Z_2 - Z_1}{Z_2 + Z_1}\right| \tag{2.1}$$

and

$$T = \frac{2Z_2}{Z_2 + Z_1} \tag{2.2}$$

where Z_1 and Z_2 are the acoustic impedances of the two materials. Acoustic impedance is the product of the velocity of the wave through the material, V and the density of the material, ρ.

$$Z = \rho V \tag{2.3}$$

The amount of ultrasonic wave energy reflected back from an interface has been shown to depend on the relative material properties of the materials. Therefore testing has involved one material that does not change with the time (the buffer) and one that changes in properties with time (the sample). The change in properties of the samples as a function of time can therefore be monitored using wave reflection. If R is measured, and Z_1 is known, then Z_2 can be determined. For the reflection of waves at the interface of a cement paste and a buffer, Z_1 becomes Z_{buffer} and Z_2 becomes Z_{paste}.

If Z_{buffer} is much higher or lower than Z_{paste}, then the value of R does not change substantially with time. Hence, small changes in the paste with time cannot be monitored. To be able to monitor small changes in the paste, the buffer must be chosen such that its acoustic impedance is close to that of the paste.

2.5. Ultrasonic wave reflection on cementitious materials

Studies have been done with both transmission and reflection of ultrasonic waves on numerous materials for several years. Ultrasonic wave reflection testing on cement pastes is, however, a more recent development. Shear waves do not pass through the initially fluid cement paste. As hydration progresses, hydration products form on the surface of cement particles and with progressive hydration, they grow outward into the pore space and into each other. This leads to an increase in the volume fraction of the solids present and results in the formation of a solid, percolated microstructure, thereby leading to an increase in the amount of transmitted shear wave energy. The transmitted shear wave energy increases continuously as the solid fraction keeps increasing. For this reason, shear waves have been used to study early age properties of cementitious materials. Longitudinal waves, which pass through liquids, unlike shear waves, have also been used to study properties of cementitious materials, though not as

much as shear waves. The longitudinal wave energy also increases with progressive hydration, and this is because of an increasing in longitudinal wave velocity as the solid content increases.

Tests have been done to correlate ultrasonic shear wave reflection coefficient and strength development [8, 9]. A high-impedance steel buffer was used, and concretes and mortars were studied. The reduction in reflection coefficient as compared to its initial value was designated the reflection loss and plotted with time. The reflection loss was reproducible, and showed a strong relationship with the compressive strength. A bilinear relationship between the reflection loss and strength was reported [10]. Reflection loss and compressive strength were compared, and the compressive strength estimated using the reflection loss. Using the reflection loss and one strength measurement, variation of strength with time was predicted [11]. The relationship between reflection loss and maturity has also been explored, and advantages of wave reflection method over maturity method proposed [12]. Reflection loss has also been related to the adiabatic heat loss, and similar trends in both were observed with changing w/c [10].

By measuring both the reflection coefficient and changes in phase angle of reflected shear waves, dynamic and loss modulii of cement pastes were found [13]. Measured values of modulus followed the same trend as those from oscillatory rheology. Modulii were affected greatly by w/c [13]. By neglecting changes in phase angle, the dynamic shear modulus was found for mortars [10, 14]. Changes in reflection coefficient controlled changes in shear modulus [14]. Shear modulii from torsional resonant frequency, shear wave velocity, and shear wave reflection loss showed similar trends [10].

Shear wave reflection was utilized to understand microstructural development in mortars [15]. The reflection loss of mortars was directly related to the development of the volume fraction of the total and connected solid phase of the cement paste obtained from numerical

simulations. The degree of inter-particle bonding of the cement paste affected the reflection loss. The time of increase of the reflection loss and the time of the percolation threshold of the solid phase were very similar. Reflection loss was also related to the degree of hydration estimated from different methods [10, 15].

Shear wave reflection was used to study the setting times of cement pastes, mortars and concretes [16, 17, 18]. The reflection loss for pastes depended on the cement composition, w/c, and admixtures [16, 17]. The shear reflection coefficient for concretes with a steel buffer was monitored with time and its numerical derivative found. The point at which the numerical derivative dips below zero was found to be related to the end of the induction period. Another critical point was found to be the point where the derivative became constant. This point seemed to have fundamental significance, but was much after final set from penetration methods. The effect of accelerator, retarder, superplasticizer, and silica fume on these points was studied, and admixtures which were supposed to delay set resulted in later times for these points, whereas admixtures which were supposed to accelerate set resulted in earlier times [17]. Lower impedance buffers, which give better sensitivity to earlier changes in cement pastes, have also been studied. PMMA was used as a buffer material, and the setting of mortar explored. The inflection point in the reflection coefficient-time curve was used as initial set, and the point of inversion, where the acoustic impedance of paste and buffer became equal was used as final set. These times matched those determined from the Proctor test fairly well. The effect of w/c, fly ash, retarder, and accelerator on these points was studied, and it was shown that increasing amounts w/c, fly ash, and retarder delayed initial and final set, whereas increasing amounts of accelerator hastened setting as measured by wave reflection [16].

Longitudinal waves have also been used to determine setting times. A study using glass buffer on cement pastes found that the inflection point on the reflection coefficient-time curve corresponded to initial set, and the point of inversion to final set. Set times compared well with those from the Vicat test. Slag was seen to delay initial and final set by wave reflection [19].

Since information is obtained both from shear and longitudinal waves, a study was undertaken in our lab to study early age properties of pastes using combined shear and longitudinal wave reflection [1]. A very low impedance HIPS buffer was used. The wave reflection response of both shear and longitudinal waves was explained. Flocculation and segregation could be detected by shear and longitudinal waves, respectively. No fundamental criterion for initial set was found, therefore, initial set was empirically assigned as the time when paste acoustic impedance reached 0.09 MRayls. Final set was assigned to be at the inflection point of the shear wave reflection response. Set times showed a moderate correlation with those obtained from the Proctor test. Premature stiffening was detected by a high initial drop in shear wave reflection coefficient. The initial value of the longitudinal wave reflection coefficient was related to the w/c. Partial debonding was seen with longitudinal waves, and it was proposed that the debonding was caused by autogenous shrinkage. The time of partial debonding was the same as final set time determined from shear wave reflection. It was shown that ultrasonic waves seemed to affect the cement paste, though the tests are usually thought to be non-destructive [1].

2.6. Formwork pressure

The American Concrete Institute guideline for formwork design does not explicitly address self-compacting concretes, but instead states that the formwork should be designed for full hydrostatic pressure [20]. Studies have found that maximum formwork pressure was almost always lower than the full hydrostatic pressure [21]. The maximum pressure was also usually not

found at the bottom. Maximum pressure also occurred before the pouring was finished, which implies that after a certain time, pouring of additional concrete did not cause a rise in pressure [21]. Prior research at the University of Illinois studied formwork pressure in the lab by using pressure sensors mounted on columns filled with concrete [22]. As shown in Figure 2.2, pressure typically drops fairly rapidly with time and becomes zero after a few hours elapse. The formwork pressure exerted is related to the thixotropic nature of the self-compacting concrete mix [22]. Aggregate proportioning, mineral and chemical admixtures, and ambient temperature also affect the pressure exerted [23]. Formwork pressure has been modeled and several models exist. The study at the University of Illinois developed a hyperbolic decay function to fit the pressure decay. The column pressures were monitored and the decay function was fitted to a mathematical expression. The pressure decay curve was used along with the filling height and the filling rate to predict pressures for larger structures such as walls. Predicted data were compared to pressure directly measured on several walls and a good agreement was found [24].

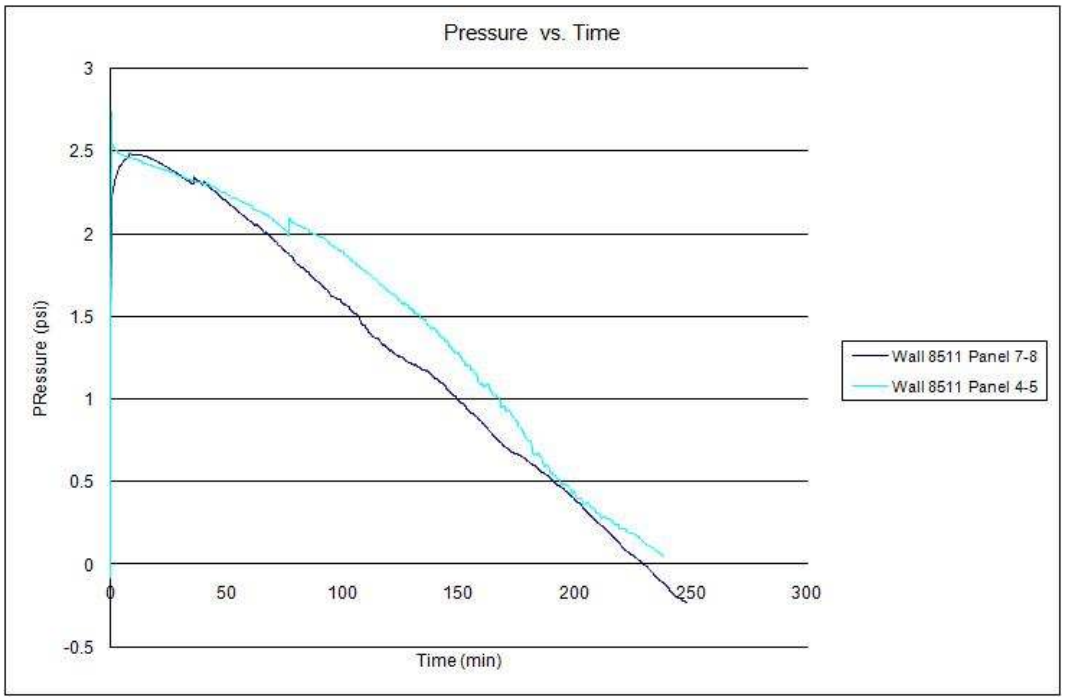

Figure 2.2. Variation of formwork pressure with time [22].

3. EXPERIMENTAL PROCEDURES AND MATERIALS

In this chapter, details of materials used and mix designs are presented. Experimental procedures of penetration resistance, ultrasonic wave reflection and formwork pressure testing are described.

3.1. Materials

The cement used in the study was a commercial Type I portland cement following standard specifications. The cement was sealed in an air tight container to prevent exposure to the atmosphere. Normal tap water was used, which was stored in a beaker in the lab for one day prior to testing to ensure that it was at ambient temperature. The symbol "w/c" refers to the ratio of the weight of the water (w) to that of the cement (c). The primary fly ash used in the study was a Class C fly ash (fa). Two other fly ashes, both Class F ashes, were also used. One (fa2) was used compare set retardation caused by different fly ashes as measured by penetration resistance. The other fly ash was used to make geopolymers. A slag was also used in making the geopolymers. Finely ground quartz (gq, average particle size between 10 – 50 microns) was used to compare its retardation of paste set with that of the fly ashes. The symbol "w/cm" refers to the ratio of the weight of the water to the overall weight of the cementitious materials. The symbols "fa/cm", "fa2/cm", and "gq/cm" refer to the ratio of weights of the materials (fa, fa2, and gq) to that of the overall cementitious materials (cm). The symbol "w/fa" refers to the weight ratio of the water and the fly ash.

Various chemical admixtures were also used. The superplasticizer ("sp") was a polycarboxylate based high range water reducer, with a solid content of 33 % by weight. The symbol "sp/c" refers to the ratio of weight of the solid superplasticizer to that of the cement. The symbol "sp/cm" refers to the ratio of weight of the solid superplasticizer to that of the

cementitious materials. A viscosity modifying agent (vma), a shrinkage reducing admixture (sra) and an air entraining admixture (aea) were also used. The symbols "vma/w", "sra/w", and "aea/w" refer to the ratio of the weight of the admixture to that of the water.

Geopolymer pastes were made with the fly ash and slag mentioned before, apart from water, potassium silicate, and potassium hydroxide. Pastes with bacteria were also tested using ultrasonic wave reflection. These pastes incorporated Bacillus pasteurii bacteria and a nutrient medium comprising of urea, yeast extract and tris base.

Self compacting concretes tested in the study they included coarse and fine aggregates apart from cement, water, fly ash, and superplasticizer mentioned above. The coarse aggregates were crushed limestone aggregates with maximum nominal sizes 9.5 mm and 19 mm aggregates, whereas the fine aggregate was siliceous concrete sand with maximum nominal size 4.75 mm.

3.2 Mix designs

All cement pastes were designed to have an overall weight of 2000 g. For pastes incorporating chemical admixtures, the weight of the mix was slightly over 2000 g, because of the admixture weigh. Self-compacting pastes incorporated both mineral and chemical admixtures. The mix designs for plain cement pastes and pastes with mineral or chemical admixtures are given in Table 3.1. The mix designs for self-compacting pastes are given in Table 3.2. Pastes differed in the w/cm, fa/cm, and sp/cm, which varied from 0.33-0.6, 0.2-0.4, and 0.00055-0.0025. The mix designs for the fly ash pastes were the same as the plain cement pastes, with fly ash replacing cement. The mix design for the fly ash-geopolymer paste was powder 1458 g, potassium silicate 160 g, potassium hydroxide 34 g, and water 348 g. The powder comprised of fly ash and slag and the mixes only differed in the powder composition, with mixes comprising 0 %, 5 %, 10 % and 15 % slag. The composition of the mix with bacteria was 1333 g

cement, 26.68 g nutrient medium (which comprised of 6.67 g urea, 13.34 g yeast extract, and 6.67 g tris base), along with 667 g water and bacteria which was grown in the nutrient medium.

Unlike pastes, concretes were batched with different overall weights. The concrete mix designs were adapted from a previous study [25]. The parameters used were w/cm, fa/cm, sp/cm, paste content, and aggregate proportion by weight. For wave reflection, the total batch weight was 50 kg. For formwork pressure tests, concrete mixes of 50 kg and 110 kg concrete were batched. For all concretes, paste content was 40 % by volume, and aggregation proportion was 20 mm aggregates: 10 mm aggregates: sand = 28: 37: 35 by weight. The only parameter that was varied was the paste composition. Two w/cm values were used, 0.33 and 0.38; two sp/cm values were used, 0.0007 and 0.0008; and two fa/cm values were used, 0.25 and 0.3. The paste compositions for the mixes Concrete 1, Concrete 2, Concrete 3, and Concrete 4, were 0.33w/cm, 0.0008sp/cm, 0.3fa/cm; 0.38w/cm, 0.0008sp/cm, 0.3fa/cm; 0.33w/cm, 0.0007sp/cm, 0.25fa/cm; and 0.33w/cm, 0.0012sp/cm, 0.3fa/cm. Concrete mix designs are presented in Table 3.3.

Table 3.1. Mix designs by weight for plain cement pastes and paste with mineral or chemical admixtures.

Mix designation	**Cement (g)**	**Water (g)**	**Mineral/Chemical admixture (g)**
0.33w/c	1504	496	--
0.35w/c	1481	519	--
0.4w/c	1429	571	--
0.5w/c	1333	667	--
0.6w/c	1250	750	--
0.33w/cm, 0.3fa/cm	1157	496	347

0.33w/cm, 0.4fa/cm	1074	496	430
0.33w/cm, 0.3fa2/cm	1157	496	347
0.33w/cm, 0.3gq/cm	1157	496	347
0.33w/c, 0.0004sp/c	1504	496	1.83
0.33w/c, 0.0008sp/c	1504	496	3.65
0.33w/c, 0.0025w/c	1504	496	11.41
0.33w/c, 0.0012vma/w	1504	496	0.60
0.5w/c, 0.0012vma/w	1333	667	0.80
0.33w/c, 0.0009sp/c, 0.0012vma/w	1504	496	sp = 4.11, vma = 0.60
0.33w/c, 0.0017sp/c, 0.0017vma/w	1504	496	sp = 7.76, vma =0.85
0.33w/c, 0.03sra/w	1504	496	15.04
0.33w/c, 0.03aea/w	1504	496	15.04

Table 3.1. (cont.) Mix designs by weight for plain cement pastes and paste with mineral or chemical admixtures.

Table 3.2. Mix designs by weight for self-compacting pastes.

Mix designation	**Cement (g)**	**Fly ash (g)**	**Water (g)**	**Super-plasticizer (g)**
0.33w/cm, 0.00055sp/cm, 0.25fa/cm	1203	301	496	2.52
0.33w/cm, 0.00055sp/cm, 0.3fa/cm	1156	347	496	2.52
0.33w/cm, 0.00055sp/cm, 0.35fa/cm	1114	390	496	2.52
0.33w/cm, 0.0007sp/cm, 0.3fa/cm	1156	347	496	3.20
0.33w/cm, 0.0008sp/cm, 0.3fa/cm	1156	347	496	3.65
0.33w/cm, 0.0008sp/cm, 0.35fa/cm	1114	390	496	3.65

0.35w/cm, 0.00055sp/cm, 0.25fa/c	1185	296	496	2.48
0.35w/cm, 0.0007sp/cm, 0.2fa/cm	1234	247	496	3.15
0.35w/cm, 0.0007sp/cm, 0.25fa/cm	1185	296	496	3.15
0.35w/cm, 0.0007sp/cm, 0.3fa/cm	1139	342	496	3.15
0.35w/cm, 0.0008sp/cm, 0.3fa/cm	1139	342	496	3.59
0.38w/cm, 0.0007sp/cm, 0.2fa/cm	1208	241	496	3.08
0.38w/cm, 0.0008sp/cm, 0.3fa/cm	1115	334	496	3.51

Table 3.2. (cont.) Mix designs by weight for self-compacting pastes.

Table 3.3. Mix designs by weight for concretes.

Component (%)	**Mix Designation**			
	Concrete 1	**Concrete 2**	**Concrete 3**	**Concrete 4**
Cement	17.20	15.92	19.82	17.20
Fly ash	7.57	7.00	4.95	7.57
Water	9.25	9.95	9.25	9.25
19 mm aggregate	18.78	19.13	18.78	18.78
9.5 mm aggregate	24.82	25.28	24.82	24.82
Sand	23.47	23.92	23.47	23.47
Superplasticizer	0.05967	0.05517	0.05221	0.08950

3.3. Mixing

Pastes were mixed in a paddle mixer (a Hobart mixer with around 3 kg paste capacity) mostly following standard procedures. Normal cement pastes were mixed for 30 seconds at

speed 1, then the mixer was stopped for 60 seconds and the sides were scraped, and the paste was mixed for 90 seconds at speed 2. Pastes with fly ash added were mixed the same way, as were fly ash-water pastes and pastes with bacteria. For pastes containing superplasticizer, including self-compacting pastes, the superplasticizer was mixed with 30 % of the water, and added after 30 seconds of mixing. Pastes were mixed for then 60 seconds at speed 1, then the mixer stopped for 60 seconds and scraped, and then mixing was continued for 120 seconds at speed 2. Pastes with viscosity modifying agent were also mixed this way, with the superplasticizer added with 30 % of the water, and the viscosity modifying agent with 10 % of the water, both added at 30 seconds. Geopolymer pastes were mixed for 4 minutes: the solids were dry mixed for 30 seconds at speed 1, and then the solution was added and mixed for 60 seconds. The mixer was stopped, paste was scraped off the sides and further mixing was done for 150 seconds at speed 2.

Concretes were mixed in a pan mixer. Batch sizes were either 50 or 110 kg. Dry aggregates and cement were mixed for 30 seconds, and then water was added and mixed for 60 seconds. The sides and bottom were scraped, and then mixing proceeded for 150 seconds.

3.4. Penetration resistance procedure

The ASTM standard for penetration resistance was followed, with minor modifications, as explained in detail elsewhere [9]. Around 2 kg of paste was placed in a plastic container for penetration resistance testing after it was mixed. The container was around 50 cm × 60 cm × 50 cm. The container was tapped on the table to level the paste and then covered with a moist towel to prevent evaporation of water. Penetration resistance was measured using a screw-driven testing machine (Instron 4500) equipped with several needles and a 1-kN load cell. Penetration resistance measurements were done at intervals of one hour. They were made in triplicate and averaged. Six needles were used, with cross sections of 645 mm^2, 323 mm^2, 161 mm^2, 65 mm^2,

32 mm^2, and 16 mm^2, and each with a length of around 90 mm. Each needle penetrated to a depth of 25 mm in 10 seconds. Larger needles were used for initial measurements, and smaller ones for later measurements. Needles were changed as required to provide the required penetration resistance within the required range of load until the smallest needle had been used. The load was divided by area of the needle to calculate penetration resistance. The decision to change needles was subjective.

3.5. Ultrasonic wave reflection procedure

The procedure developed by Chung for wave reflection testing was followed, which is explained in detail elsewhere [1]. Cement paste was mixed and approximately 300 gm (3 kg for concrete) was poured into the ultrasonic wave reflection container. Contact-type 2.25-MHz P-wave and S-wave transducers were attached to the bottom of the container. The container was made of high impact polystyrene (HIPS). HIPS buffer was chosen because it has relatively low acoustic impedance, thus providing sensitivity to small changes in the cement paste. The size of the container was around approximately 50 mm × 60 mm × 50 mm (scaled up three times in all directions for concrete). Solid phenol salicylate was used to couple the transducer to the buffer. The thickness of the HIPS buffer at the bottom of the container was 6.25 mm, and this was selected based on wave velocity and other similar considerations. The transducers were connected to two Panametrics 5077 pulser-receiver units. The output power level of the pulser-receiver units were set to obtain large amplitude for the first reflected wave pulses. The pulser-receiver units were connected to a computer equipped with a National Instruments 5102 PCI type digitizer (8–bit, 2–channel), using a sampling rate of 10 MHz for each transducer. The computer program LabView was used to collect and process data. Time domain signals were obtained, and then converted to frequency domain data by use of a fast Fourier transform. Once the frequency

data were obtained, the wave reflection coefficient was calculated using a single pulse compensating procedure [1] which uses the ratio of the amplitude of reflection with cement paste and air. The testing apparatus is shown in Figure 3.1. A photo of the same is shown in Figure 3.2.

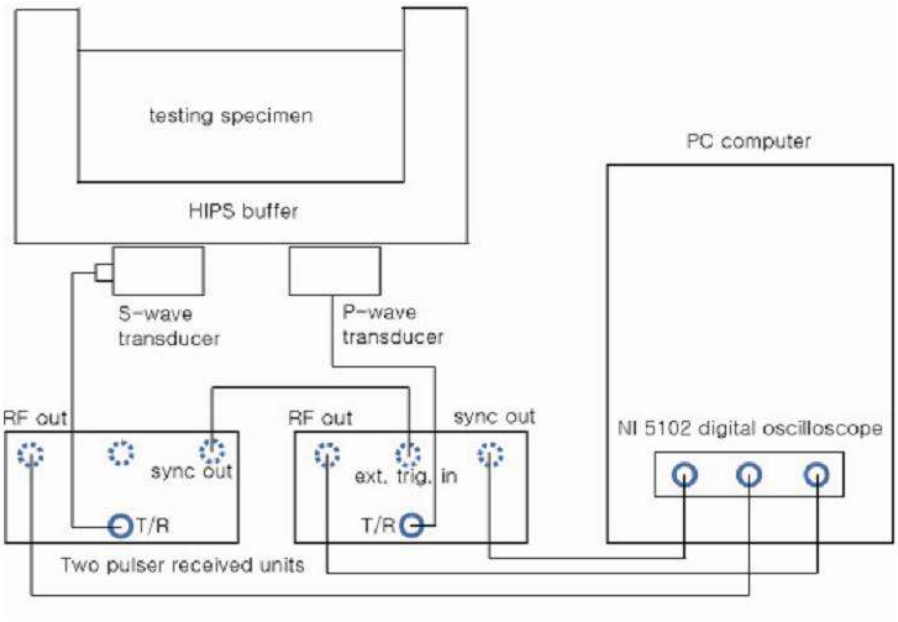

Figure 3.1. Ultrasonic wave reflection testing apparatus [1].

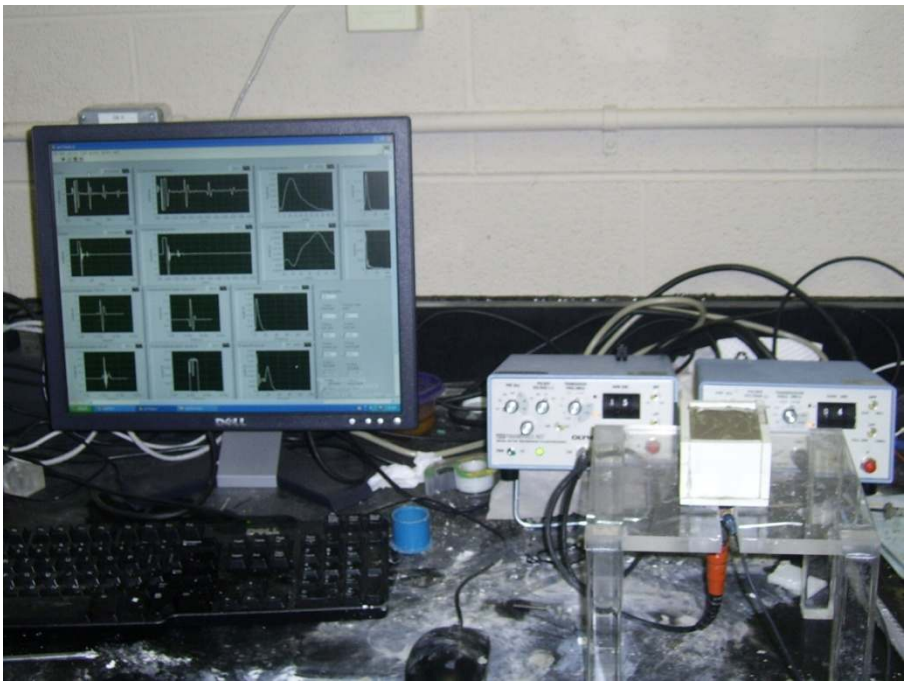

Figure 3.2. Photo of the ultrasonic wave reflection testing apparatus.

3.6. Formwork pressure procedure

The procedure developed by Birch for formwork pressure testing was used, and is described in detail elsewhere [24]. Pressures were measured using a commercially available flush diaphragm-type pressure transducer with a face diameter of 20 mm. The sensors were connected to a Vishay Model P-3 data logger for recording data. The test columns used in the experimental program were 0.25 m diameter Polyvinyl chloride pipes 1 m in height. The columns were made of two halves, which were fastened with metal hose clamps. They were designed such that they could be assembled and disassembled with ease. This system also made it easy to clean off any concrete that may have dripped on the form. Holes were machined into the side of the columns at various heights for mounting sensors. The bottom column was secured to a wooden base so that the column would not tip over during filling. Sensors were secured to the column, at the location of the holes, using flat square metal mounting plates. In addition, a cling film with a small amount of talc powder on it was placed over the sensors prior to mounting to prevent sticking of the concrete and eliminate any suction due to shrinkage of the concrete. A photo of the sensors is shown in Figure 3.3, the data logger in Figure 3.4, and the test column in Figure 3.5.

Figure 3.3. Formwork pressure sensor [24].

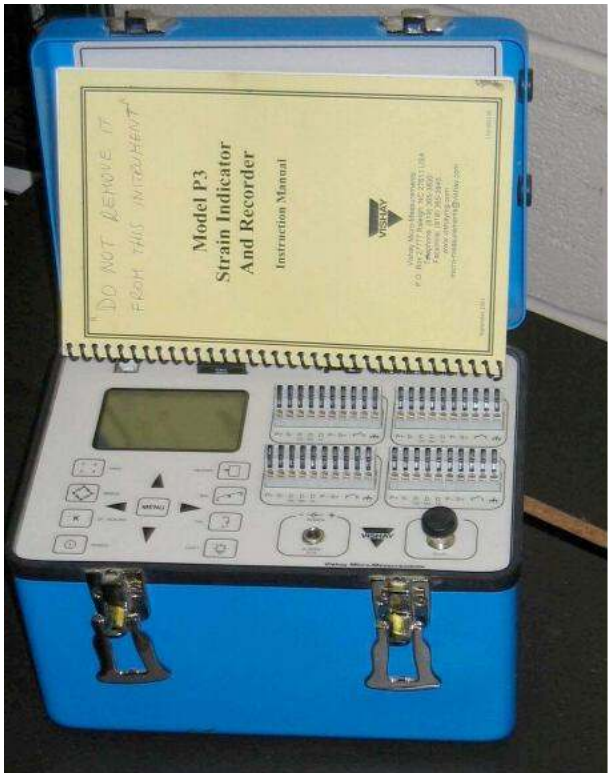

Figure 3.4. Formwork pressure data logger [24].

Figure 3.5. Formwork pressure test column [21].

4. PENETRATION RESISTANCE

The standard test for determining concrete setting times is the Proctor penetration resistance test [5]. It is noted that the test is not actually done on concrete, but on mortar extracted from the concrete. According to the standard [5], initial set is when the penetration resistance is 3.5 MPa and final set when the penetration resistance is 27.6 MPa. Previous studies by our research group focused on the adaption of the standard penetration test for cement pastes. It was concluded that for cement pastes, initial set is at a penetration level of 2 MPa, and final set at a penetration level of 14 MPa [9]. One drawback of the penetration resistance test is its empirical nature–the levels of penetration levels corresponding to initial and final set in the standard (and our modification of the standard) are arbitrary and no specific change occurs in the mortar or paste at these levels.

In this chapter, penetration resistance results of normal and self-compacting cement pastes are presented. The setting times obtained using penetration resistance for these pastes are determined. Results of pastes modified with mineral and chemical admixtures, fly ash pastes, and geopolymers are also presented. The effect of temperature on the setting time of cement pastes is also investigated.

4.1. Results

4.1.1. Normal cement pastes

Penetration resistance was performed on cement pastes of varying w/c to investigate the effect of w/c on setting times. In this study, w/c values of 0.35, 0.4, 0.5, and 0.6 were used. Penetration resistance values of these pastes were plotted as a function of time. The curves shifted to the right with higher w/c, indicating later setting times. Exponential functions were fitted to these curves, and initial and final set times were found as the times the fitted penetration

resistance curves reached values of 2 MPa and 14 MPa, respectively. The correlation coefficient, R^2, was over 0.99 for all the curves, indicating that the fits were good. These results are shown in Figure 4.1. The setting times increased with w/c, and the test clearly distinguished between the various w/c values tested and, therefore, is sensitive to changes in w/c. Values of initial and final set are shown in Table 4.1. The setting times were plotted against w/c (Figure 4.2), and it was concluded from the plot that the setting times depend linearly on w/c. The linear dependence of setting time on w/c has not been explored in prior work, and is an important observation, as it can be extrapolated or interpolated to find the setting times of other w/c pastes. The exact nature of this relationship most likely depends on various factors such as cement type, temperature, and relative humidity.

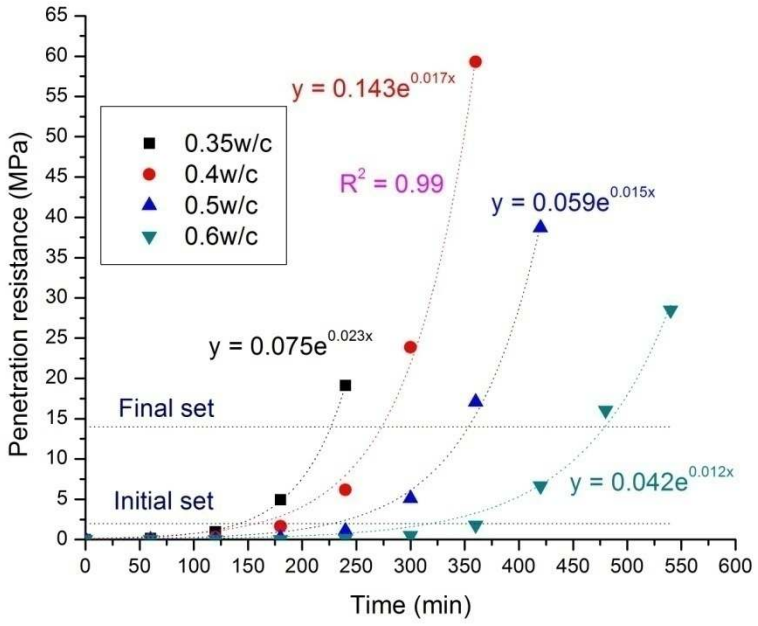

Figure 4.1. Penetration resistance of cement pastes with varying w/c. Exponential curves were fitted to the data. Initial and final set levels of 2 MPa and 14 MPa are shown. The value of R^2 applies to all the curves shown.

Table 4.1. Setting times of cement pastes with varying w/c from penetration resistance.

w/c	Initial set (min)	Final set (min)
0.35	142	220
0.4	157	264
0.5	228	344
0.6	319	467

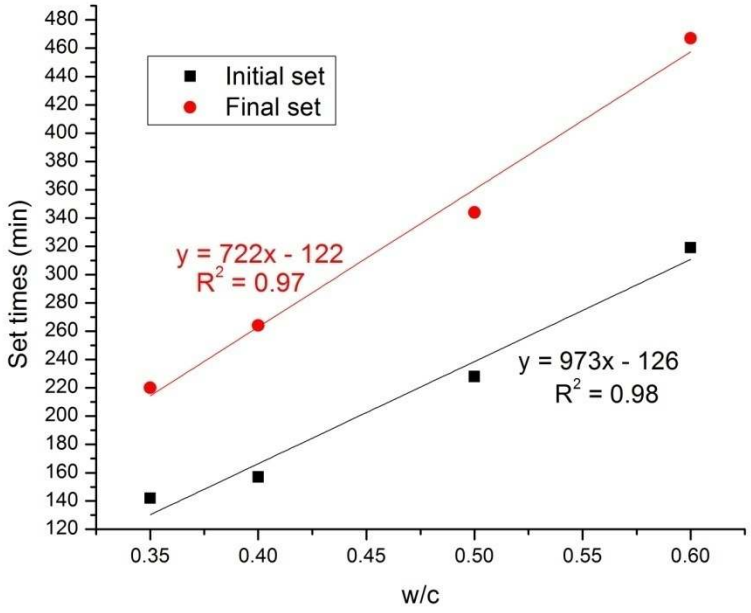

Figure 4.2. Setting times of cement pastes from penetration resistance plotted against w/c. The dependence is highly linear.

4.1.2. Cement pastes with fly ash or superplasticizer

Self-compacting pastes were made by incorporating both fly ash and superplasticizer in the pastes. To understand the combined effect of these materials on setting times, it was important to know their individual effects on the setting times. For this purpose, the following

mixes were tested: 0.33w/c; 0.33w/cm, 0.3fa/cm; 0.33w/cm, 0.4fa/cm; 0.33w/c, 0.0004sp/c; and 0.33w/c, 0.0008sp/c. The effect of increasing amounts of fly ash (Figure 4.3) and superplasticizer (Figure 4.4) on the penetration resistance of cement pastes was studied. The curves shifted to the right with both increasing fly ash and superplasticizer content, indicating higher setting times. These responses were expected, since both fly ash and superplasticizer usually delay set. The test was easily able to distinguish the setting times of the different mixes. At the respective dosages used, the fly ash retarded set more than the superplasticizer did. When compared to normal cement paste, the fly ash pastes showed a higher difference in time between initial and final set, however, the superplasticized pastes showed roughly the same difference. The setting times of all pastes with fly ash or superplasticizer are shown in Table 4.2.

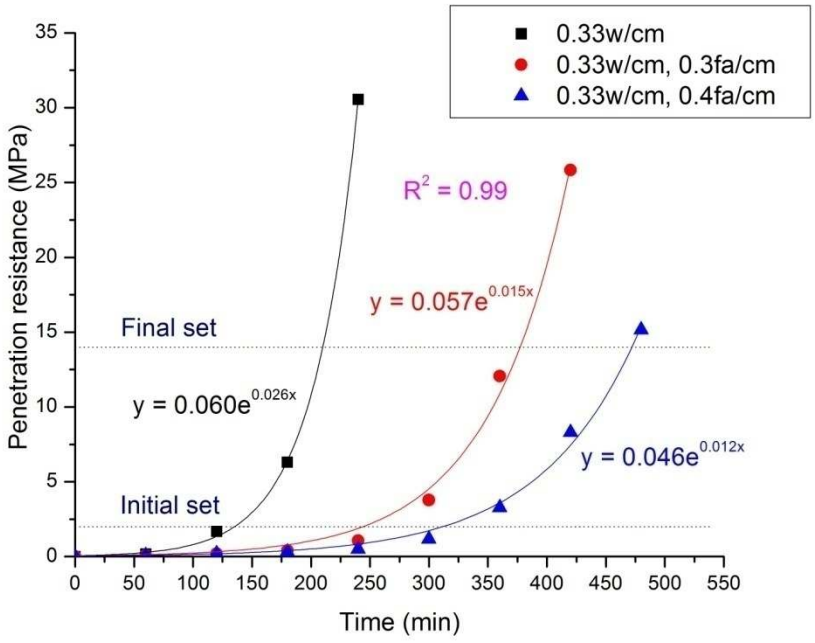

Figure 4.3. Penetration resistance of cement pastes with increasing amounts of fly ash.

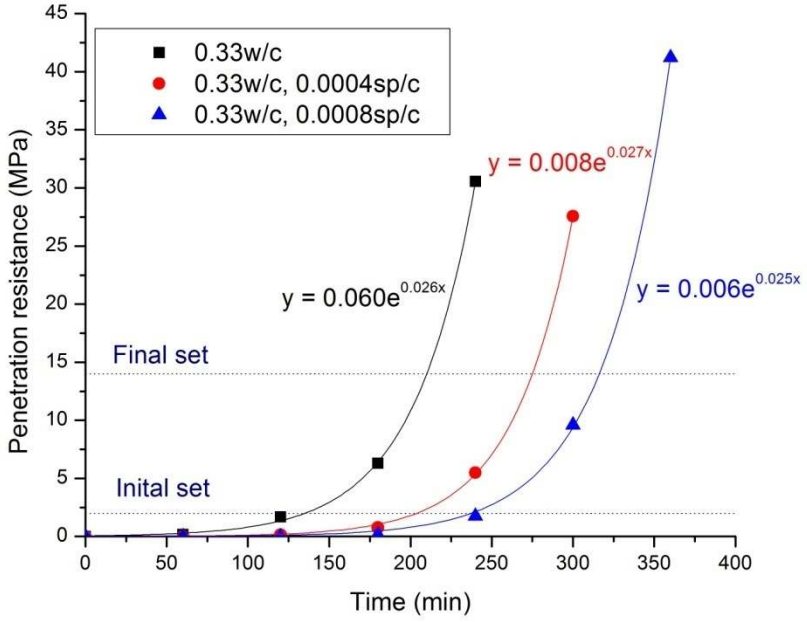

Figure 4.4. Penetration resistance of cement pastes with increasing amounts of superplasticizer.

Table 4.2. Setting times of cement pastes with fly ash or superplasticizer.

Mix	Initial set (min)	Final set (min)	Difference between initial and final set (min)
0.33w/c	135	210	75
0.33w/cm, 0.3fa/cm	244	377	133
0.33w/cm, 0.4fa/cm	312	472	160
0.33w/c, 0.0004sp/c	204	275	71
0.33w/c, 0.0008sp/c	237	316	79

4.1.3. Self-compacting pastes

Several self-compacting pastes were tested for penetration resistance. These pastes had both fly ash and superplasticizer added to achieve the required self-compacting behavior. For different pastes, the w/cm, the fa/cm, and the sp/cm were varied.

To check the reproducibility of the penetration resistance method, three trials each were performed on two mixes: 0.33w/cm, 0.00055sp/cm, 0.3fa/cm; and 0.38w/cm, 0.0007sp/cm, 0.2fa/cm. The results of these trials are shown in Figure 4.5 and Figure 4.6. Setting times and statistical parameters are shown in Table 4.2.

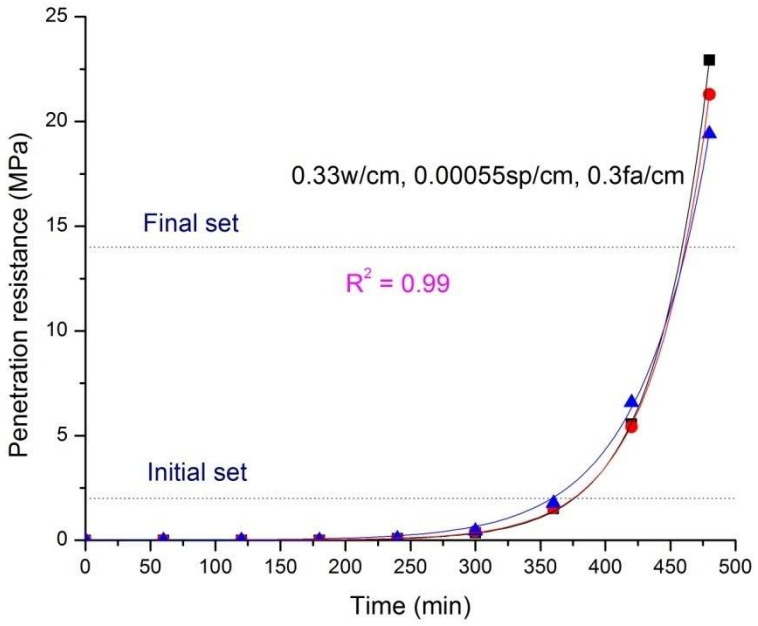

Figure 4.5. Reproducibility of the penetration resistance method with self-compacting pastes for a paste with the composition 0.33w/cm, 0.00055sp/cm, 0.3fa/cm.

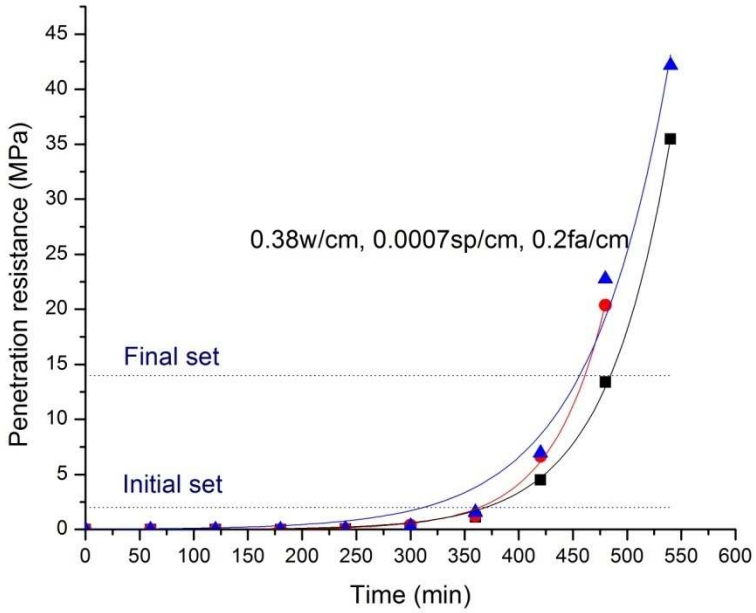

Figure 4.6. Reproducibility of the penetration resistance method with self-compacting pastes for a paste with the composition 0.38w/cm, 0.0007sp/cm, 0.2fa/cm.

Table 4.3. Setting times and statistical parameters for self-compacting paste reproducibility.

Parameter	0.33w/cm, 0.00055sp/cm, 0.3fa/cm			0.38w/cm, 0.0007sp/cm, 0.2fa/cm		
	Trial 1	Trial 2	Trial 3	Trial 1	Trial 2	Trial 3
IS (min)	376	375	359	364	369	312
FS (min)	459	461	462	461	456	485
Average, IS (min)	370			348		
Average, FS (min)	461			467		
Standard deviation, IS (min)	9.54			31.56		
Standard deviation, FS (min)	1.53			15.50		
Coefficient of variation, IS (%)	2.58			9.06		
Coefficient of variation, FS (%)	0.33			3.32		

*IS denotes initial set, and FS denotes final set.

From Table 4.3, it is seen that the coefficient of variation values for final set were generally very low. The coefficient of variation values for initial set were higher, especially for the mix 0.38w/cm, 0.0007sp/cm, 0.2fa/cm. The average coefficient of variation was around 6.2 % for initial set and 1.5 % for final set. Additional tests need to be done to more completely determine the reproducibility of the method.

Figure 4.7 shows the effect of increasing fa/cm on the penetration resistance of self-compacting pastes with the same w/cm and sp/cm. Figure 4.8 shows the effect of increasing sp/cm on the penetration resistance of self-compacting pastes with the same w/cm and fa/cm. Figure 4.9 shows the effect of increasing w/cm on the penetration resistance of self-compacting pastes with the same sp/cm and fa/cm. As expected, increase in any of fa/cm, sp/cm, and w/cm led to shifting of the penetration resistance curves to the right. The setting time values are shown in Table 4.4, and it was seen that increase in any of the three parameters resulted in a considerable increase in final set times. On the other hand, results with initial set were not as clear, however, initial set times seemed to generally increase with increase in fa/cm and sp/cm. Therefore, it appears that the method was able to distinguish fairly small changes in w/cm, sp/cm, and fa/cm. Hence, penetration resistance can be used to accurately determine the setting times of various self-compacting pastes (more so for final set than for initial set). The effect of an increase in both fa/cm and sp/cm is shown in Figure 4.10, and the set times are given in Table 4.4. Such an increase led to an increase of over 100 minutes in both initial and final set, and thus the setting times of such pastes were easily distinguishable using penetration resistance. Set values with normal and self-compacting pastes are compared with those obtained from ultrasonic wave reflection in chapter 5 and chapter 6.

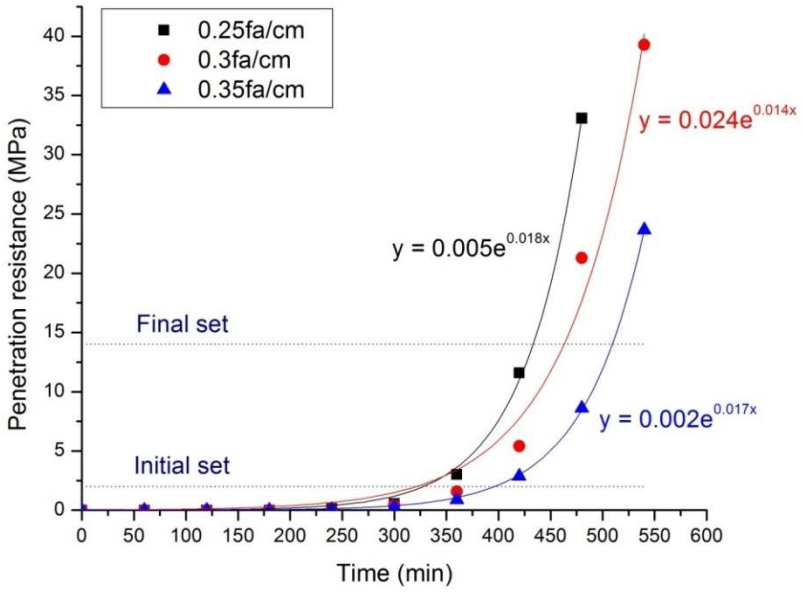

Figure 4.7. Penetration resistance of self-compacting pastes with 0.33w/cm, 0.00055 sp/cm and differing fa/cm.

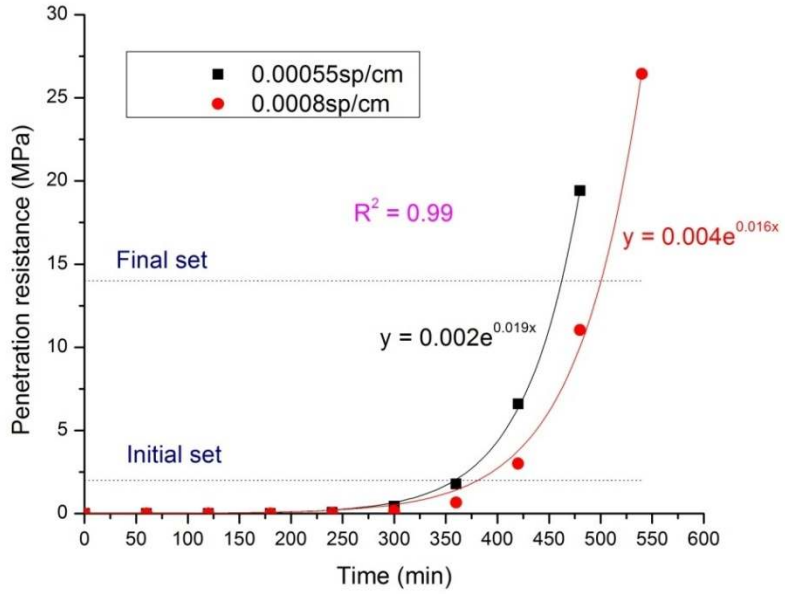

Figure 4.8. Penetration resistance of self-compacting pastes with increasing 0.33w/cm, 0.3fa/cm and differing sp/cm.

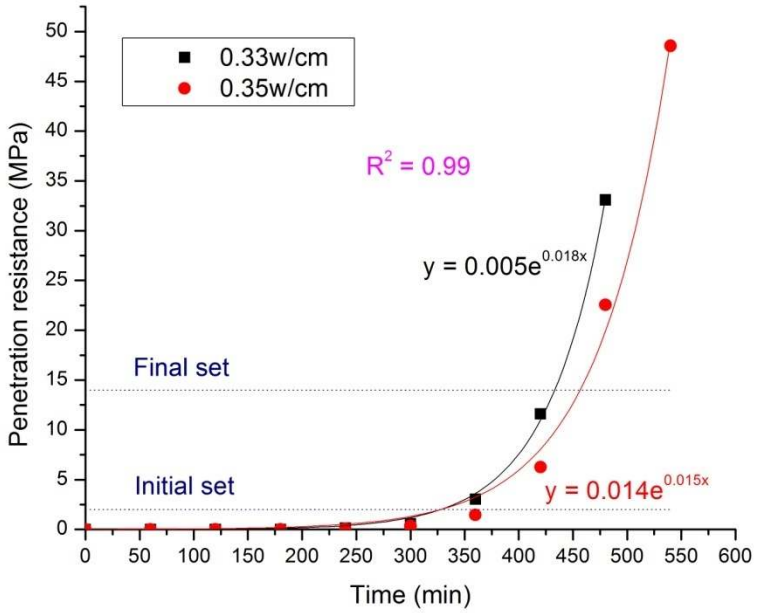

Figure 4.9. Penetration resistance of self-compacting pastes with 0.055sp/cm, 0.25fa/cm and differing w/cm.

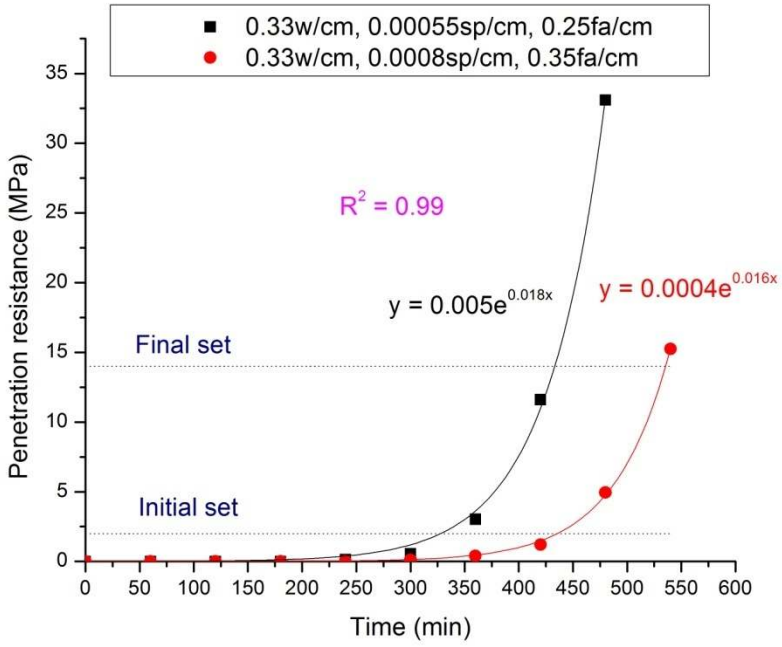

Figure 4.10. Penetration resistance of self-compacting pastes with differing sp/cm and fa/cm.

Table 4.4. Setting times of various self-compacting pastes.

Mix	Change	Initial set (min)	Final set (min)
0.33w/cm, 0.00055sp/cm, 0.25fa/cm	Increasing fa/cm	328	433
0.33 w/cm, 0.00055sp/cm, 0.3fa/cm		321	463
0.33w/cm, 0.00055sp/cm, 0.35fa/cm		396	509
0.33w/cm, 0.00055sp/cm, 0.3fa/cm	Increasing sp/cm	359	462
0.33w/cm, 0.0008sp/cm, 0.3fa/cm		381	500
0.33w/cm, 0.00055sp/cm, 0.25fa/cm	Increasing w/cm	328	433
0.35w/cm, 0.00055sp/cm, 0.25fa/cm		327	457
0.33w/cm, 0.00055sp/cm, 0.25fa/cm	Increasing sp/cm and fa/cm	328	435
0.33w/cm, 0.0008sp/cm, 0.35fa/cm		433	557

4.1.4. Other pastes

Pastes modified with mineral and chemical admixtures, fly ash-water pastes, and geopolymer pastes were also studied. The effect of a viscosity modifying agent on the setting times was studied, as self-compacting concretes sometimes incorporate these admixtures. Dosages of 0.0012 and 0.0017 vma/w were used. Addition of viscosity modifying agent resulted in the penetration resistance curves shifting to the right, indicating increase in the set times. Self-compacting pastes with superplasticizer and viscosity modifying agent were also tested. Increasing both sp/cm and vma/w resulted in substantially higher setting times. Results with viscosity modifying agents are shown in Figure 4.11 and Figure 4.12.

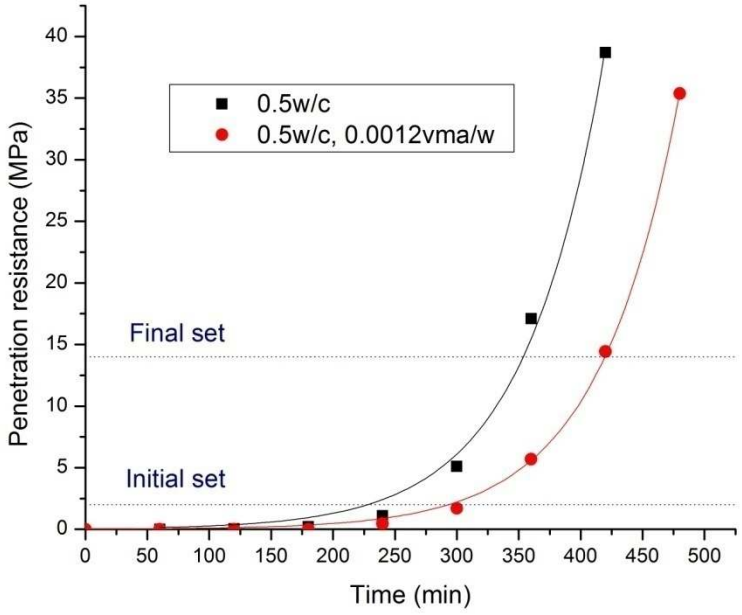

Figure 4.11. Effect of viscosity modifying agent on penetration resistance of 0.5w/c paste.

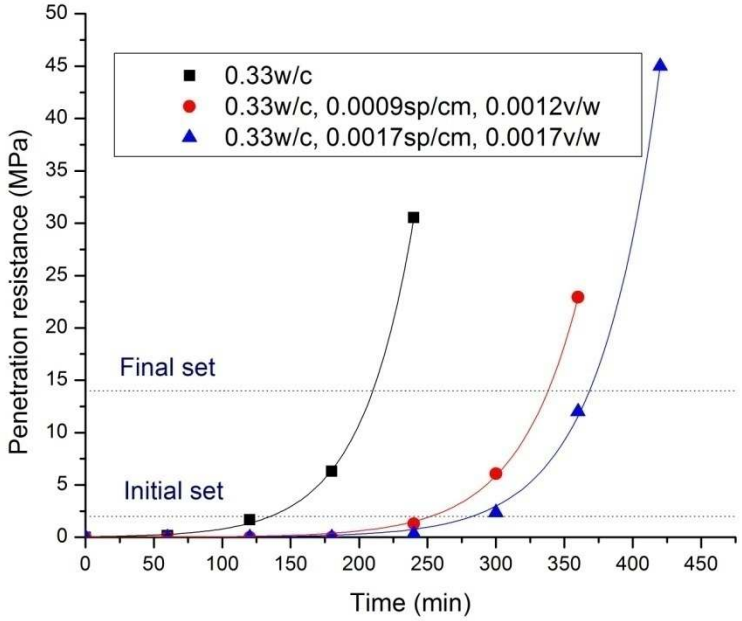

Figure 4.12. Effect of viscosity modifying agent and superplasticizer on penetration resistance of 0.33w/c paste.

Tests were done to see if the set retardation caused by the fly ash was due to the fly ash retarding cement hydration or due to cement being replaced by inert material. Finely powdered ground quartz was added to cement paste, and the setting time of this paste was compared to that of the paste with fly ash at the same replacement ratio. A 0.33w/c paste was made with another fly ash (a Class F fly ash, designated fa2) at the same replacement ratio as the fly ash used in the study (a Class C) and the setting times of all three pastes compared (Figure 4.13). The paste with ground quartz showed later setting when compared to the normal cement paste; however, it set substantially earlier than the pastes with fly ash. These results indicated that the fly ashes were retarding setting more than an inert filler was, indicating that the fly ash was probably retarding the cement hydration reaction.

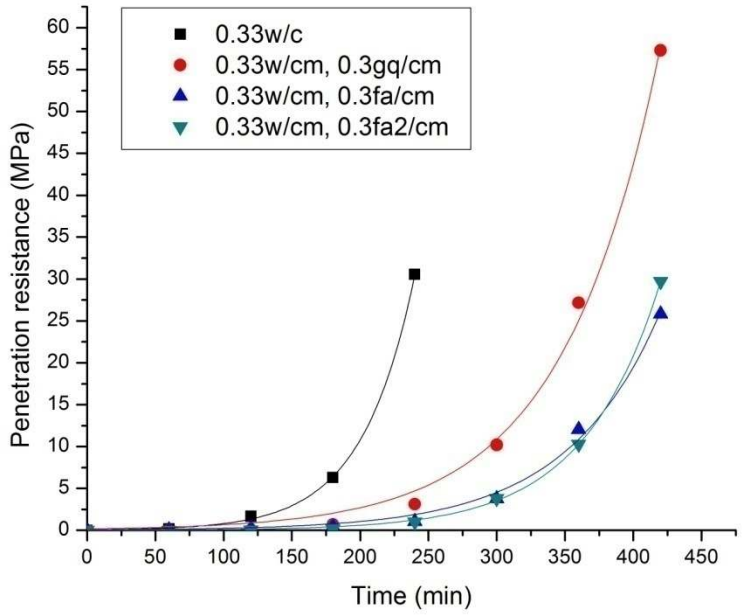

Figure 4.13. Effect of ground quartz and fly ashes on penetration resistance of 0.33 w/c paste.

The fly ash used in the study was a Class C fly ash, which is sometimes reported to react with water. The penetration resistance of fly ash-water mixtures was tested using pastes with

various w/fa values. The penetration resistance of paste made with a low w/fa of 0.24 exceeded the testing machine limit of 65 MPa at the first measurement. Rapid and strong initial stiffening was also observed for the mix with w/fa 0.33 (the mix showed a penetration resistance value of 24 MPa at the first measurement, whereas cement paste of the same w/c showed around 0.2 MPa at that time). It is noted that to thoroughly analyze the setting of such mixtures, the testing procedure has to be changed to collect more data at earlier times in the setting process. The amount of (initial) stiffening decreased with increasing w/fa ratio. The mixes showed unusual responses, and did not fit the exponential curve shape usually associated with cement pastes. For example, the mix with 0.5w/fa showed almost constant penetration resistance with time. Results are shown in Figure 4.14. Although some of the fly ash-water pastes showed rapid stiffening, cement pastes containing this fly ash actually showed set retardation and no rapid stiffening.

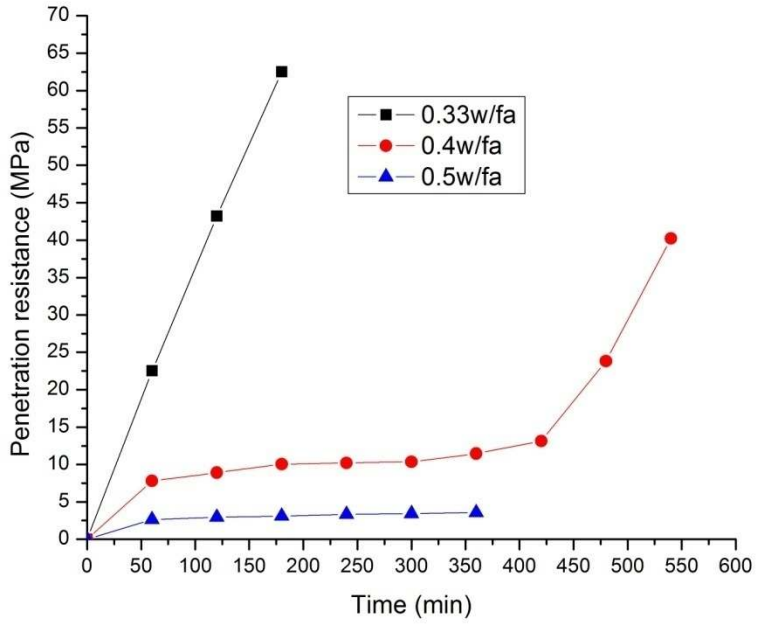

Figure 4.14. Penetration resistance of fly ash pastes.

Penetration testing was also done on a fly ash-slag geopolymer paste with 15 % slag. However, the test method was modified in terms of data collection with more frequent data collection in the earlier part of the test as compared to the later part, since the mixes had showed early stiffening. The results are shown in Figure 4.15. On comparison with a cement paste of similar water content, it was seen that the geopolymer showed very different stiffening behavior. It had rapid initial stiffening and showed much higher initial penetration resistance than the cement paste. However, the penetration resistance considerably slowed down later, and did not follow the exponential increase seen in the cement paste.

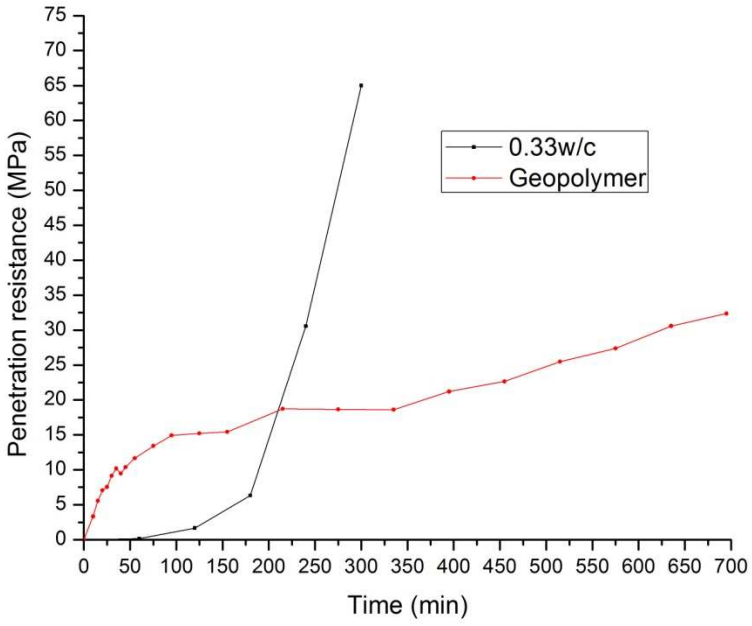

Figure 4.15. Penetration resistance of a geopolymer and normal cement paste.

4.1.5. Effect of changing temperature on setting times

It is well known that increasing temperature results in faster setting for cementitious materials. The above penetration resistance tests were all performed at 75 °F. To investigate the effect of temperature on set times, penetration testing was carried out at different temperatures. Tests were performed on a self compacting paste with composition 0.33w/cm, 0.00055sp/cm,

0.3fa/cm. Results are shown in Figure 4.16. Setting was considerably slower at a temperature of 66 °F as compared to a temperature of 75 °F. Setting at 82 °F and 84 °F was almost the same, and slightly faster than at 75 °F. Hence, set seemed to be retarded considerably at lower temperatures, but not considerably accelerated at higher temperatures.

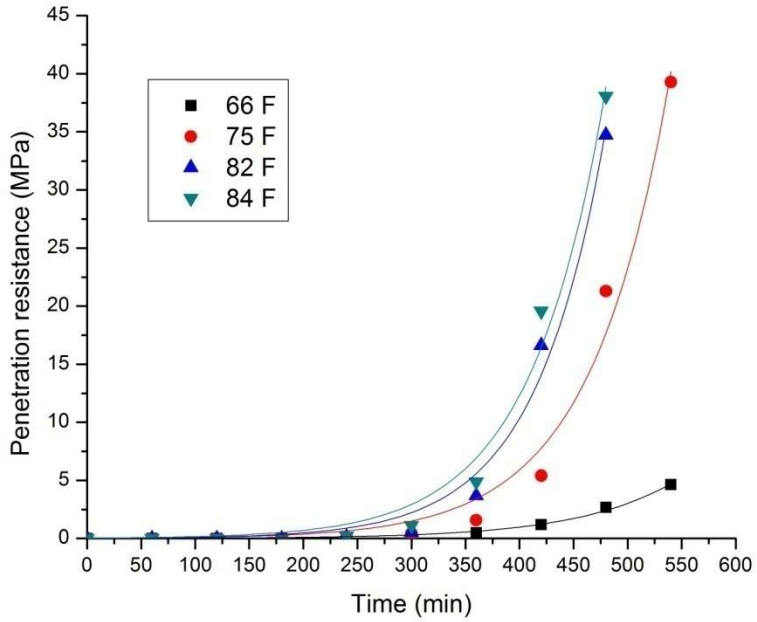

Figure 4.16. Effect of temperature on the penetration resistance of cement pastes.

4.2. Conclusions

The following conclusions were drawn from penetration resistance testing:

1. Penetration resistance can distinguish pastes of varying w/c. Setting times varied linearly with w/c.
2. Penetration resistance with self-compacting pastes showed good reproducibility. Coefficient of variation values for final set were lower than those for initial set.
3. Fly ash, superplasticizer, and viscosity modifying agent retard setting in cement pastes. Increase in w/cm, fa/cm, and sp/cm in self-compacting pastes caused shifting of the

penetration resistance curves to the right. Retardation of final set was more than that of initial set. Penetration resistance distinguished fairly small changes in w/cm, fa/cm, and sp/cm.

4. Fly ash pastes showed extremely rapid stiffening at low w/fa ratio. Fly ash-slag geopolymers showed different stiffening characteristics from cement pastes with much higher initial stiffening and lower later stiffening. These stiffening behaviors were easily detected by penetration resistance.
5. Set using penetration resistance was retarded considerably at lower temperatures, but not as strongly accelerated at higher temperatures.

5. ULTRASONIC SHEAR WAVE REFLECTION

Penetration resistance tests have been used to determine setting time of cementitious materials, but these methods have several drawbacks. They are laborious, time consuming, and do not give continuous data output. For these reasons, several attempts have been made to develop other methods to determine setting times. Non-destructive ultrasonic methods, primarily transmitted ultrasonic waves have being researched for this purpose. In this study, a newer method, ultrasonic wave reflection has been used to analyze setting behavior. Both shear (S-wave) and longitudinal (P-wave) waves have been used in the study; S-wave results are presented in this chapter, and P-wave results are presented in the next chapter. The reflection coefficient of hydrating cementitious materials at their interface with a buffer is monitored as a function of time and conclusions about setting times are made from the resulting reflection coefficient-time curve.

Results with both normal and self-compacting pastes are presented. Setting times are found and compared with those obtained using penetration resistance. Results of pastes modified with mineral and chemical admixtures, pastes showing rapid stiffening, fly ash pastes, and geopolymers are presented, to show the general applicability of this method. Results with self-compacting concretes are shown, and compared to the results of the corresponding pastes. Curve fitting to S-wave reflection data is explored.

5.1. Results

5.1.1. Normal cement pastes

It was shown in earlier work in our laboratory that high impact polystyrene (HIPS) buffer showed more sensitivity to early changes in cement pastes [1]. Hence, all testing in this study was done with HIPS as buffer.

To check reproducibility of the S-wave reflection method, seven trials of the same 0.5 w/c paste were performed. The reflection coefficient, R, of these pastes was plotted against time (the R-t curve, shown in Figure 5.1). Though there was some variation in the data, the trials showed similar responses.

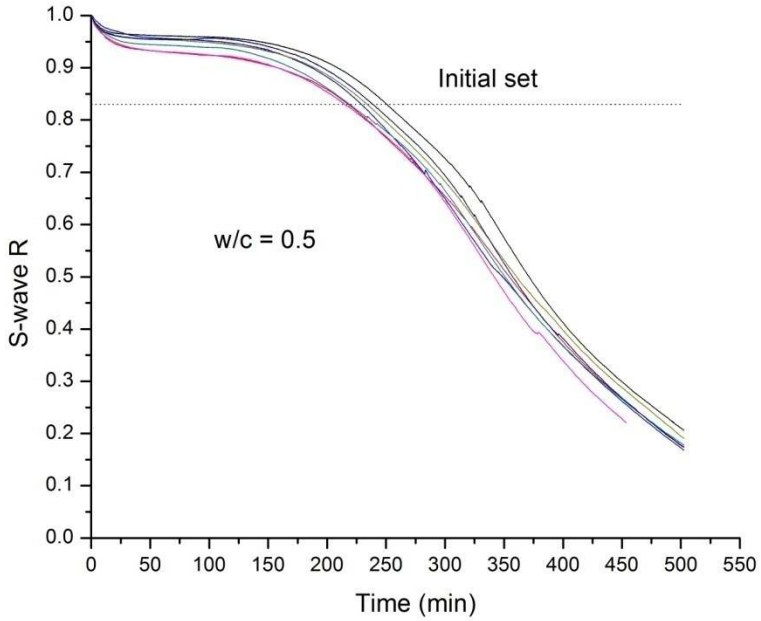

Figure 5.1. R-t curve for seven trials of 0.5w/c paste.

S-waves cannot pass through liquids, and so did not pass through the initially fluid cement paste. Hence, R was equal to one. The value of R dropped from 1 to around 0.95 in the first 20 minutes. This drop was attributed to reflocculation of the cement paste after being poured into the wave reflection container. After this, R remained roughly constant for some time (around 150 minutes for 0.5w/c paste). This response was considered to be due to the induction period in the paste hydration. After the induction period, R started to drop rapidly and then reached an inflection point, after which the rate of drop slightly decreased. R then steadily decreased until it reached its minimum value. The minimum on the R-t curves, called an inversion, is the time

when the acoustic impedances of the paste and buffer are equal. This point is eye-catching, however, it does not have any fundamental significance. After inversion, R increased gradually. R increased as long as the cement hardens; however, there was a steady decrease in the rate of change of R. Tests carried out for long periods of time showed very little change in R after 2 days. The curves shown in Figure 5.1 are truncated; and inversion and post-inversion response are shown in Figure 5.3. It is noted that the response is rather similar to that of the heat curves of cement paste discussed before: an initial drop, an induction period, a rapid decrease, a slower decrease, and then a steady decrease in wave reflection correspond to an initial peak, an induction period, rapid heat evolution, slower heat evolution, and a steady state, respectively in the heat evolution curve of cement paste.

In our previous research [1], an attempt was made to find initial and final set from the S-wave R-t curve. No fundamental point was found for initial set, and initial set was assigned at an empirical level of R = 0.83. The point of inflection was considered to be final set since that point was presumed to correspond to a change in the rate of hydration (when the hydration kinetics changed from dissolution control to diffusion control). This point was found as the minimum on the smoothed numerical time derivative of the R data, designated $\frac{\Delta R}{\Delta t}$. The derivative was computed using points spaced two minutes apart, and then it was smoothed by averaging over a moving window twelve minutes wide. The averaging did not change the curves in any way, apart from reducing the noise. The $\frac{\Delta R}{\Delta t} - t$ curves for the seven trials are shown in Figure 5.2. Initial and final set were found using these parameters and listed for the seven trials in Table 5.1. Statistical parameters are listed in Table 5.2. The coefficient of variation values for initial and final set were fairly low, and hence S-wave reflection can be used to determine set times in a

reproducible manner. It is worth noting that the coefficient of variation for final set, 3 % was half that for initial set, 6 %.

Table 5.1. Setting times for w/c = 0.5 trials.

Trial/ Parameter	**Initial set (min)**	**Final set (min)**
1	249	339
2	216	336
3	228	308
4	217	325
5	213	324
6	233	332
7	237	325

Table 5.2. Statistical parameters for w/c = 0.5 trials.

Trial/ Parameter	**Initial set**	**Final set**
Average (min)	228	327
Standard deviation (min)	13.13	10.23
Coefficient of variation (%)	5.77	3.13

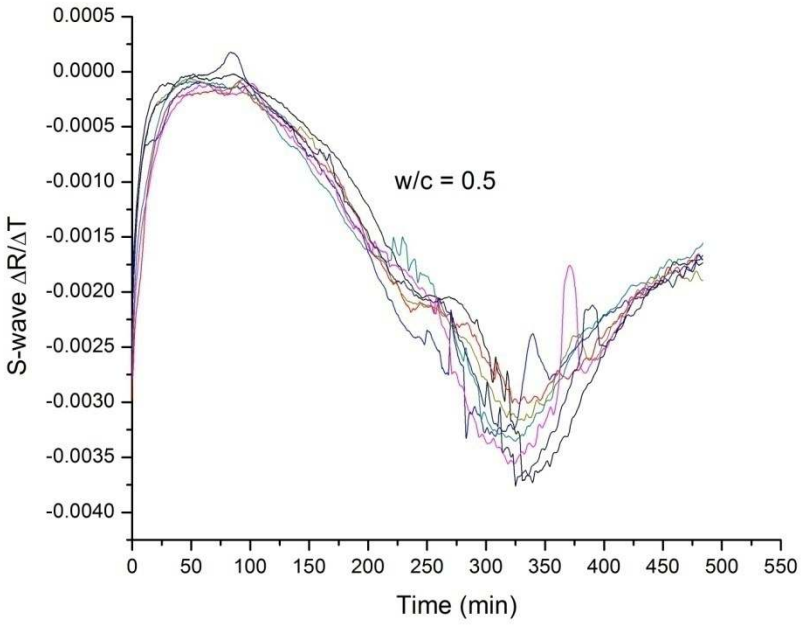

Figure 5.2. $\frac{\Delta R}{\Delta t} - t$ curves for seven trials of w/c = 0.5 paste.

Tests were done on pastes with w/c values of 0.35, 0.4, 0.5, and 0.6, which were the same w/c values on which penetration resistance tests were done. The R-t curves are presented in Figure 5.3 and the $\frac{\Delta R}{\Delta t} - t$ curves in Figure 5.4. The response of the different w/c pastes was considerably different. The curves shifted to the right with higher w/c, indicating higher setting times, as with penetration resistance. The values of initial and final set were found using the methods outlined above, and these values are shown in Table 5.3. From these values, the method can distinguish between w/c values for initial set, as the differences between these times were of the order of 16-27 minutes, which was more than the 13 minute standard deviation for repetitions of 0.5 w/c. S-wave reflection can also clearly distinguish between the w/c values tested for final set, as the differences between final set times for various w/c values were of the order of 24-41 minutes, which was considerably more than the 10 minute standard deviation for repetitions of 0.5w/c. A strong linear relationship was seen when setting times were plotted against w/c (Figure

5.5), though the correlation was slightly lower than that for penetration resistance. The penetration and S-wave reflection results indicate that the w/c affected the setting time in a linear manner.

Initial and final set times from both S-wave reflection and penetration resistance were compared (Figure 5.6). The relationship was roughly linear, though the correlation was only moderately strong. The setting times determined from the two methods were different, since the relationship deviated considerably from the unity line. For lower w/c, set times determined by penetration resistance were earlier, but for higher w/c, set times determined by penetration resistance were later, which suggests penetration resistance is affected more strongly than S-wave reflection by w/c. Pastes with higher w/c often showed segregation, thereby leading to the formation of a harder layer at the bottom, which may have affected the S-wave reflection more than the penetration resistance, since the wave reflection used transducers placed at the bottom. This hard layer at the bottom may have caused pasted with higher w/c to show earlier set by S-wave UWR. Higher w/c pastes also showed bleeding, which reduced the penetration resistance, but may not have significantly affected the wave reflection. Therefore, bleeding and segregation might explain earlier setting times for higher w/c pastes with S-wave reflection.

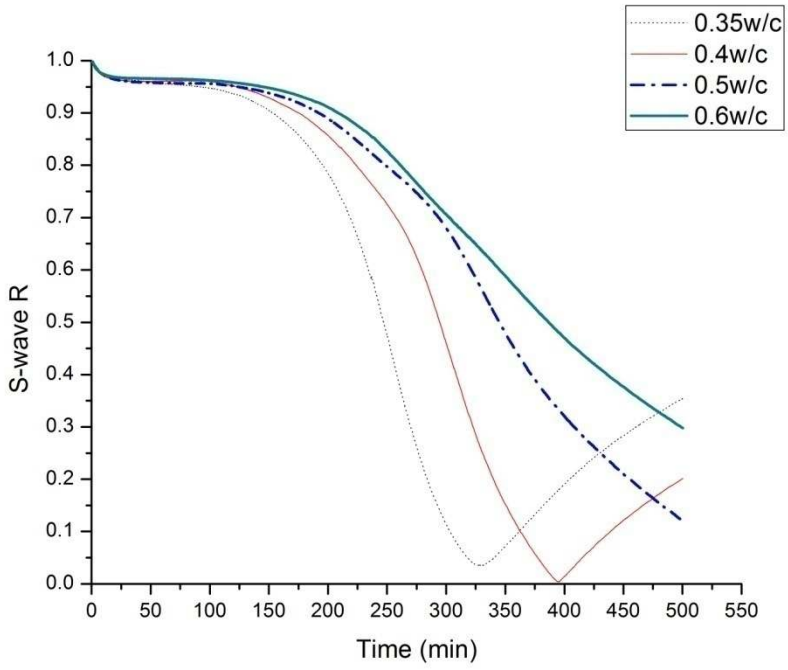

Figure 5.3. R-t curves for pastes with varying w/c.

Table 5.3. Setting times for pastes of varying w/c.

w/c	**Initial set (min)**	**Final set (min)**
0.35	185	250
0.4	212	291
0.5	228	327
0.6	247	351

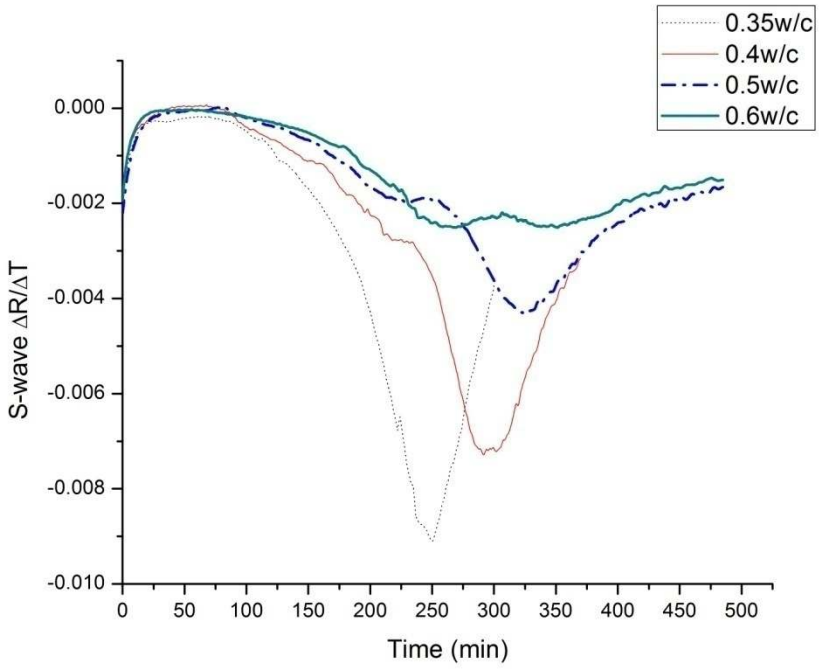

Figure 5.4. $\frac{\Delta R}{\Delta t} - t$ curves for pastes with varying w/c.

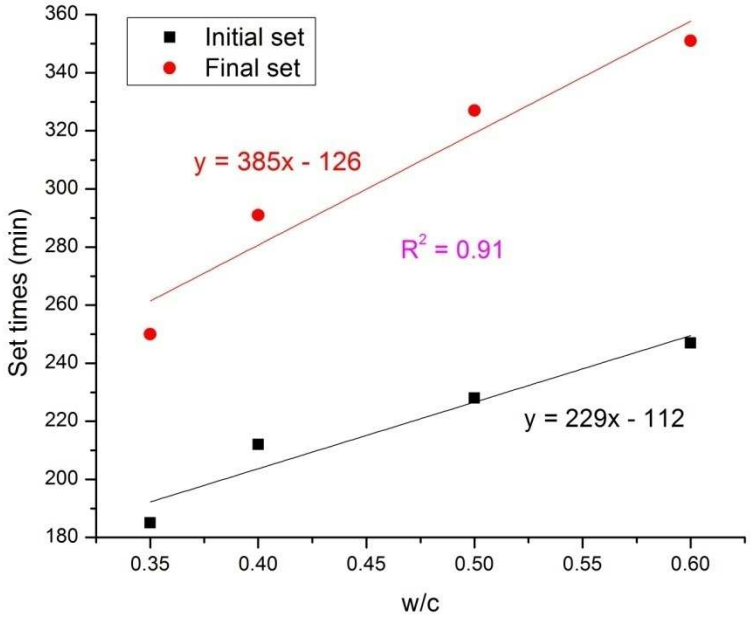

Figure 5.5. Setting times plotted against w/c for pastes with varying w/c.

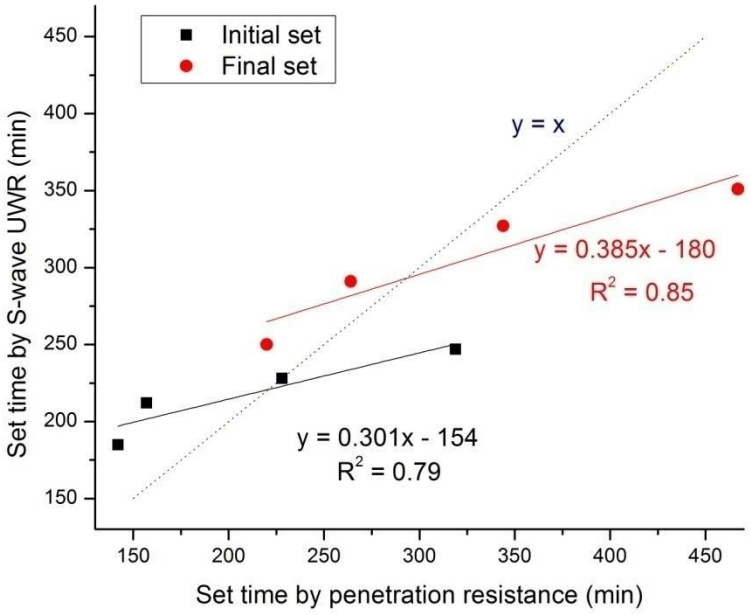

Figure 5.6. Comparison of set times from S-wave reflection and penetration resistance.

5.1.2. Self-compacting pastes

S-wave reflection was done on pastes with fly ash and pastes with superplasticizer, since self-compacting pastes incorporate both. The R-t curves and the $\frac{\Delta R}{\Delta t} - t$ curves for 0.33w/c pastes with fly ash and superplasticizer are shown in Figure 5.7 and Figure 5.8, respectively, and it can be seen that in the dosages used, addition of either of these materials considerably delay setting.

S-wave reflection was done on several self-compacting pastes. To check reproducibility of the method with self-compacting pastes, three trials of a mix with the composition 0.38w/cm, 0.0008sp/cm, 0.3fa/cm were tested. The R-t curves are presented in Figure 5.9 and the $\frac{\Delta R}{\Delta t} - t$ curves in Figure 5.10. The three trials showed similar response. Setting times were computed, and are presented in Table 5.4. The standard deviations were 10.8 minutes for initial set and 1.2 minutes for final set. The coefficient of variation values were around 3.8 % for initial set and 0.3 % for final set, which indicated very good reproducibility. As with plain cement pastes, and with

penetration resistance results, coefficient of variability was lower for final set as compared to initial set. The coefficient of variation values were lower than those from penetration measurements, which were around 5.8 % for initial set and 1.8 % for final set.

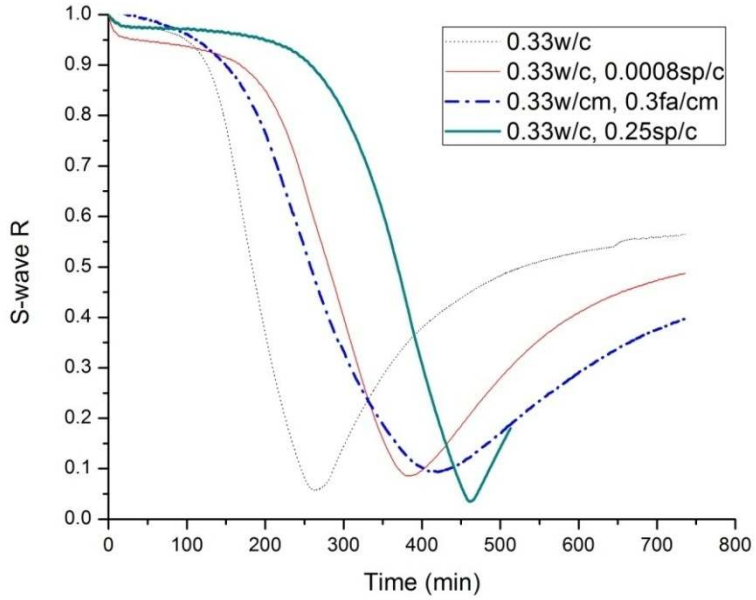

Figure 5.7. R-t curves for pastes with fly ash and pastes with superplasticizer.

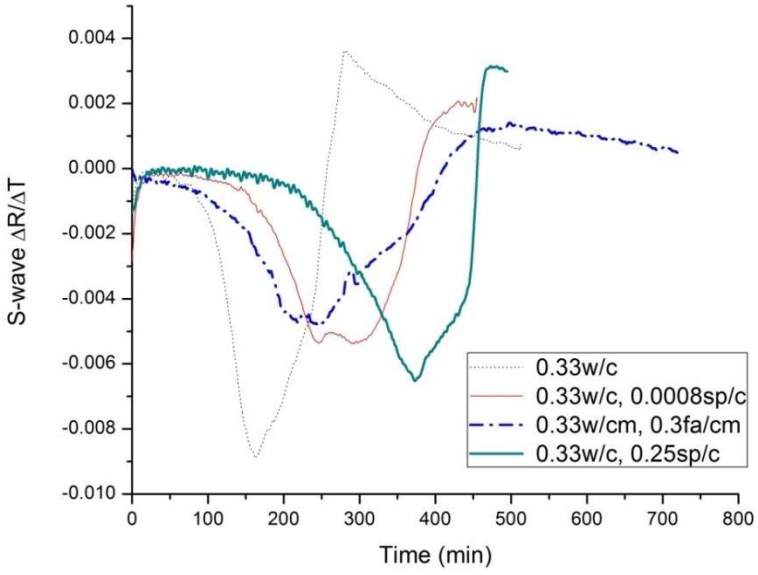

Figure 5.8. $\frac{\Delta R}{\Delta t} - t$ curves for pastes with fly ash and pastes with superplasticizer.

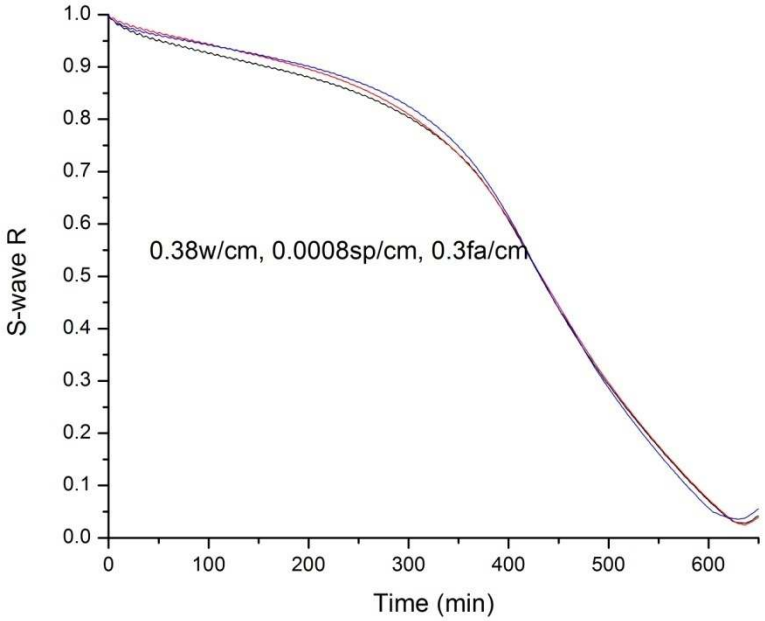

Figure 5.9. R-t curves for three trials of one self-compacting paste mix.

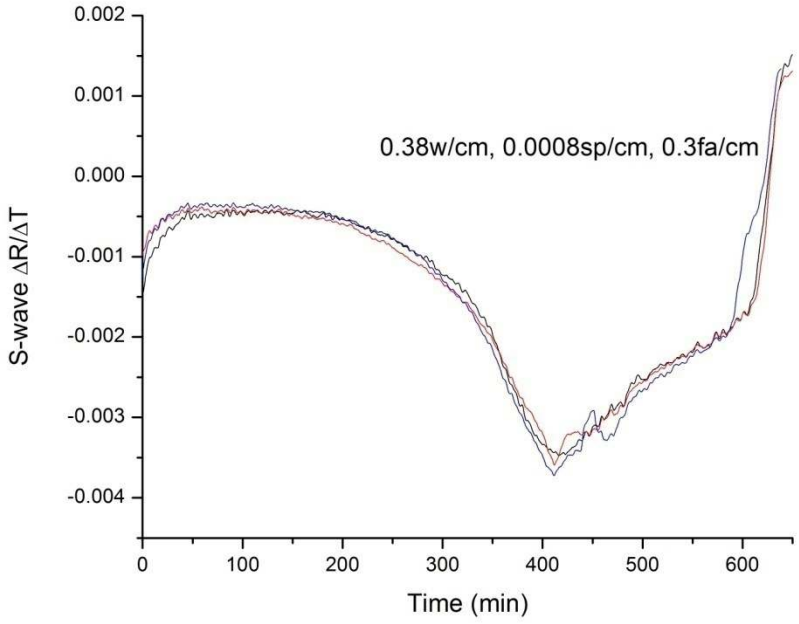

Figure 5.10. $\frac{\Delta R}{\Delta t} - t$ curves for three trials of one self-compacting paste mix.

Pastes with different fa/cm, sp/cm, and w/cm ratios were tested to see if the method could be used to differentiate between self-compacting pastes of different compositions. The R-t curves and $\frac{\Delta R}{\Delta t} - t$ curves for pastes with differing fa/cm but the same sp/cm and w/cm are shown in Figure 5.11 and Figure 5.12, respectively. The R-t curves and $\frac{\Delta R}{\Delta t} - t$ curves for pastes with differing sp/cm but the same fa/cm and w/c are shown in Figure 5.13 and Figure 5.14, respectively. The R-t curves and $\frac{\Delta R}{\Delta t} - t$ curves for pastes with differing w/cm but the same sp/cm and fa/cm are shown in Figure 5.15 and Figure 5.16, respectively. In general, higher w/cm, sp/cm and fa/cm led to the curves shifting to the right, indicating higher setting times. The results for these pastes are shown in Table 5.4. It can be seen that the method clearly distinguished the different mixes with respect to final set, but not as well with respect to initial set.

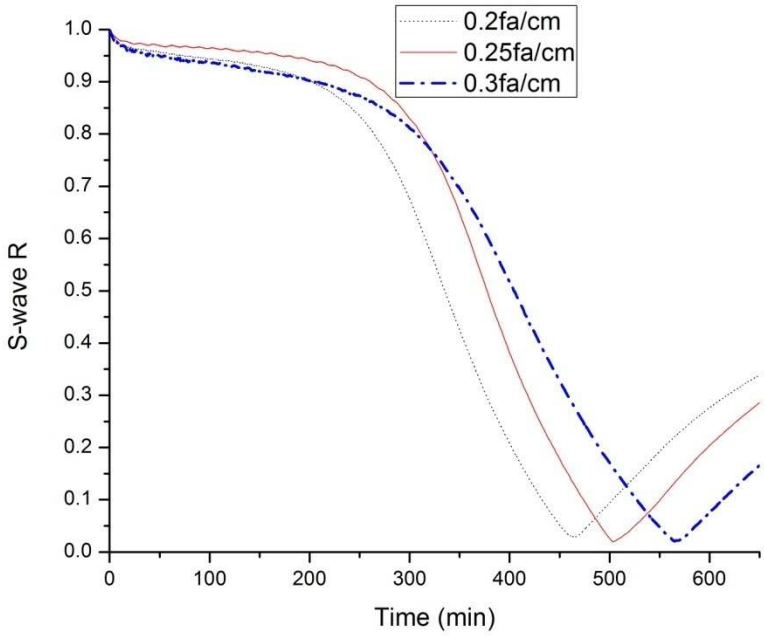

Figure 5.11. R-t curves for self-compacting pastes with 0.35w/cm, 0.0007sp/cm and differing fa/cm.

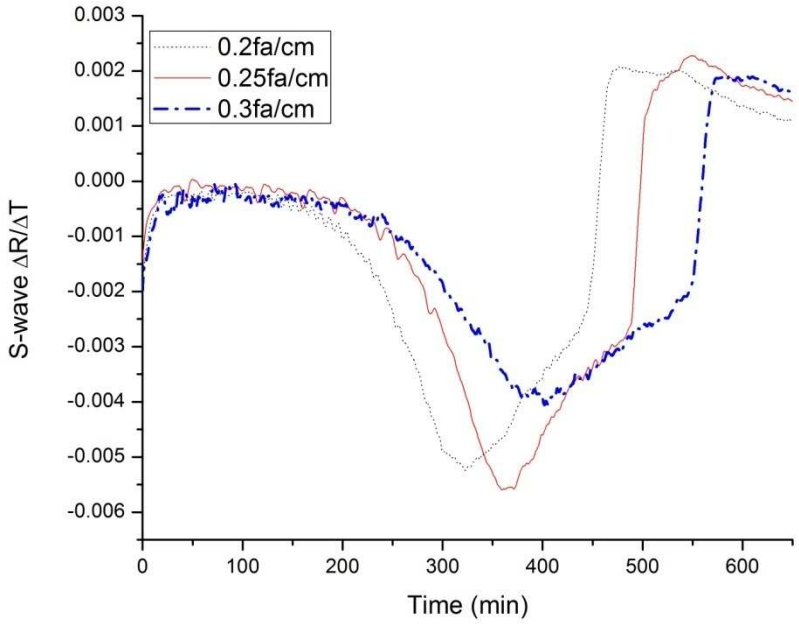

Figure 5.12. $\frac{\Delta R}{\Delta t} - t$ curves for self-compacting pastes with 0.35w/cm, 0.0007sp/cm and differing fa/cm.

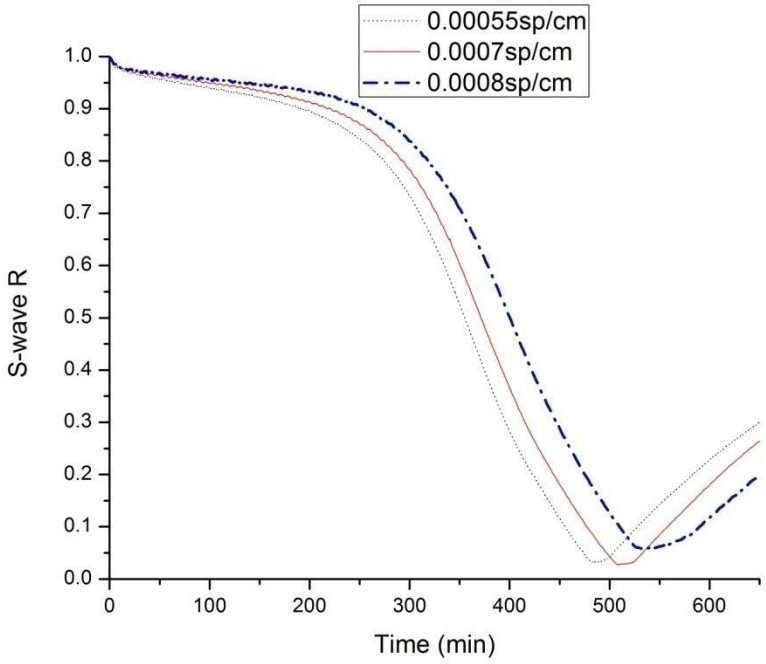

Figure 5.13. R-t curves for self-compacting pastes with 0.33w/cm, 0.3fa/cm and differing sp/cm.

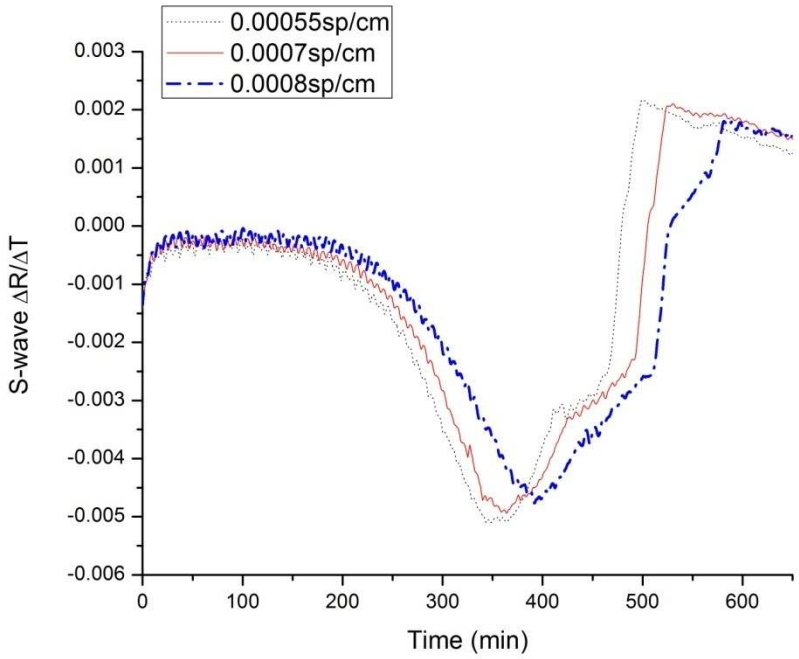

Figure 5.14 $\frac{\Delta R}{\Delta t} - t$ curves for self-compacting pastes with 0.33w/cm, 0.3fa/cm and differing sp/cm.

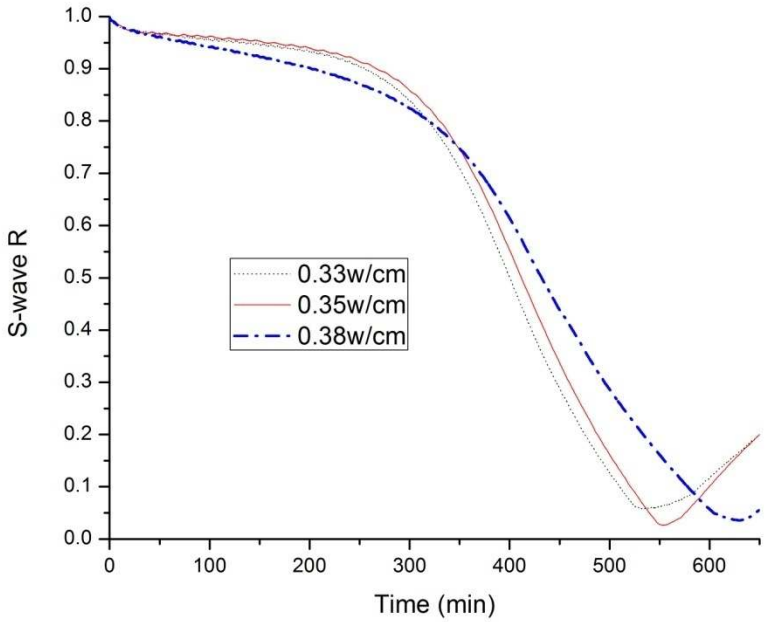

Figure 5.15. R-t curves for self-compacting pastes with 0.0008sp/cm, 0.3fa/cm and differing w/cm.

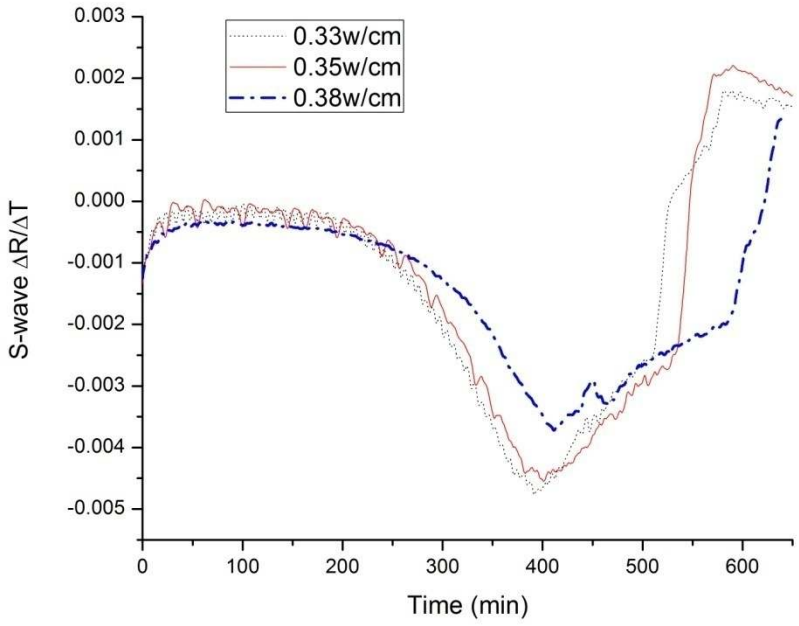

Figure 5.16. $\frac{\Delta R}{\Delta t} - t$ curves for self-compacting pastes with 0.0008sp/cm, 0.3fa/cm and differing w/cm.

Table 5.4. Setting times of various self-compacting pastes.

Mix	Change	Initial set (min)	Final set (min)
0.35w/cm, 0.0007sp/cm, 0.2fa/cm	Increasing fa/cm	252	319
0.35w/cm, 0.0007sp/cm, 0.25fa/cm		300	363
0.35w/cm, 0.0007sp/cm, 0.3fa/cm		288	400
0.33w/cm, 0.00055sp/cm, 0.3fa/cm	Increasing sp/cm	259	342
0.33w/cm, 0.0007sp/cm, 0.3fa/cm		277	353
0.33w/cm, 0.0008sp/cm, 0.3fa/cm		305	390
0.33w/cm, 0.0008sp/cm, 0.3fa/cm	Increasing w/cm	305	390
0.35w/cm, 0.0008sp/cm, 0.3fa/cm		316	396

0.38w/cm, 0.0008sp/cm, 0.3fa/cm		281	408
0.38w/cm, 0.0008sp/cm, 0.3fa/cm	Repeats	275	410
0.38w/cm, 0.0008sp/cm, 0.3fa/cm		281	410
0.38w/cm, 0.0008sp/cm, 0.3fa/cm		296	408

Table 5.4. (cont.) Setting times of various self-compacting pastes.

Set times from penetration resistance and S-wave reflection were compared for various self-compacting pastes (Table 5.5). Figure 5.17 shows a comparison of the setting times. Initial sets from the two methods were not well correlated, but final sets were moderately well correlated. The relationship was linear, though it was considerably off the unity line. In all cases, set times from penetration resistance were much later than those from wave reflection.

Table 5.5. Comparison of S-wave reflection and penetration resistance setting times for self-compacting pastes.

Mix	**IS, SWR**	**IS, PR**	**FS, SWR**	**FS, PR**
0.33w/cm, 0.00055sp/cm, 0.25fa/cm	254	328	335	433
0.33w/cm, 0.00055sp/cm, 0.3fa/cm	259	376	342	459
0.33w/cm, 0.0008sp/cm, 0.3fa/cm	305	381	390	500
0.33w/cm, 0.00055sp/cm, 0.35fa/cm	298	396	395	509
0.33w/cm, 0.0008sp/cm, 0.35fa/cm	303	433	423	557
0.35w/cm, 0.0007sp/cm, 0.20fa/cm	252	382	319	468
0.35w/cm, 0.00055sp/cm, 0.25fa/cm	273	327	330	457
0.35w/cm, 0.0007sp/cm, 0.25fa/cm	300	391	363	474

*IS denotes initial set, FS denotes final set, SWR denotes S-wave reflection, and PR denotes penetration resistance.

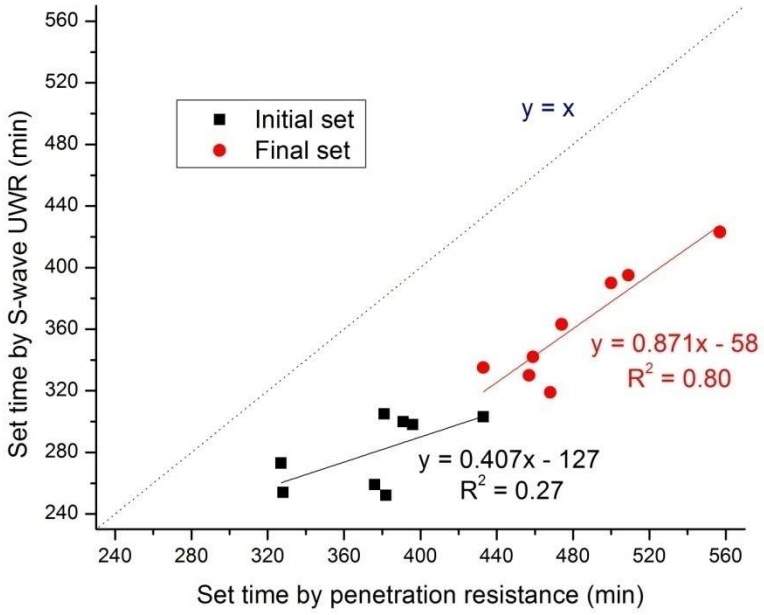

Figure 5.17. Comparison of S-wave reflection and penetration resistance setting times for self-compacting pastes.

5.1.3. Other pastes

Shrinkage reducing admixture, air entraining admixture, and viscosity modifying agent were added to 0.33w/c pastes and their (individual) effect on setting explored. The R-t curves and the $\frac{\Delta R}{\Delta t} - t$ curves for these pastes are shown in Figure 5.18 and Figure 5.19, respectively. The shrinkage reducing admixture showed roughly the same initial set, delayed final set, and slightly higher initial stiffening. The air entraining admixture showed slightly delayed initial and final set. The viscosity modifying agent completely modifies the setting behavior; the R-t curve is almost linear with added viscosity modifying agent. Further experiments need to be done to more fully analyze the effects of these admixtures on hydration and stiffening, but these preliminary results seem to show that S-wave reflection can be used to study such effects.

Research has been done in our laboratory to study the use of bacteria for the development of self-healing concrete. Pastes with bacteria were visually observed to have high initial stiffening and delayed setting times. The R-t curves and the $\frac{\Delta R}{\Delta t} - t$ curves for normal pastes, pastes with nutrient medium, and pastes with nutrient medium and bacteria are shown in Figure 5.20 and Figure 5.21, respectively. The nutrient medium and bacteria each individually caused high initial stiffening and considerably delayed setting (for example, the paste with nutrient medium and bacteria had a final set almost 500 minutes later than the normal paste).

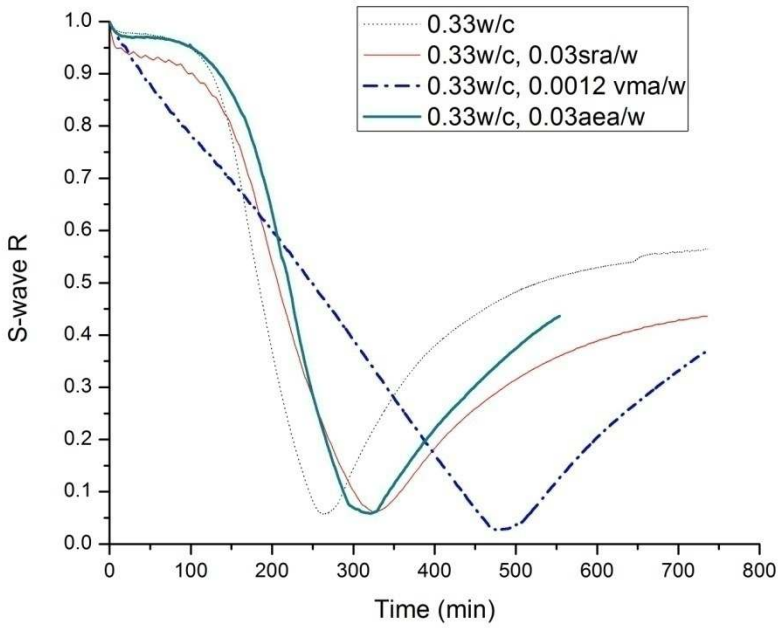

Figure 5.18. R-t curves for pastes with chemical admixtures.

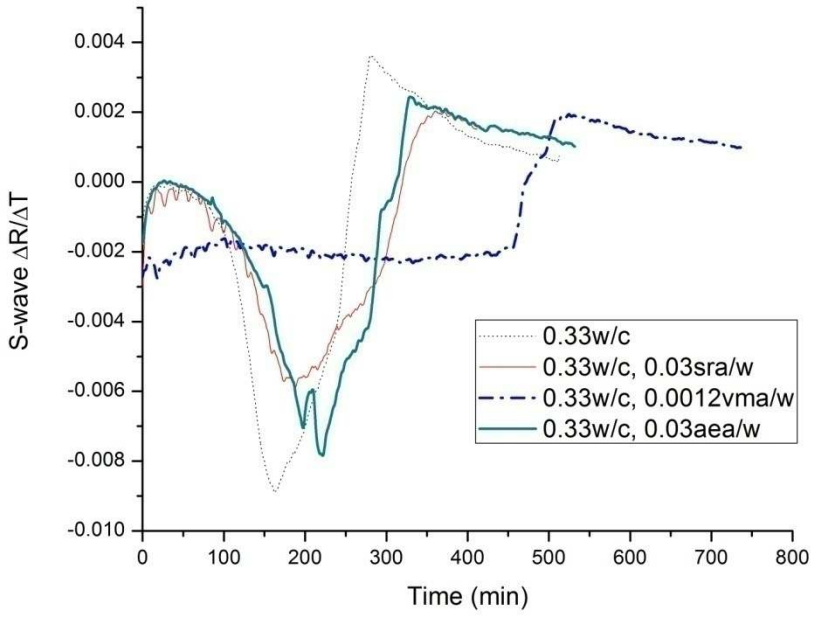

Figure 5.19. $\frac{\Delta R}{\Delta t} - t$ curves for pastes with chemical admixtures.

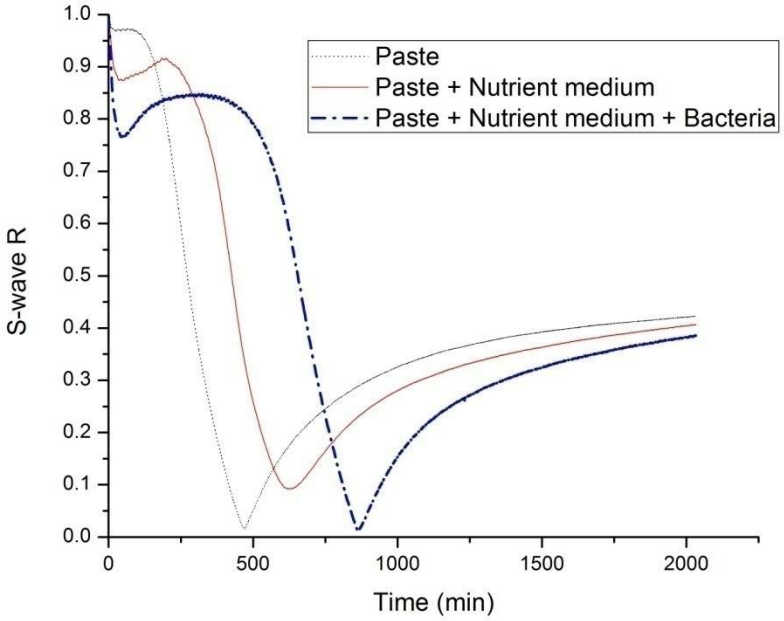

Figure 5.20. R-t curves for pastes with nutrient medium and bacteria.

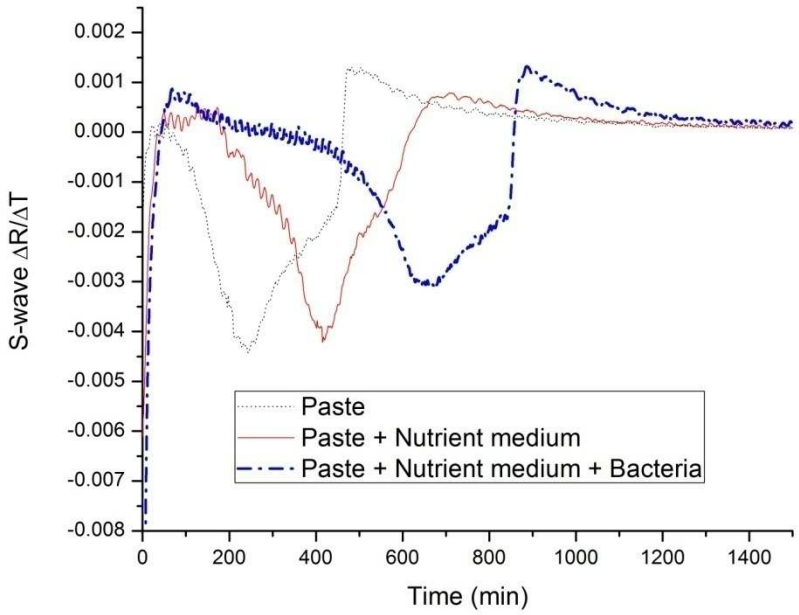

Figure 5.21. $\frac{\Delta R}{\Delta t(t)}$ curves for pastes with nutrient medium and bacteria.

As mentioned in the previous chapter, the fly ash used in the study rapidly stiffened when mixed with water. S-wave reflection was used to study the setting of such mixes. The R-t curves and the $\frac{\Delta R}{\Delta t} - t$ curves for fly ash pastes are shown in Figure 5.22 and Figure 5.23, respectively. There was extremely strong and rapid initial stiffening. For example, the paste with 0.33w/fa showed an initial drop in R of almost 0.95; as opposed to a drop of around 0.05 for normal cement pastes. The extent of stiffening decreased as the w/fa increased, an expected result. The $\frac{\Delta R}{\Delta t} - t$ curves showed that most of the stiffening occurred in the first 50 minutes. The results from S-wave reflection agreed broadly with penetration resistance, which showed rapid stiffening and higher rapid stiffening for lower w/fa values. The continuous data obtained through wave reflection makes it more useful than penetration resistance to study such stiffening.

The results with admixture modified pastes, bacteria modified pastes and fly ash pastes showed that S-wave reflection can be used to study the stiffening characteristics of any modified pastes. The continuous data obtained gives it an advantage over the penetration resistance test which gives only discrete data.

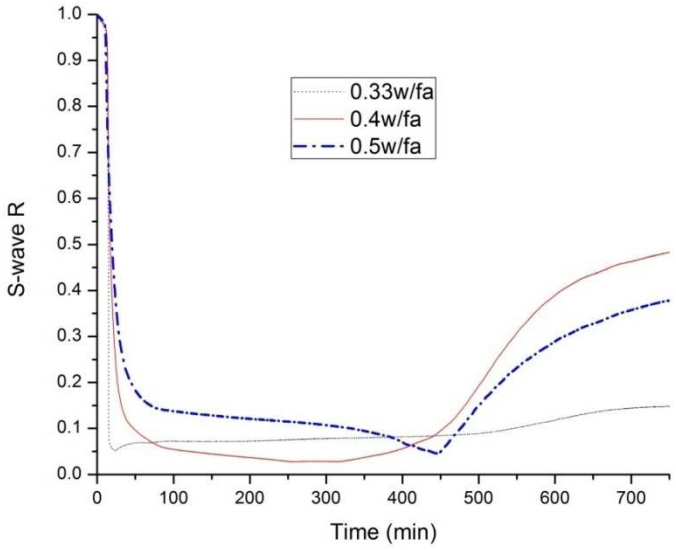

Figure 5.22. R-t curves for fly ash pastes with varying w/fa.

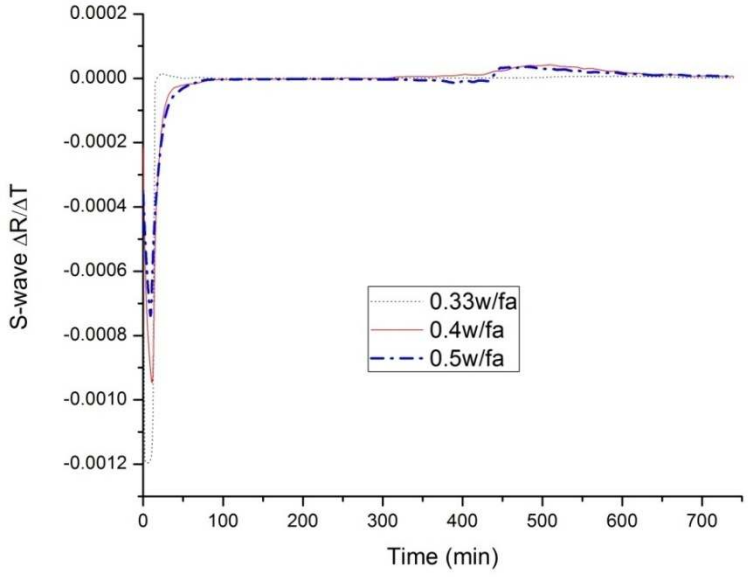

Figure 5.23. $\frac{\Delta R}{\Delta t} - t$ curves for fly ash pastes with varying w/fa.

S-wave reflection on fly ash-slag geopolymers was carried out to study their stiffening characteristics. The R-t curves and $\frac{\Delta R}{\Delta t} - t$ curves for geopolymer pastes are shown in Figure 5.24 and Figure 5.25 respectively. The geopolymers showed higher initial stiffening as compared to cement pastes, but lower later stiffening. The geopolymer without slag did not show significant stiffening. At 5 and 10 % slag levels, R rapidly increased to a value of one at around 550 and 350 minutes respectively. A value of one for R indicated air, and this phenomenon, called debonding, is caused by the pulling away of the paste from the buffer. This occurred due to high shrinkage in these pastes, which was also observed visually. The 15 % slag paste did not show debonding. Set times could not be determined for these pastes using the methods outlined before as the nature of the geopolymer stiffening is different from cement pastes. However, the curves could be compared amongst themselves, and as with admixture modified pastes, S-wave reflection results revealed critical information about setting.

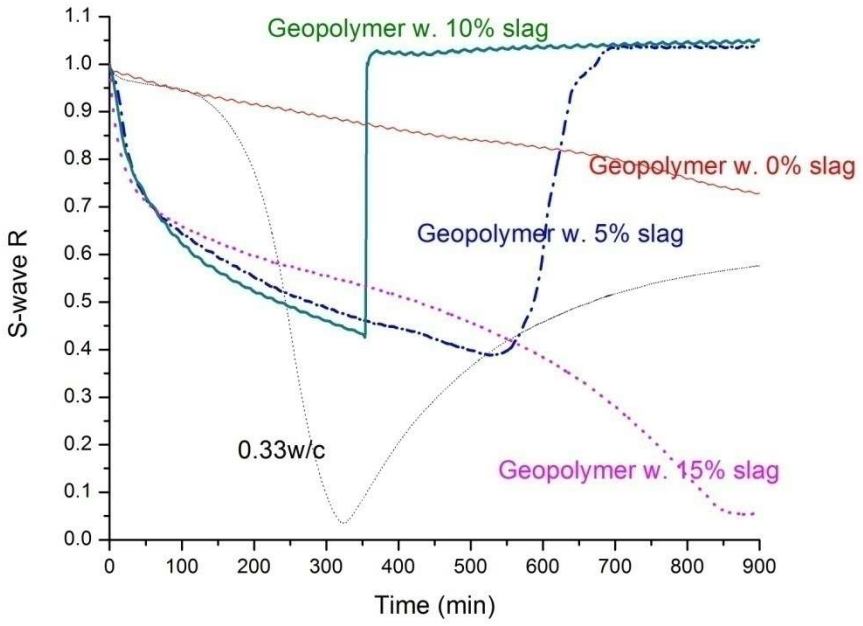

Figure 5.24. R-t curves for geopolymer pastes.

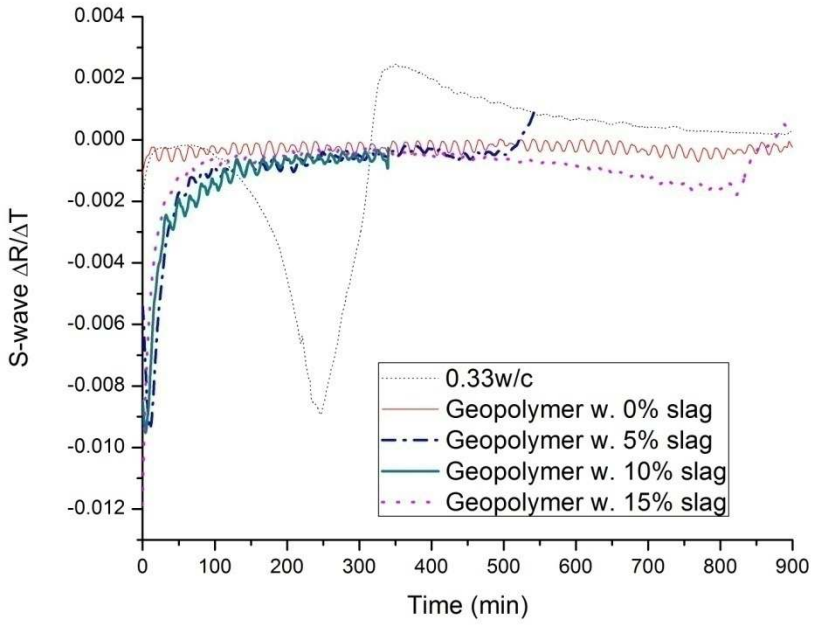

Figure 5.25. $\frac{\Delta R}{\Delta t} - t$ curves for geopolymer pastes.

5.1.4. Curve fitting for S-wave reflection

Curve fitting was done to the S-wave reflection data. An Avrami type curve was fit for the R-t curves. The Avrami fit worked fairly well for a few w/c values, but the fit was not as good for other w/c values. Also, the exact fitting parameters used influenced the quality of the fit very strongly. Hence, this fit was not found to be acceptable. S-wave reflection data were corrected for inversion, by flipping the data after the inversion point around that point. Inversion corrected S-wave R-t curves were found to fit well to a logistic function of the form $y = A_2 + \frac{A_1 - A_2}{1 + (\frac{x}{x0})^p}$. Curves for three pastes were fit using this method, and as can be seen from Figure 5.26, the fits were fairly good. $\frac{\Delta R}{\Delta t} - t$ curves were found and compared with a numerical derivative from the fitted R data, and the two curves agreed well. Results for one paste are shown in Figure 5.27. The final setting times computed from the actual data and the fit data differed on an

average by 3 % for the three pastes tested. The initial set times showed more variation, with the differences being around 11 %. Therefore, the logistic function was in general a good fit for the S-wave reflection data, though the utility of fitting such a complex function is debatable.

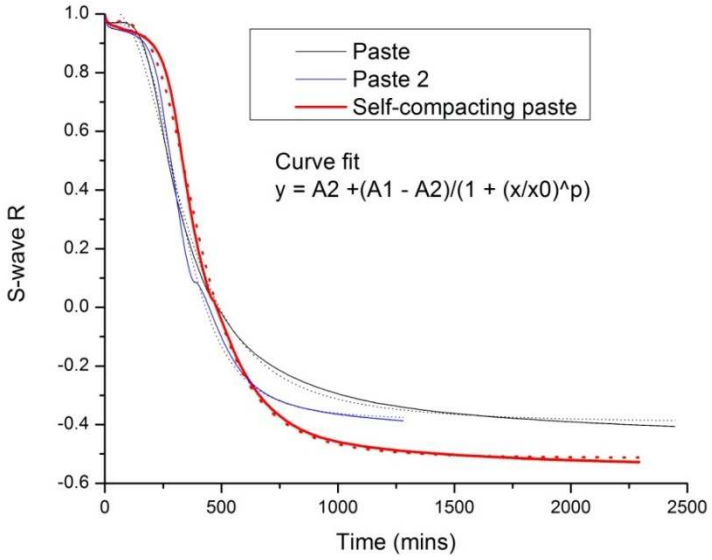

Figure 5.26. Logistic function fit to S-wave R data for three pastes.

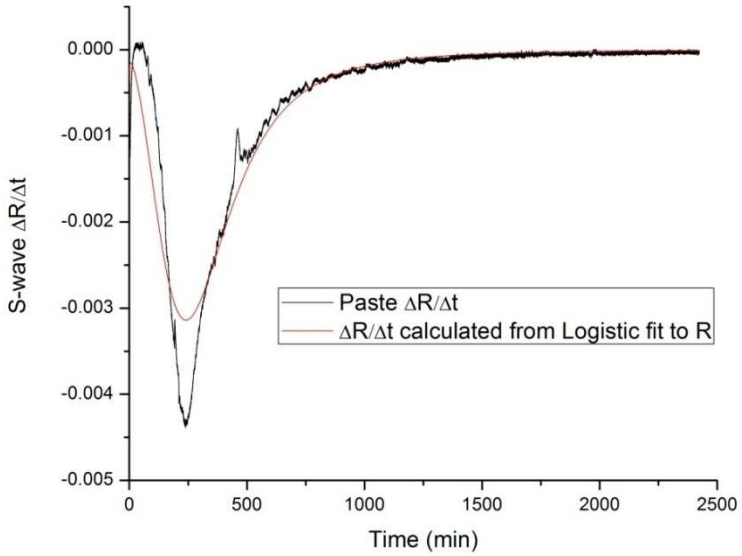

Figure 5.27. Comparison of $\frac{\Delta R}{\Delta t} - t$ curves from R data and $\frac{\Delta R}{\Delta t} - t$ curves from a numerical derivative of the fit data.

5.1.5. Self-compacting concretes

One of the main objectives of this study was to study the adaptability of UWR to concretes. To this effect, S-wave reflection tests were done on several self-compacting concretes with paste compositions which had already been tested. Four trials each of two different self-compacting concretes (Concrete 1 and Concrete 2) were tested. The pastes corresponding to these concretes were 0.33w/cm, 0.0008sp/cm, 0.3fa/cm and 0.38w/cm, 0.0008sp/cm, 0.3fa/cm, respectively. The R-t curves and the $\frac{\Delta R}{\Delta t} - t$ curves for Concrete 1 are shown in Figure 5.28 and Figure 5.29, respectively. The R-t curves and the $\frac{\Delta R}{\Delta t} - t$ curves for Concrete 2 are shown in Figure 5.29 and Figure 5.30, respectively. The paste and concrete results were not very different in terms of the overall shape of the curves. The S-wave reflection response did not seem to depend to a large extent on whether paste or concrete was tested. The setting times are presented in Table 5.6 and statistical parameters are presented in Table 5.7. The coefficient of variation values averaged around 8.1 % for initial set and 5.1 % for final set. The percentage differences in set times between paste and concrete were not very high; they averaged around 10.4 % for initial set and 5.8 % for final set. These numbers indicated that the method is fairly reproducible for concretes, and that paste and concrete setting times are similar, and that S-wave reflection gave more accurate results for final set as compared to initial set. Therefore, we can conclude that S-wave reflection can be used on concretes and that the results are similar to those of pastes.

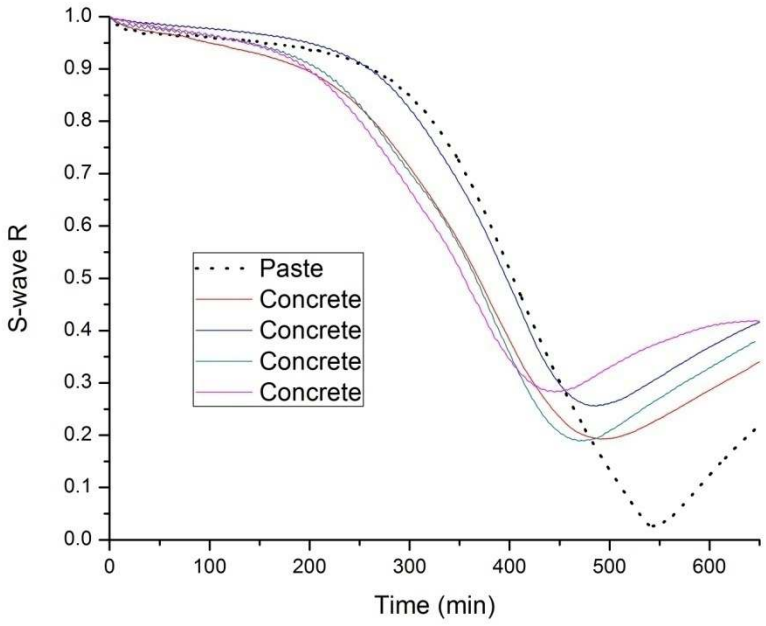

Figure 5.28. R-t curves for a paste and four corresponding concretes (Concrete 1).

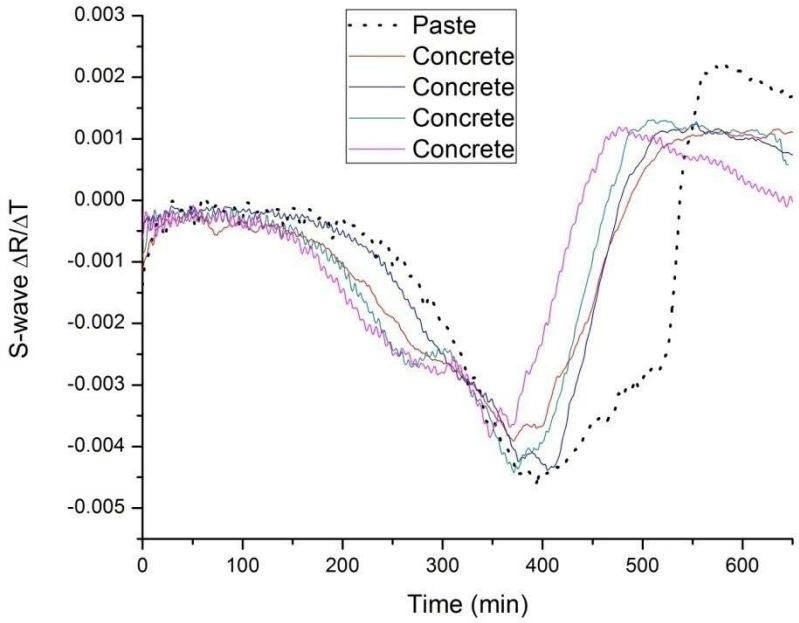

Figure 5.29. $\frac{\Delta R}{\Delta t} - t$ for a paste and four corresponding concretes (Concrete 1).

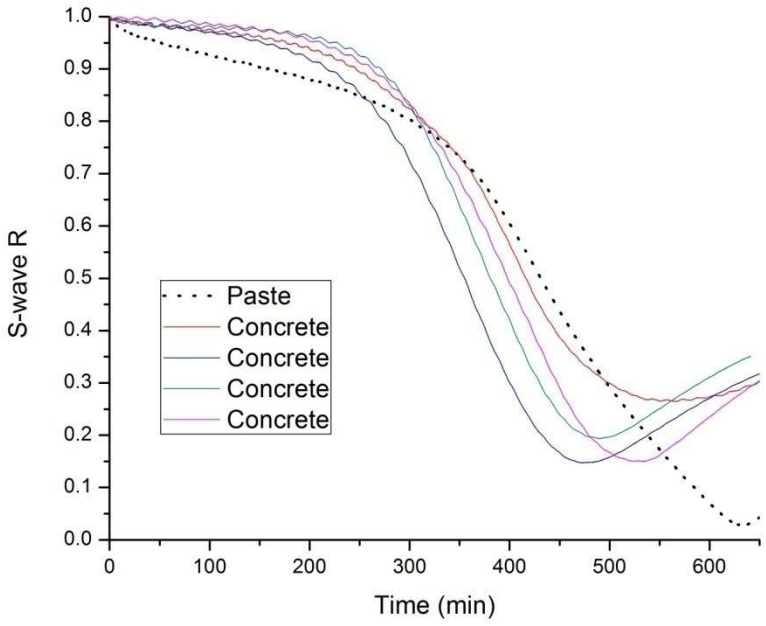

Figure 5.30. R-t curves for a paste and four corresponding concretes (Concrete 2).

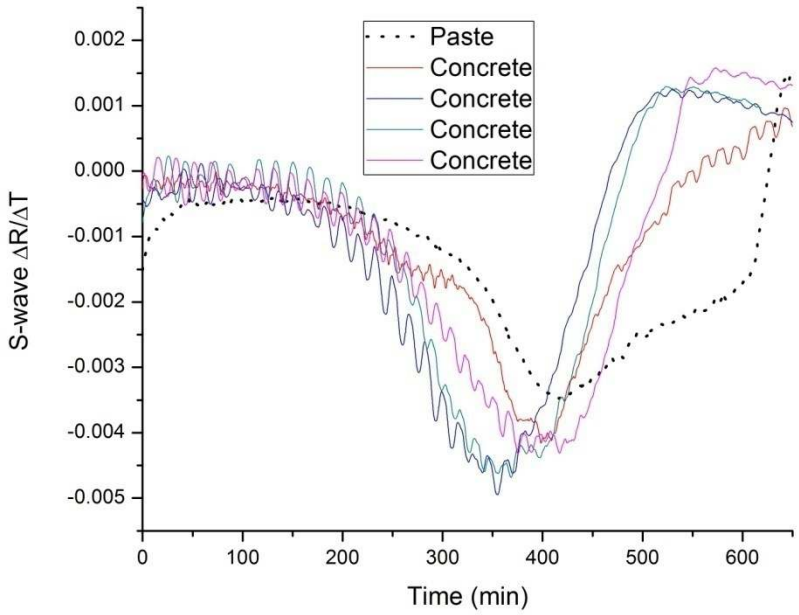

Figure 5.31. $\frac{\Delta R}{\Delta t} - t$ curves for a paste and four corresponding concretes (Concrete 2).

Table 5.6. Setting times of pastes and corresponding concretes

Mix	Initial set (min)	Final set (min)
Paste 1	309	388
Concrete 1	253	371
Concrete 1	303	406
Concrete 1	255	374
Concrete 1	245	357
Paste 2	273	408
Concrete 2	295	394
Concrete 2	263	366
Concrete 2	301	352
Concrete 2	300	374

Table 5.7. Statistical parameters for paste and self-compacting concrete setting times.

Parameter	Initial set	Final set
Paste 1 (min)	309	388
Average, Concrete 1 (min)	264	377
Standard deviation, Concrete 1 (min)	26.36	20.70
Coefficient of variation, Concrete 1 (%)	9.98	5.49
Difference between Paste 1 and Concrete 1 (%)	14.56	2.84
Paste 2 (min)	273	408
Average, Concrete 2 (min)	290	372
Standard deviation, Concrete 2 (min)	18.02	17.54
Coefficient of variation, Concrete 2 (%)	6.22	4.72
Difference between Paste 2 and Concrete 2 (%)	6.23 %	8.82 %

5.2. Conclusions

The following conclusions were drawn from ultrasonic S-wave testing:

1. S-wave reflection on normal and self-compacting cement pastes gave reproducible responses. Initial and final set values showed less than 5 % coefficient of variation values. The coefficient of variation values were higher for initial set than for final set.
2. Initial and final setting times of mixes with varying w/c were clearly different and S-wave reflection can be used to identify changes in w/c. Setting times varied linearly with w/c; the correlation was slightly weaker than for penetration resistance.
3. For normal and self-compacting pastes, final set times from S-wave reflection were linearly related to those from penetration resistance, and correlation was moderately strong. The correlation was stronger for final set than for initial set. For normal pastes, w/c had a stronger effect on penetration resistance than on S-wave reflection. For self-compacting pastes, set times by penetration resistance were higher than by S-wave reflection.
4. Fly ash and superplasticizer act to retard set. Increasing w/cm, fa/cm, and sp/cm caused the R-t curves to shift to the right. Changes in final set were more easily detected than changes in initial set.
5. S-wave reflection can be used to study the effect of various admixtures and additives on cement stiffening including set acceleration, retardation, change in initial stiffening, and rapid stiffening.
6. Stiffening behavior of fly ash pastes and geopolymer pastes was monitored using S-wave reflection; and rapid stiffening and high shrinkage were detected.

7. Avrami curves did not fit well to S-wave R-t data. Complicated logistic functions offered better fits.
8. Self-compacting concretes gave similar R-t responses to corresponding self-compacting pastes. Concrete and paste set times differed by less than 10 %. Coefficient of variation values for concrete set times were less than 8 %.

6. ULTRASONIC LONGITUDINAL WAVE REFLECTION

Ultrasonic studies on cementitious materials have used both shear (S-waves) and longitudinal (P-waves) waves, since there are distinct advantages to using each of the techniques. In this research, both S-wave and P-wave reflection were simultaneously performed, in order to obtain more data, and make the best use of ultrasonic techniques. Though the results are presented in separate chapters, during testing, both S-wave and P-wave transducers were attached to the buffer, and wave reflection data were collected for both simultaneously. Ultrasonic P-wave reflection results are presented in this chapter. Results with normal cement pastes are presented, and the shape of the reflection curve is explained. A method to determine final set using P-wave reflection data is explored. Results with self-compacting pastes are presented. Final set times from P-wave reflection are compared to those from S-wave reflection and from penetration resistance. Results of pastes modified with mineral and chemical admixtures, and geopolymer pastes are presented. Results with self-compacting concretes are also shown, and compared to the results of the corresponding pastes. The phenomenon of partial debonding is discussed.

6.1. Results

6.1.1. Normal cement pastes

It was shown in earlier work in our laboratory that high impact polystyrene (HIPS) was more sensitive to small changes in hydrating cement paste [1]. Hence, all testing in this study was done with HIPS as buffer.

To check reproducibility of the P-wave reflection method, seven trials of the same 0.5w/c paste were performed. The R-t curves of these pastes are shown in Figure 6.1. Though there was some variation in the data, the trials showed very similar response.

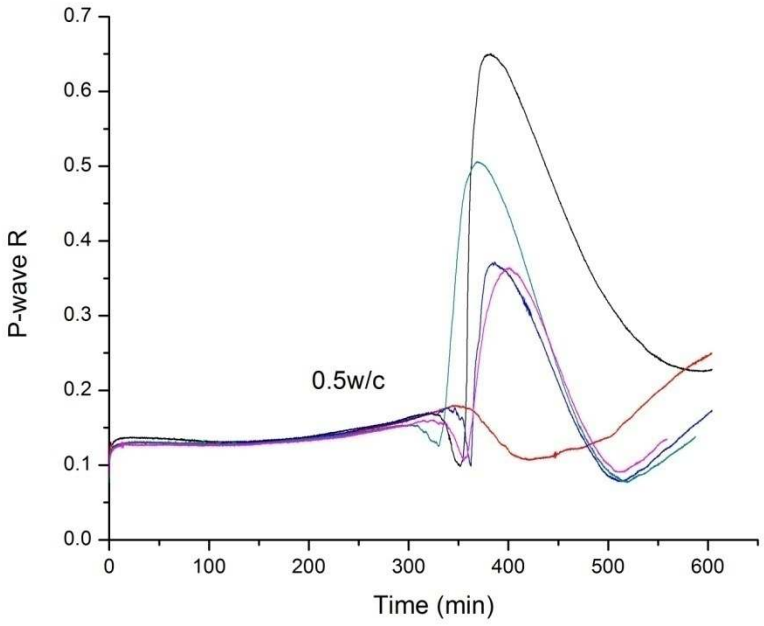

Figure 6.1. R-t curves for five trials of 0.5w/c paste.

The initial reflection value was not one because P-waves pass through fluids, unlike S-waves. For 0.5 w/c pastes, the initial value was around 0.12. There was an initial stable period, in which R increased very gradually with time. At around 300 minutes, the curves showed a response termed "partial debonding", in which the R value suddenly increased and reached a maximum. Often this rapid increase was preceded by a slight dip. The maximum value of R, which ranged from 0.35-0.65, indicates the extent of partial debonding. Partial debonding was presumed to be caused by partial loss of contact of the cement paste with the buffer material which resulted in air replacing some of the cement paste at the interface (debonding is only partial because complete loss of contact would mean only air present at the interface, which gives a R value of one). After reaching its maximum, the R value decreased until it reached a minimum (which appeared to be an inversion), and then increased again. The decrease and subsequent increase was attributed to gradual recovery of contact between the buffer and cement

paste. A more detailed analysis of the shape of the curve and partial debonding is presented towards the end of this chapter.

Tests were done on pastes with w/c values of 0.35, 0.4, 0.5, and 0.6, which were the same w/c values on which penetration resistance tests were done. The R-t curves are presented in Figure 6.2. The curves shifted to the right with higher w/c, similar to S-wave R-t curves. Partial debonding was seen for the three lower w/c pastes, but not for 0.6 w/c paste. For the pastes which showed partial debonding, the onset of partial debonding, that is, the time at which the R values started to dip from their initial stable values, occurred at roughly the same time as final set obtained from the S-wave inflection point, and was therefore considered final set from P-wave reflection. The onset of partial debonding increased as the w/c increased. The exact time at which this decrease occurred was somewhat uncertain, and therefore difficult to accurately determine, and hence, the time of the first minimum after the curve started to drop was used as final set from P-wave reflection. Sometimes, the curves did not show a drop, and directly increased. In these cases, the time when this increase occurred was estimated and used as final set. Final set times from P-wave reflection were roughly 240, 265, and 335 minutes for the 0.35, 0.4, and 0.5 w/c pastes respectively. These values matched fairly closely with the S-wave reflection final set times of 250, 291, and 327 minutes for 0.35, 0.4, and 0.5 w/c pastes. The initial value of R decreased with increasing w/c. A strong linear correlation was seen when the value of R at 30 minutes was plotted against w/c [1]. This correlation is presumed to be caused by w/c determining density, and density controlling the R value.

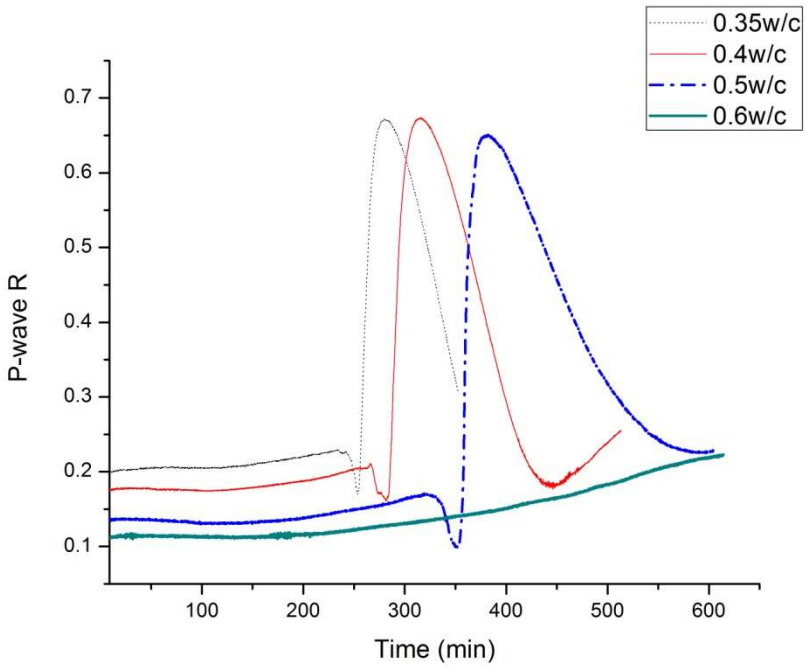

Figure 6.2. R-t curves for pastes with varying w/c.

6.1.2. Self-compacting pastes

The R-t curves for 0.33w/c pastes with fly ash and 0.33w/c pastes with superplasticizer are shown in Figure 6.3. Both fly ash and superplasticizer these considerably retard set (the onset on partial debonding increases) in the dosages used, which is the same result as obtained from penetration resistance and S-wave reflection.

Reproducibility of the method with self-compacting pastes was checked by testing three trials of a mix with the composition 0.38w/cm, 0.0008sp/cm, 0.3fa/cm. The R-t curves are presented in Figure 6.4. The three curves were very similar, especially before partial debonding occurred. Final set times were computed, and are presented in Table 6.1. The standard deviation was around 1.2 minutes and the coefficient of variation was 0.3 % which indicated very good reproducibility. Final set times from P-wave and S-wave reflection were almost the same; the difference in times was less than 3 %.

To see if the method could be used to differentiate between self-compacting pastes of different compositions, pastes with different sp/cm, fa/cm, and w/cm were tested. The R-t curves for pastes with differing fa/cm but the same w/cm and sp/cm are shown in Figure 6.5. The R-t curves for pastes with differing sp/cm but the same w/cm and fa/cm are shown in Figure 6.6. The R-t curves for pastes with differing w/cm but the same sp/cm and fa/cm are shown in Figure 6.7. No clear trend in the initial R value was seen with changes in w/cm, fa/cm, and sp/cm, however, in general, higher w/cm, fa/cm, and sp/cm led to the curves and the onset of partial debonding shifting to the right, indicating higher setting times. The method clearly distinguished the different mixes tested with respect to final set (Table 6.1).

Because of the approximations made in determining final set from P-wave reflection, the time was not extremely accurate. However, even with these approximations, the values of final set from S-wave reflection and P-wave reflection matched each other well. For all mixes tested, the values were within 5 % of each other. The S-wave and P-wave final set times for sixteen self-compacting pastes were plotted against each other (Figure 6.8). Final set times determined by S-wave and P-wave reflection were about the same. The correlation was moderately strong, and may have been higher but for a few outliers.

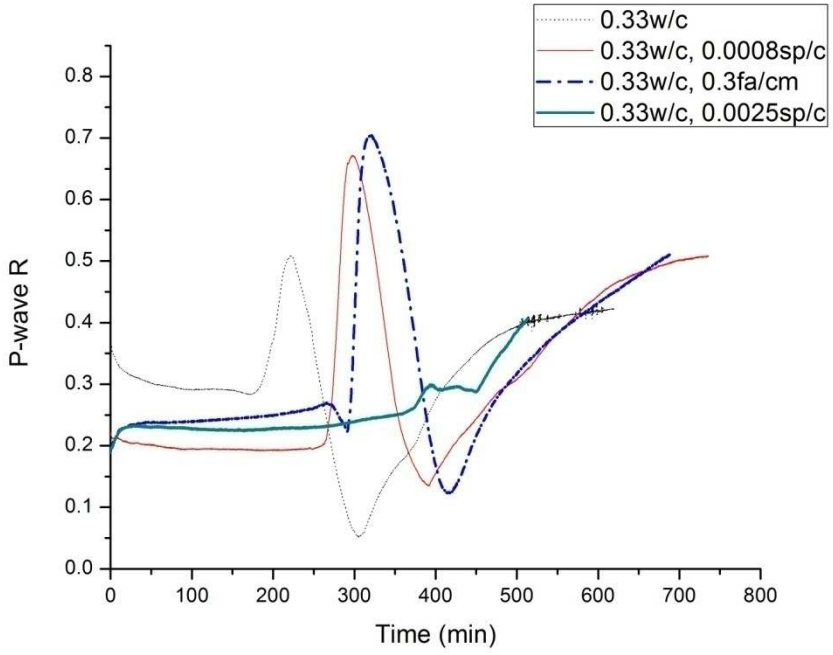

Figure 6.3. R-t curves for pastes with fly ash and pastes with superplasticizer.

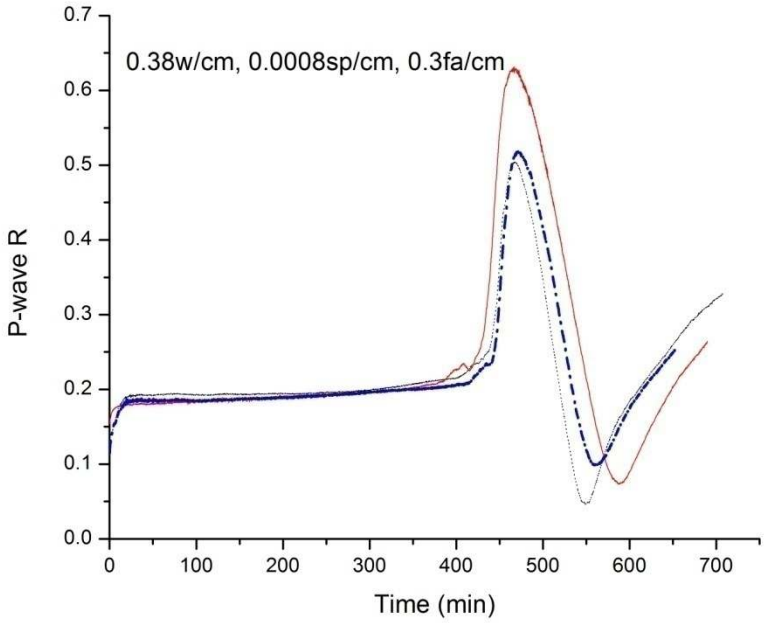

Figure 6.4. R-t curves for three trials of one self-compacting paste mix.

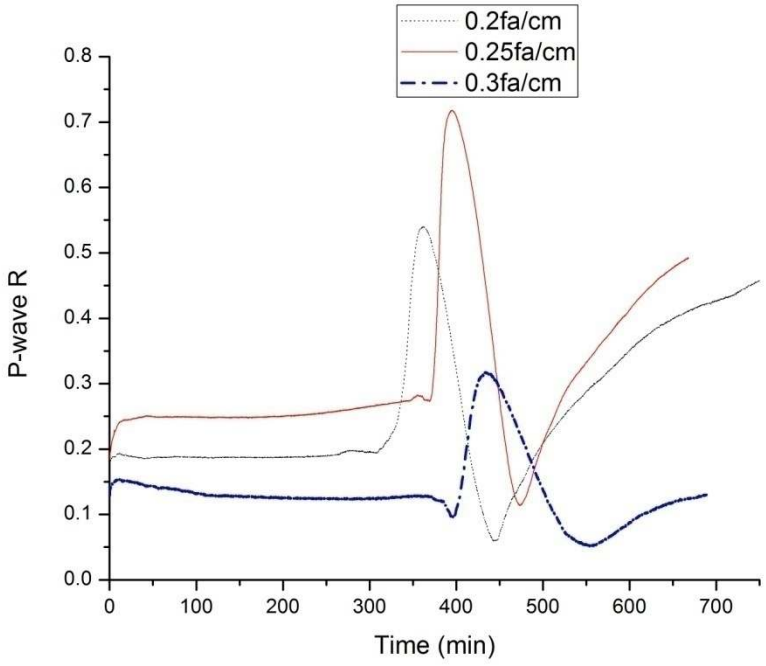

Figure 6.5. R-t curves for self-compacting pastes with 0.35w/cm, 0.0007sp/cm and differing fa/cm.

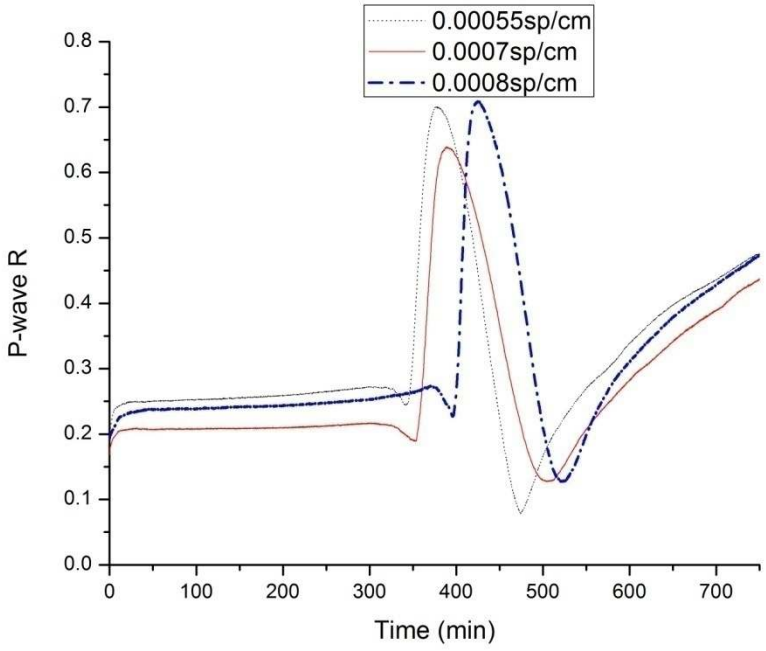

Figure 6.6. R-t curves for self-compacting pastes with 0.33w/cm, 0.3fa/cm and differing sp/cm.

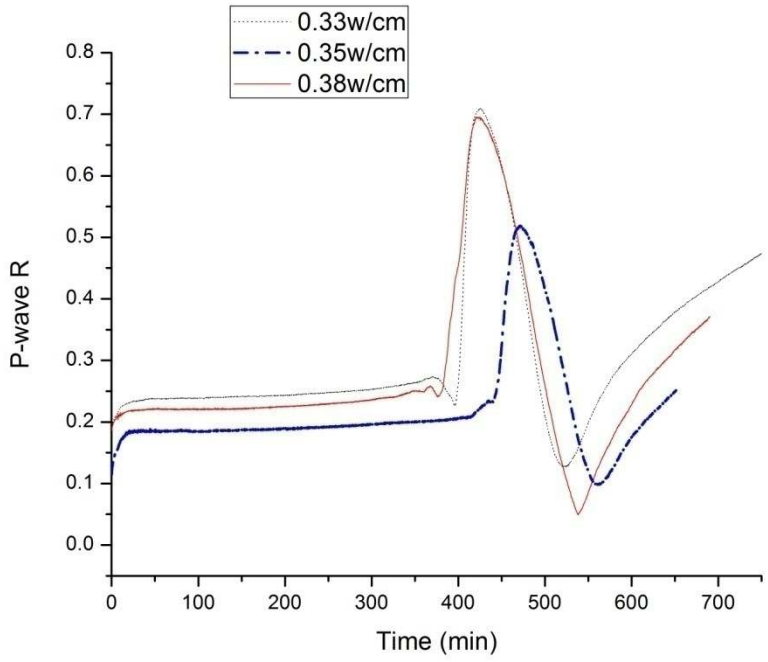

Figure 6.7. R-t curves for self-compacting pastes with 0.0008sp/cm, 0.3fa/cm and differing w/cm.

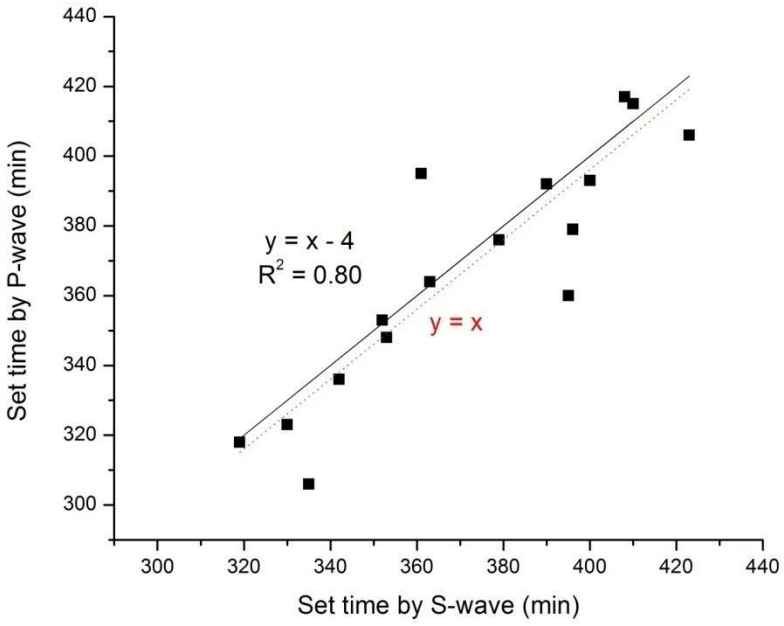

Figure 6.8. Comparison of final set times from S-wave and P-wave reflection.

Table 6.1. Final set times of various self-compacting pastes from S-wave and P-wave reflection.

Mix	Change	P-wave (min)	S-wave (min)
0.35w/cm, 0.0007sp/cm, 0.2fa/cm	Increasing fa/cm	318	319
0.35w/cm, 0.0007sp/cm, 0.25fa/cm		364	363
0.35w/cm, 0.0007sp/cm, 0.3fa/cm		393	400
0.33w/cm, 0.00055sp/cm, 0.3fa/cm	Increasing sp/cm	336	342
0.33w/cm, 0.0007sp/cm, 0.3fa/cm		336	353
0.33w/cm, 0.0008sp/cm, 0.3fa/cm		392	390
0.33w/cm, 0.0008sp/cm, 0.3fa/cm	Increasing w/cm	392	390
0.35w/cm, 0.0008sp/cm, 0.3fa/cm		379	396
0.38w/cm, 0.0008sp/cm, 0.3fa/cm		417	410
0.38w/cm, 0.0008sp/cm, 0.3fa/cm	Repeats	415	410
0.38w/cm, 0.0008sp/cm, 0.3fa/cm		417	410
0.38w/cm, 0.0008sp/cm, 0.3fa/cm		417	408

Penetration resistance, S-wave, and P-wave reflection final set times are compared for various self-compacting pastes in Table 6.2 and Figure 6.9. The final sets from UWR were moderately correlated with those from penetration resistance. The relationships were linear; though considerably off from the unity line. In all cases, set times from penetration resistance were much later than those from UWR. The relationship between P-wave final set time and penetration resistance was very similar to that between S-wave setting time and penetration resistance.

Table 6.2. Comparison of final set times of self-compacting pastes from UWR and penetration resistance.

Mix	P-wave (min)	S-wave (min)	Penetration (min)
0.33w/cm, 0.00055sp/cm, 0.25fa/cm	306	335	433
0.33w/cm, 0.00055sp/cm, 0.3fa/cm	336	342	459
0.33w/cm, 0.0008sp/cm, 0.3fa/cm	392	390	500
0.33w/cm, 0.00055sp/cm, 0.35fa/cm	379	395	509
0.33w/cm, 0.0008sp/cm, 0.35fa/cm	406	423	557
0.35w/cm, 0.0007sp/cm, 0.2fa/cm	318	319	468
0.35w/cm, 0.00055sp/cm, 0.25fa/cm	323	330	457
0.35w/cm, 0.0007sp/cm, 0.25fa/cm	364	363	474

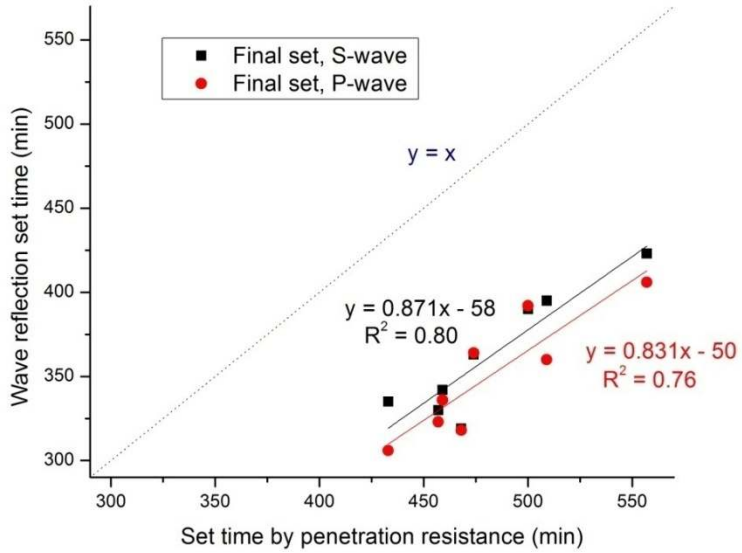

Figure 6.9. Comparison of final set times of self-compacting pastes from UWR and penetration resistance.

6.1.3. Other pastes

P-wave reflection was done on pastes modified with chemical admixtures to study the effect of these admixtures on stiffening. Shrinkage reducing admixture, air entraining agent, and viscosity modifying agent were added to 0.33w/c pastes. The R-t curves for pastes with these admixtures are shown in Figure 6.10. Shrinkage reducing admixture showed roughly the same final set, and higher extent of partial debonding. Air entraining agent showed a completely different response, with R starting from 0.8 and then decreasing with time. This response was attributed to air at the interface, which was detected by the P-wave (like during partial debonding). The viscosity modifying agent seemed to completely modify the stiffening, with the shape of the R-t curve resembling a broad hump. Some of the results obtained were similar to those from S-wave reflection, but some additional information was also obtained (as with air entraining agent). Further experiments need to be done to better understand the effects of these admixtures on stiffening, but these results show that UWR can be used to analyze such effects, and that using both S-wave and P-wave reflection gave more comprehensive results.

P-wave reflection on fly ash-slag based geopolymers was carried out to study their stiffening. The R-t curves are shown in Figure 6.11. The pastes with 5 and 10 % slag content showed full debonding. Data obtained after full debonding was useless, since the value is then simply that of air at the interface (R = 1). The paste without slag did not show significant stiffening, as its R value remained roughly constant with time. The 15 % slag mix did not show full debonding. The geopolymers showed similar results with both P-wave and S-wave reflection. Set times could not be determined for these pastes using the methods outlined before, as the nature of stiffening was different, but the geopolymers could be compared amongst themselves using UWR. Wave reflection results revealed critical information about setting, and

using both S-wave and P-wave gave complimentary information. These results show that UWR can be used to study the stiffening characteristics of any pastes which harden with time. The continuous data obtained gives it an advantage over the discrete data from penetration resistance.

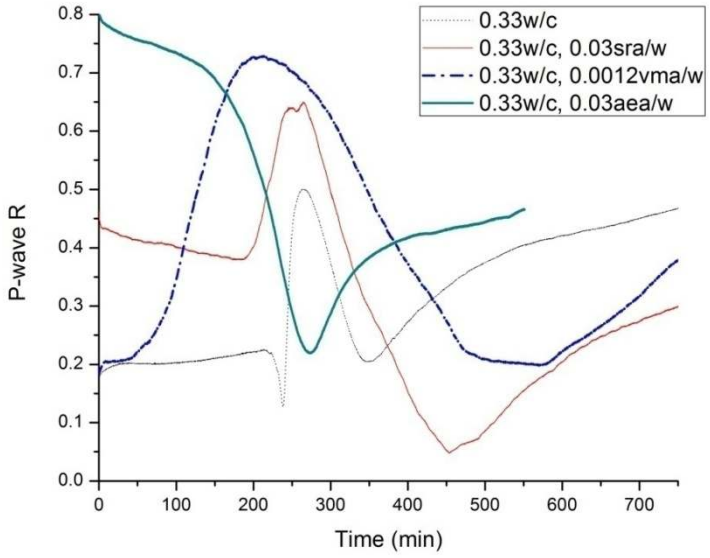

Figure 6.10. R-t curves for pastes with admixtures.

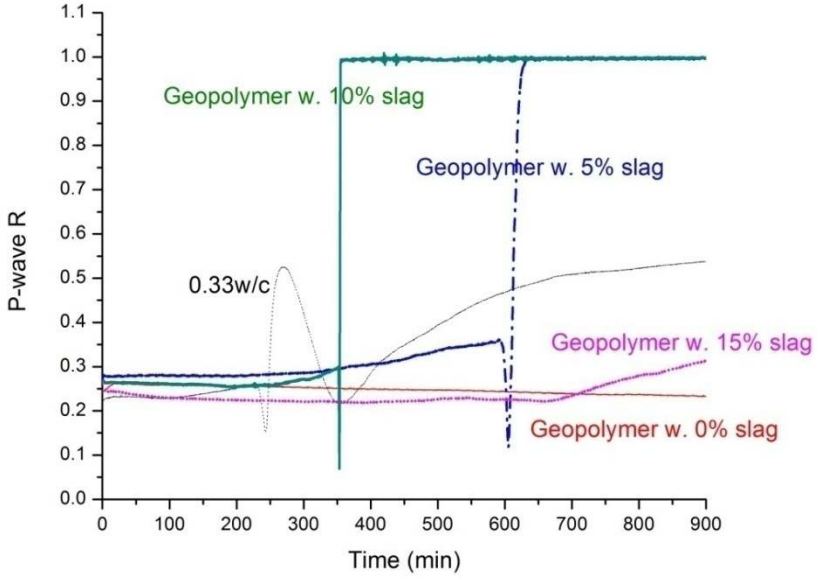

Figure 6.11. R-t curves for geopolymer pastes.

6.1.4. Self-compacting concretes

P-wave reflection tests were done on several self-compacting concretes with paste compositions which had already been tested. Four trials each of two different self-compacting concretes were tested (Concrete 1 and Concrete 2). The R-t curves for the first paste and its corresponding concretes are shown in Figure 6.12. The R-t curves for the second paste and its corresponding concretes are shown in Figure 6.13. The time at which partial debonding occurred was roughly the same for paste and the concretes, though the exact shape of the curves, and the extent of partial debonding varied. Some of the concrete curves were similar to the paste curves, whereas others seemed to be a flipped over version of the paste curves. These differences and variations were probably due to aggregate in the concrete. Presence of different amounts of aggregate at the buffer interface may change the value of concrete acoustic impedance, and thus lead to different R-t curves.

Setting times for concrete were determined. The setting times are shown in Table 6.3 and averages and statistical parameters are shown in Table 6.4. The coefficient of variation values for concrete averaged around 6 % for P-wave final set, and 5 % for S-wave final set. These numbers indicated that UWR was reproducible for final set. The percentage differences between paste and concrete final set times averaged 2.8 % for P-wave reflection and 5.8 % for S-wave reflection. The differences were low, and therefore, paste and concrete had similar final set times, and P-wave reflection showed marginally more similar final set times for paste and concretes than S-wave reflection. From these results, it can be seen that UWR can be used on concretes, and that the results are fairly reproducible, and the final set times are not very different from those of the corresponding pastes.

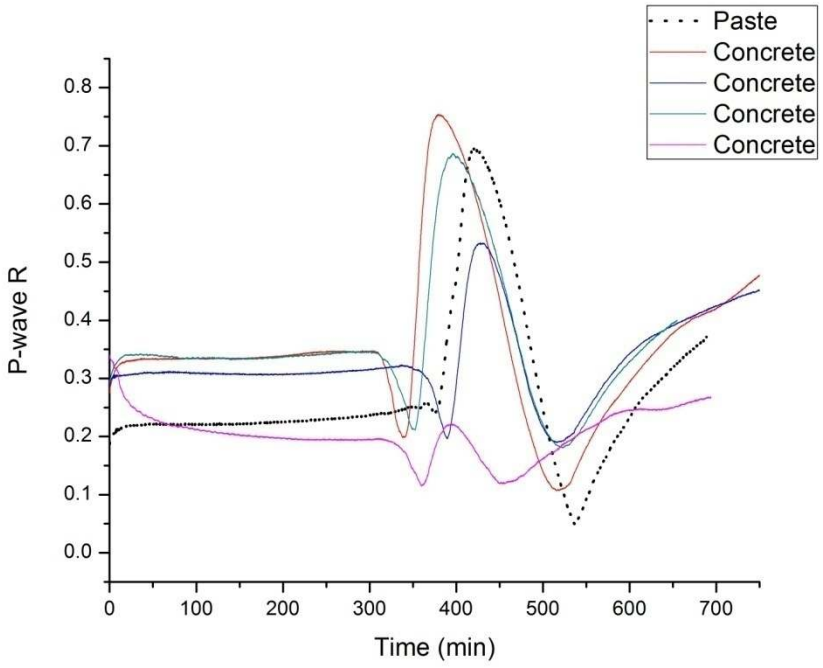

Figure 6.12. R-t curves for a paste and four corresponding concretes (Concrete 1).

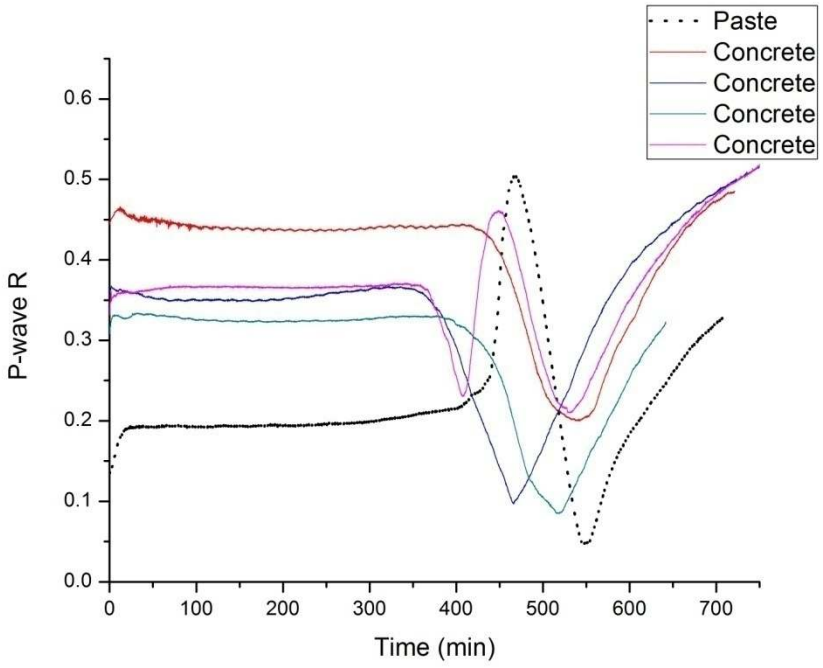

Figure 6.13. R-t curves for a paste and four corresponding concretes (Concrete 2).

Table 6.3. Setting times of self-compacting pastes and corresponding concretes.

Mix	P-wave (min)	S-wave (min)
Paste 1	363	388
Concrete 1	336	371
Concrete 1	380	406
Concrete 1	346	374
Concrete 1	363	357
Paste 2	404	408
Concrete 2	406	394
Concrete 2	395	366
Concrete 2	352	352
Concrete 2	403	374

Table 6.4. Statistical parameters for setting times of self-compacting paste and corresponding concretes.

Parameters for Final Set	P-wave	S-wave
Paste 1 (min)	363	388
Average, Concrete 1 (min)	356	377
Standard deviation, Concrete 1 (min)	19.36	20.70
Coefficient of variation, Concrete 1 (%)	5.44	5.49
Difference between Paste 1 and Concrete 1 (%)	1.86	2.84
Paste 2 (min)	404	408
Average, Concrete 2 (min)	389	372

Standard deviation, Concrete 2 (min)	25.10	17.54
Coefficient of variation, Concrete 2 (%)	6.45	4.72
Difference between Paste 2 and Concrete 2 (%)	3.71	8.82

Table 6.4. (cont.) Statistical parameters for setting times of self-compacting paste and corresponding concretes.

6.1.5. Partial debonding

The phenomenon of partial debonding in P-wave reflection is explained in some detail below. The three important characteristics of partial debonding are the time of debonding, the extent of debonding, and whether or not recovery occurred. Full debonding was seen in both P- and S-wave reflection for geopolymers, but cement pastes only showed partial debonding with P-wave reflection. Cement pastes did not show partial debonding with S-wave reflection. Partial debonding was always associated with recovery; no recovery was seen after full debonding. The value of R became 1 after full debonding, and this was because the cement paste at the interface was completely replaced by air. Geopolymers showed high shrinkage, so it made sense that the debonding was at least partially due to shrinkage. The time of debonding varied depending on the paste tested, but this time was roughly the same as final set for all pastes tested.

When paste is fluid, the autogenous shrinkage (the volume change when there is no moisture movement into or out of the specimen) is the same as the chemical shrinkage (the internal volume change because the volume of hydration products is smaller than the volume of reactants). Autogenous and chemical shrinkage deviate from each other with progressive hydration. Previous research [26] showed that the autogenous shrinkage substantially deviated from chemical shrinkage at final set. Near final set, the solid particles in the paste impinge on

one another and this causes an underpressure to develop in the paste. This underpressure is possibly caused by shrinkage promoting suction of moisture to fill the spaces produced by hydration. The underpressure results in a three dimensional volume change and draws water into the interior of the paste. Therefore, the contact between the sample and the buffer is reduced, and partial debonding is observed.

P-wave partial debonding was not affected by the addition of a shrinkage reducing admixture (Figure 6.10), and it is unclear why this was so. The debonding was considerably reduced by addition of excessive superplasticizer (Figure 6.9). Cement paste with high w/c did not show partial debonding (Figure 6.2). Since the superplasticizer allows for a dispersed system and thereby more available free water in the system and the high w/c paste naturally has more free water available, it was postulated that the partial debonding was controlled by the presence of water.

Tests were run with water ponded on top of 0.33w/c pastes. The results are shown in Figure 6.14 and no partial debonding was seen in the two trials with ponded water. These results indicated that the partial debonding occurred at the time of final set due to the partial removal of water from the paste-buffer interface, presumably due to autogenous shrinkage. The addition of ponded water on top of the paste provided a reservoir of additional water on top and reduced the autogenous shrinkage and prevented the partial debonding.

Based on the hypothesis of partial debonding, the shape of the curve was analyzed (Figure 6.15). The P-wave reflection curve was divided into four stages–Stage 1 was the initial stable region, Stage 2 was the region from the onset of partial debonding to where R reached its maximum, Stage 3 from the maximum to the next minimum, and Stage 4 from the minimum onwards. In Stage 1, cement paste was in contact with the buffer. Partial debonding started at the

onset of Stage 2, when water was driven away, and some of the paste was replaced by air at the interface. R was reduced, since the cement paste was replaced by air, which had lower acoustic impedance. R decreased until it reached a local minimum and then it increased. Since debonding was clearly not complete at this point, a reasonable way to explain this minimum was that it was an inversion–the acoustic impedance of the paste in contact with the buffer, which was originally higher than the buffer, was now lower than the buffer, due to replacement by air. The acoustic impedance of the paste further decreased, below the buffer acoustic impedance, and this led to an increase in R (R changes direction at inversion). R increased until it reached a maximum, the end of the partial debonding. There was a subsequent decrease in R after the maximum, which is due to recovery, that is, the air was replaced by paste or water. This happened in Stage 3 and R decreased. It was not clear what caused recovery, but it may be due to the effect of gravity and stiffening due to deposition of hydration products in the air gaps or due to the movement of water into the gap. R reached a minimum at the end of Stage 3, which was another inversion, which occurred because the acoustic impedance of the paste at the interface, which was previously lesser than the buffer increased due to recovery and was equal to that of the buffer. Recovery and stiffening progressed in Stage 4 and R gradually increased with continuing hydration. Stage 3 and Stage 4 were not fundamentally different, and recovery took place in both these stages.

Time domain data, which showed the number of reflected waves and their amplitude, was collected in the four stages to understand what was happening at the interface during partial debonding (Figure 6.16). The number of reflected waves is directly proportional to the difference in acoustic impedance–more reflected waves are seen when a wave goes from a medium of very high (low) acoustic impedance to one of very low (high) acoustic impedance. Air has very low

acoustic impedance, and shows seven reflected waves at the air-buffer interface. In stage 1, the acoustic impedances of the paste and buffer were similar and there was only one reflected wave. As partial debonding progressed (stage 2), the number of reflected waves increased fairly rapidly from one to four, with four reflected waves being seen at the maximum. During stage 3, recovery, the number of reflected waves decreased fairly rapidly from four to one. An inversion occurred at this point, and then the number of reflected waves increased gradually and progressively to four after three to five days. The sudden increase in the number of reflected waves during partial debonding clearly indicated that paste was partially removed and air was introduced at the interface. This air was consequently replaced by paste during recovery.

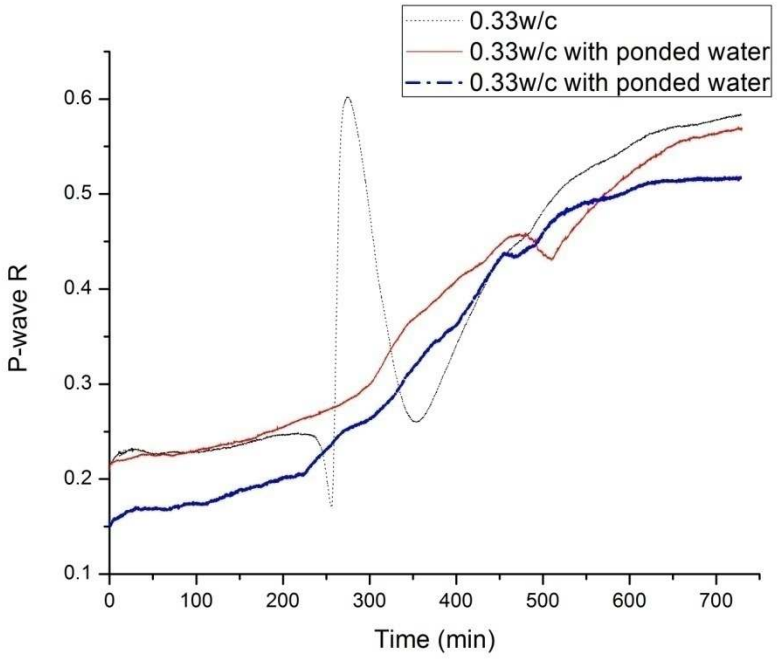

Figure 6.14. Effect of ponded water on partial debonding.

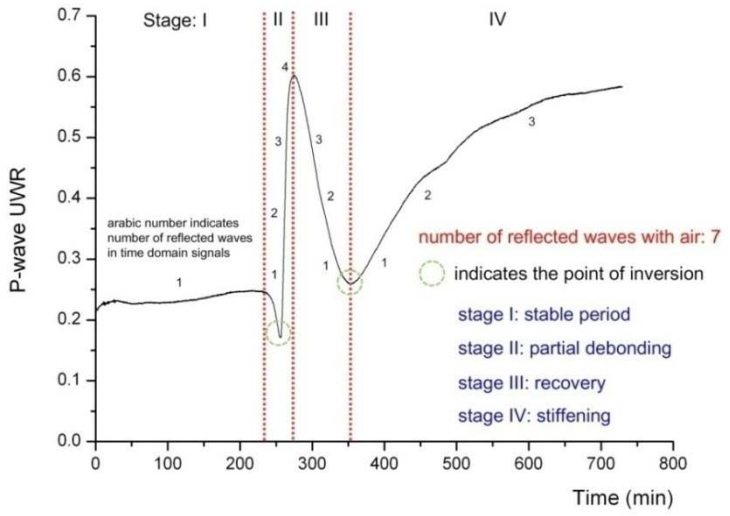

Figure 6.15. R-t curve for 0.33 w/c cement paste showing different stages in the curve. The Arabic numbers in the Figure indicates the number of reflected waves in time domain signals.

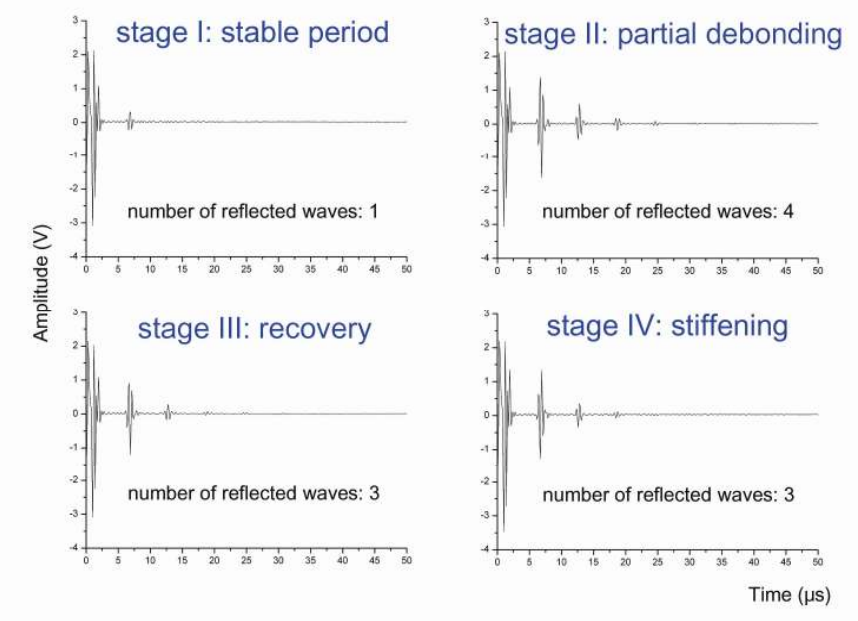

Figure 6.16. The time domain signals from various stages shown in Figure 6.15.

6.2. Conclusions

The following conclusions were drawn from ultrasonic P-wave testing:

1. Final set was found as the time of onset of partial debonding.

2. P-wave reflection on normal and self-compacting cement paste gave reproducible responses, especially before partial debonding. Coefficient of variation values were less than 1 %.
3. Final setting times of mixes with varying w/c were different and P-wave reflection can be used to identify changes in w/c. Final setting times varied linearly with w/c. Final set times for normal and self-compacting pastes with S-wave and P-wave reflection were similar.
4. For normal and self-compacting pastes, final set times from P-wave reflection were linearly related to those from penetration resistance; correlation was moderately strong.
5. Fly ash and superplasticizer act to retard set. Increasing w/cm, fa/cm, and sp/cm caused the R-t curves to shift to the right.
6. P-wave reflection can be used to find the effect of various admixtures and additives on stiffening including set acceleration, retardation, and change in extent of partial debonding. Entrained air was easily detected using P-wave reflection. Stiffening behavior of geopolymer pastes was monitored; high shrinkage was detected.
7. Response of self-compacting concretes was fairly similar to those of corresponding pastes; however, the curves seemed to be flipped over in some cases. Final set times were found and they differed from paste set times by less than 6 %. Coefficient of variation values for concrete final set times were less than 6 %.
8. Partial debonding is probably caused by autogenous shrinkage at final set. Partial debonding was controlled by water; the response was not seen when there was excess free water in the system. Time domain data were used to explain the changes occurring in the paste during partial debonding.

7. INSTRUMENTATION EFFECTS

In this chapter, instrumentation effects on S-wave and P-wave reflection results are explored. The work presented in previous chapters largely focused on changes in the material being tested, but various settings of the pulser-receiver units and other equipment parameters can potentially lead to differences in results obtained. To verify if the observed response of the cement paste was an actual response of the paste itself or just the "energy signature" of the pulser-receiver unit, the unit was switched on midway through the measurement and this response compared with a normal response. Results with two different power levels of the pulser-receiver unit were also compared to see the effect of the power input on the response. The location of the transducers was varied and the effect of such changes in location on partial debonding was analyzed.

7.1. Results

7.1.1. Effect of pulser-receiver unit settings

A test was devised in which the pulser-receiver units were switched on three hours after the cement paste was poured into the test container. The S-wave and P-wave R-t curves are compared with those in which the pulser-receiver units were on during the entire experiment in Figure 7.1 and Figure 7.2, respectively. The responses in the two cases were not considerably different, which indicated that the response is due to changes in the paste rather than due to interaction with the pulser-receiver units. There did seem to be some effect of the pulser-receiver units, since the responses were not exactly the same, but this was to be expected, since the amount of energy put into the system determined how it behaved to a certain extent. Partial debonding was seen when the unit is switched on three hours into the measurement as well, and thus was a response of the paste, and not caused by the pulser-receiver unit energy.

To study the effect of the pulser-receiver unit power on the response, tests were performed at a lower power level than before (previous tests were all done at the highest power setting). The S-wave and P-wave R-t curves are shown in Figure 7.3 and Figure 7.4 respectively. The S-wave R-t curves were similar in both cases, though the inversion occurs at a higher R value for the lower power case. Since the inversion is time when the acoustic impedances of the buffer and the paste are equal, it should ideally occur at R = 0. However, inversion always occurred at a non-zero, slightly positive value, which was presumed to be due to energy losses in the viscoelastic buffer and cement paste. The inversion occurring at higher R at lower power level supported this argument. The P-wave R-t curve was considerably different at a lower power level. The recovery and stiffening (stage 3 and stage 4) were particularly different, with the second inversion occurring at a much higher R value than with the higher power level. Though the detailed explanation for these differences was unclear, it was evident that the power level affects UWR measurements to some extent. From these results, it was concluded that to obtain consistent results, the pulser-receiver unit settings must not be changed. It is possible that other instrument parameters like the frequency of the transducer used can affect the wave reflection response. These factors were not considered in this study, but it is clear that several instrument related factors can affect the UWR response; and while the response appears to be consistent across different pastes when these factors were not changed, the response may change considerably due to a change in these factors.

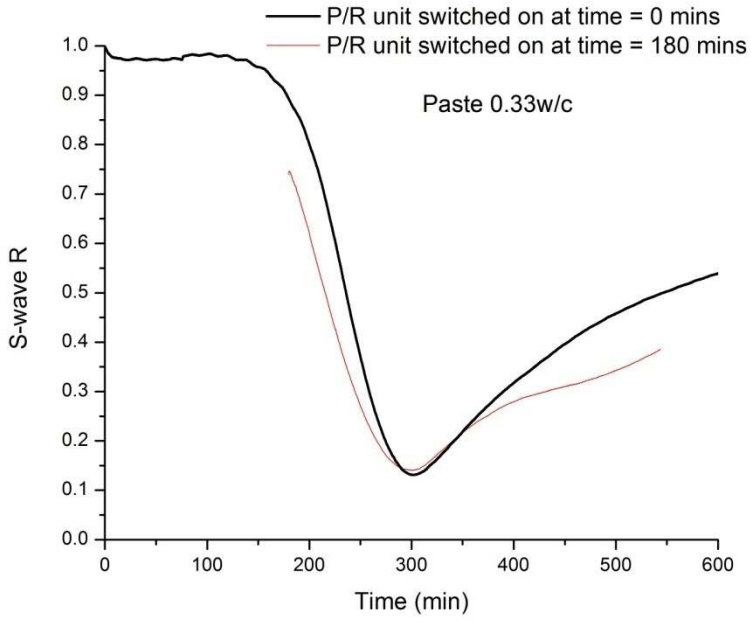

Figure 7.1. Effect of pulser-receiver unit being turned on three hours after start of test on S-wave R-t curve.

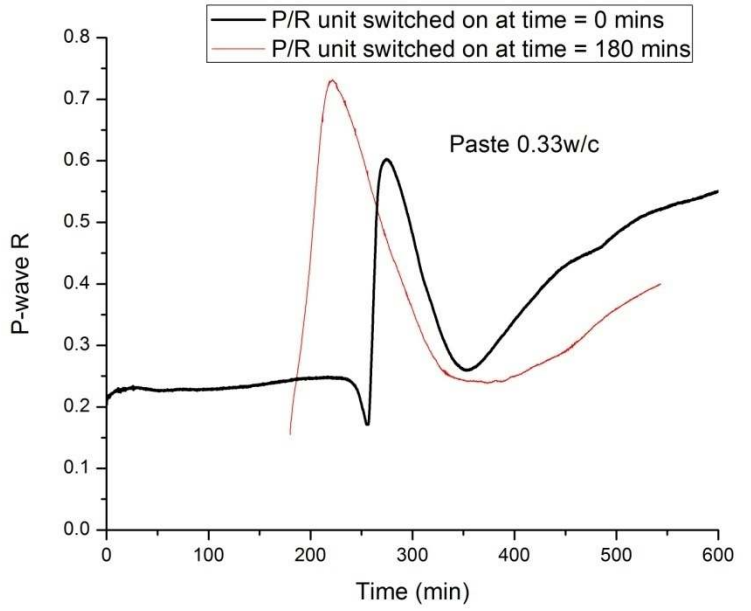

Figure 7.2. Effect of pulser-receiver unit being turned on three hours after start of test on P-wave R-t curve.

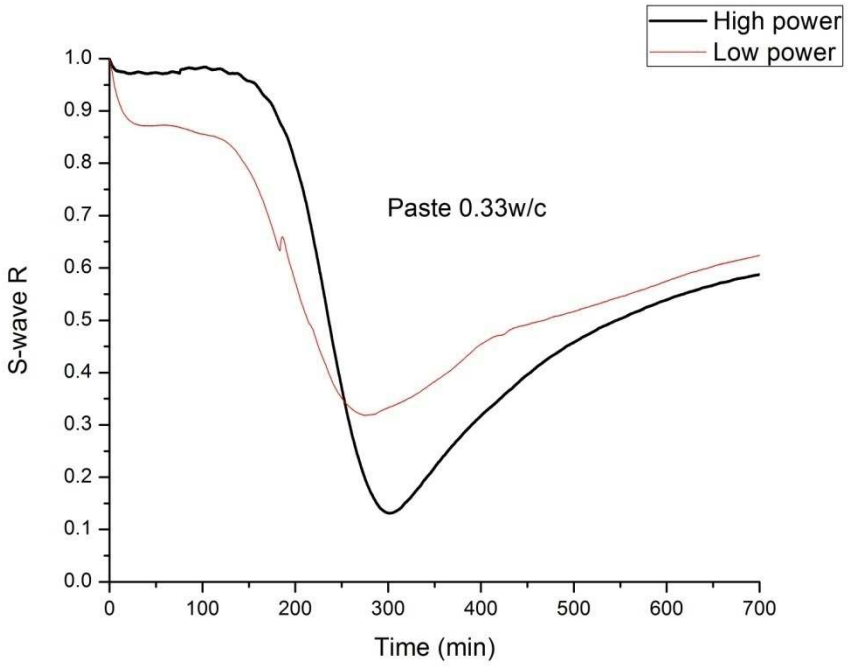

Figure 7.3. Effect of change in pulser-receiver power level on S-wave R-t curve.

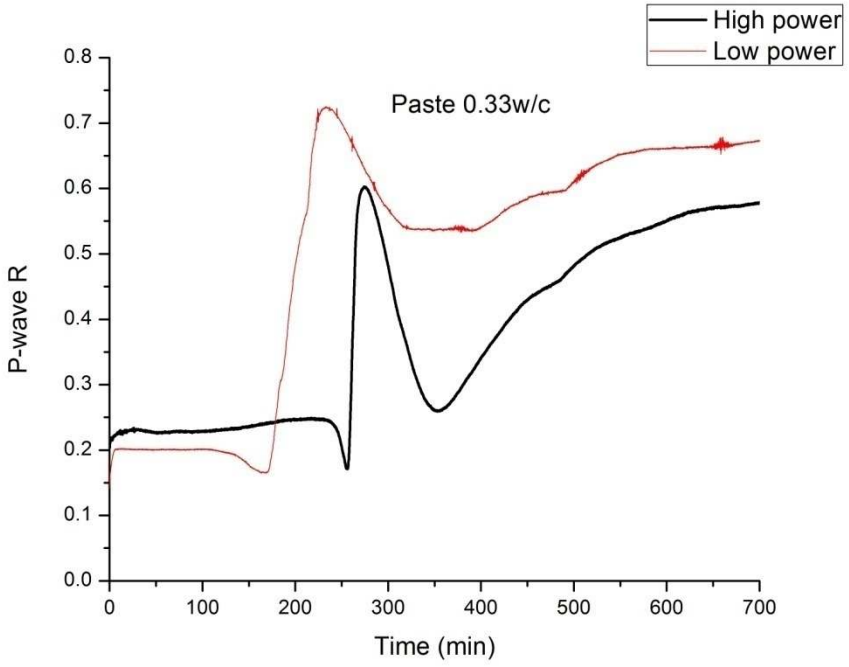

Figure 7.4. Effect of change in pulser-receiver power level on P-wave R-t curve.

7.1.2. Effect of transducer location

For all the results presented so far, the P-wave and S-wave transducers were attached to the bottom of the buffer. Tests were also performed with the transducers located on the side of the buffer. The results of various 0.33w/c pastes with transducers placed in various combinations of side and bottom locations are presented below. The results were compared with those in which both transducers were attached at the bottom. Figure 7.5 and Figure 7.6 show the S-wave and P-wave R-t curves with the S-wave transducer attached on the side and the P-wave transducer on the bottom. The S-wave reflection also showed debonding when the S-wave transducer was attached on the side. Debonding was never seen with S-wave reflection when the transducer was attached at the bottom. In one case, the debonding was full, and in the other only partial, with recovery. The P-wave response showed that the extent of partial debonding with the P-wave transducer at the bottom and S-wave transducer on the side was much lesser than when both the transducers were at the bottom. This showed that the S-wave transducer was actually promoting the partial debonding in the P-wave reflection.

Figure 7.7 and Figure 7.8 show the S-wave and P-wave R-t curves with the S-wave transducer attached on the bottom and the P-wave transducer on the side. The S-wave response did not substantially change, so it did not seem that the P wave transducer substantially affected the S-wave reflection. The P-wave reflection showed a high partial debonding extent, which was slightly higher than the extent with both the transducers on the bottom. The P-wave partial debonding extent (with the transducer at the bottom) without the S-wave transducer beside it was around R = 0.3 as opposed to around R = 0.6 when the S-wave transducer was beside it. The extent was around R = 0.7 with the P-wave transducer on the side, which indicated that the debonding on the side was much higher than on the bottom. This was true for both P-wave and

S-wave responses (the S-wave reflection did not show debonding at all when it was placed at the bottom), and was presumably because gravity acted to reduce the partial debonding on the bottom, whereas it made partial debonding worse on the side.

Figure 7.8 and Figure 7.9 show the S-wave and P-wave R-t curves with the transducers attached on opposite sides. The S-wave reflection showed full debonding in all three cases. The time of debonding was different in the three cases. The P-wave showed high debonding, around R = 0.6, but it was always partial and followed by recovery. The time of debonding was very similar in the three cases, indicating that there was probably something fundamental about the P-wave debonding but not about the S-wave debonding. The S-wave reflection was clearly more prone to full debonding than the P-wave reflection, though the P-wave reflection was more prone to debonding in general.

Figure 7.10 and Figure 7.11 show the S-wave and P-wave R-t curves with the transducers attached on the same side. The S-wave reflection showed partial debonding and recovery in both cases. The P-wave reflection showed partial debonding in one case, but full debonding in the other case; the only time full debonding was seen with P-wave reflection on cement pastes.

The following observations were therefore made from varying the transducer locations. The S-wave transducer seemed to be increasing the P-wave debonding. The P-wave transducer also seemed to slightly decrease the S-wave debonding (the S-wave transducer on the side showed full debonding four of five times with the P-wave transducer away from it, but did not show full debonding either of the two times the P-wave transducer was beside it). The S-wave was more prone to full debonding than the P-wave (four times for the S-wave reflection as opposed to once for the P-wave reflection). Debonding on side was much higher than on bottom, due to the effect of gravity.

The response of the air entraining agent was used to further understand some of these responses. The P-wave response clearly showed entrained air due to the air entraining agent, but the S-wave response did not. Hence, if there was a small amount of air at the interface, it would be detected by the P-wave transducer, but not by the S-wave transducer. Also, the S-wave transducer increased the P-wave debonding, and the P-wave transducer decreased the S-wave debonding, hence when both the transducers were at the bottom, only the P-wave reflection showed debonding. When both the transducers were at the side, there was more debonding due to gravity. This higher debonding may have provided enough air which was detected by both the S-wave and the P-wave transducers. The way the S-wave is transmitted may mean that debonding, when it occurred, was usually full, though it may occur less easily than the P-wave debonding (if there is any air at the interface, it is detected by the P-wave, since the P-wave passes through the air; the S-wave ignores this little amount of air and instead travels through the solid portion, but if there is only air at the interface, then it is detected by the S-wave). The S-wave showing full debonding more often than the P-wave supports the hypothesis that recovery is caused (at least partially) by movement of water into the air gap–the P-wave can detect the difference between water and air, but the S-wave cannot.

Previously, it was shown that the presence of ponded water resulted in the vanishing of the partial debonding response when both the transducers were attached at the bottom. A test was done with ponded water with the transducers placed on opposite sides and the response compared to the response without any ponded water. The S-wave and P-wave R-t curves are shown in Figure 7.13 and Figure 7.14 respectively. The P-wave reflection clearly showed that there was no partial debonding with the ponded water. The S-wave reflection showed a very slight debonding, but complete recovery, with the curve going back to normal. In three other

cases without ponded water, full debonding was always seen. Hence, (ponded) water was effective in controlling debonding, whether P-wave or S-wave, whether full or partial.

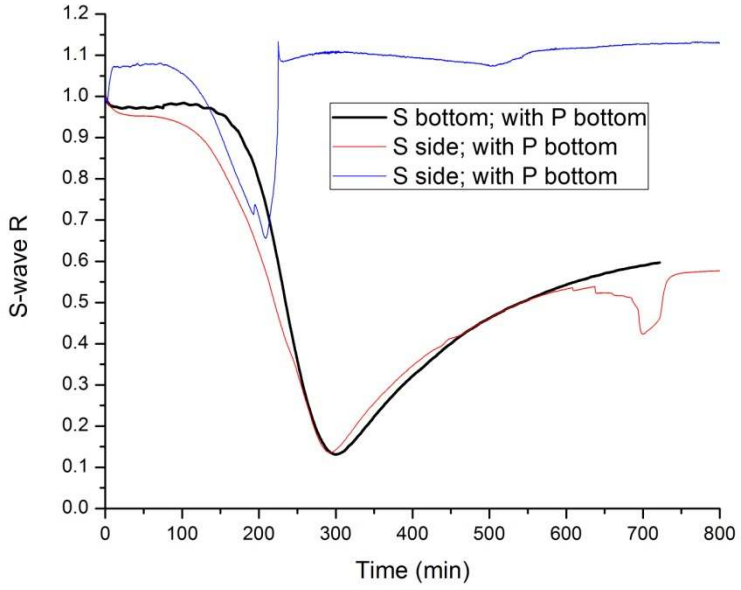

Figure 7.5. S-wave R-t curve with S-wave transducer on side and P-wave transducer on bottom.

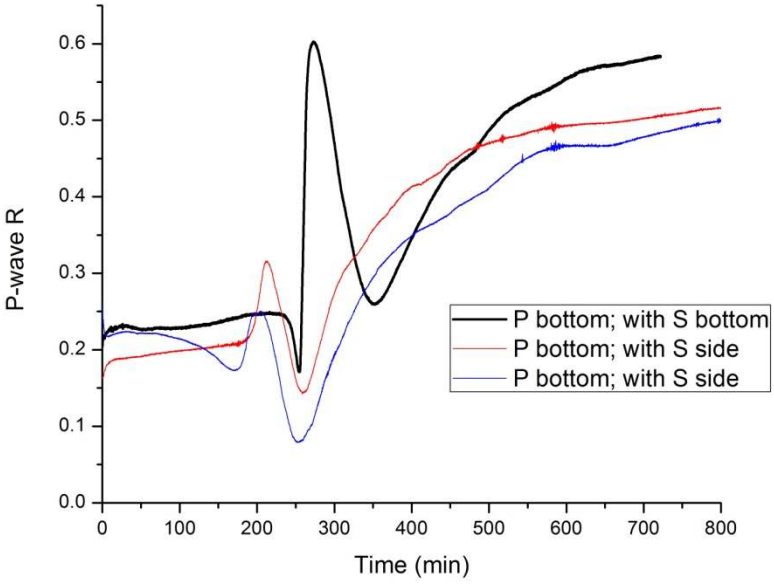

Figure 7.6. P-wave R-t curve with S-wave transducer on side and P-wave transducer on bottom.

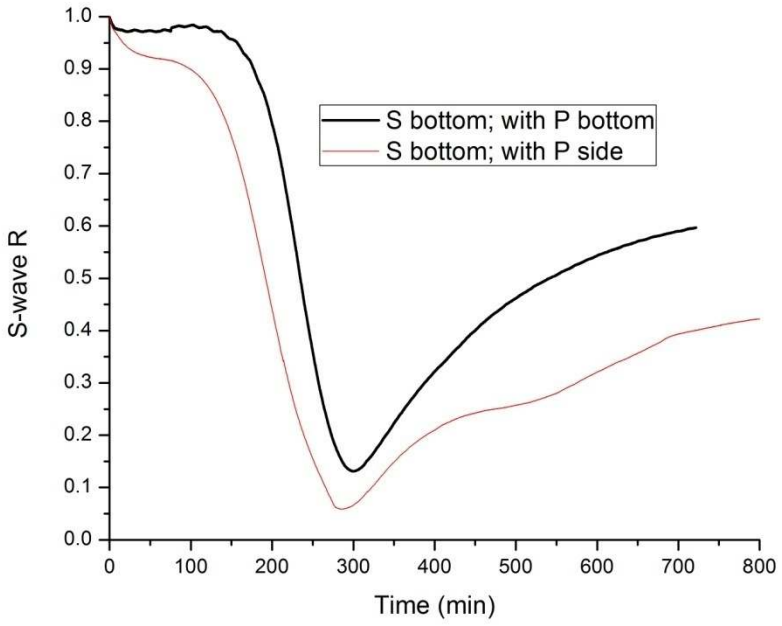

Figure 7.7. S-wave R-t curve with S-wave transducer on bottom and P-wave transducer on side.

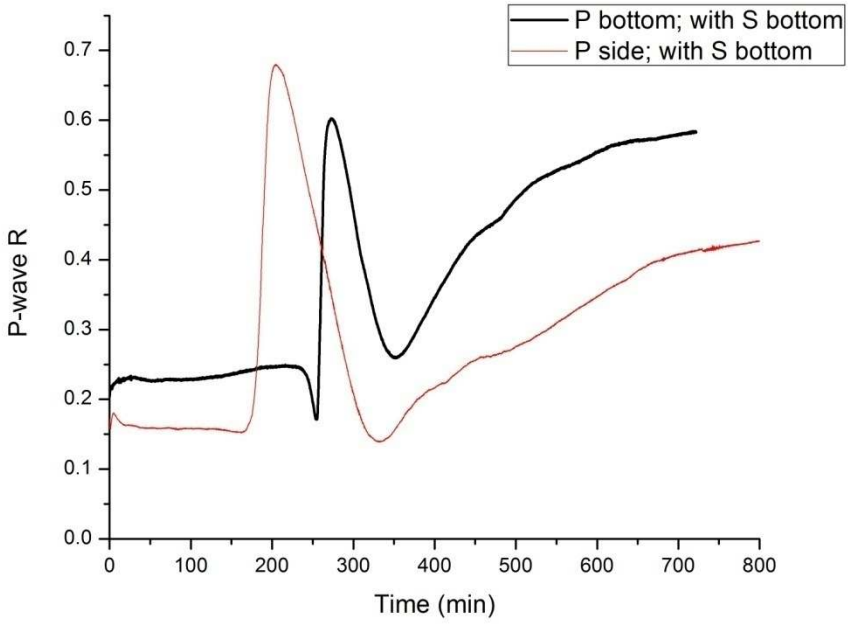

Figure 7.8. P-wave R-t curve with S-wave transducer on bottom and P-wave transducer on side.

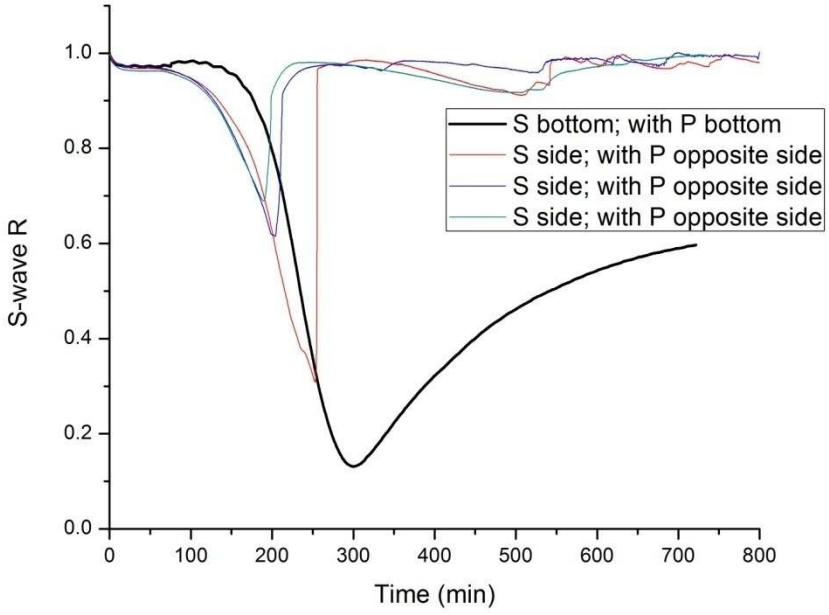

Figure 7.9. S-wave R-t curve with S-wave and P-wave transducers on the opposite side.

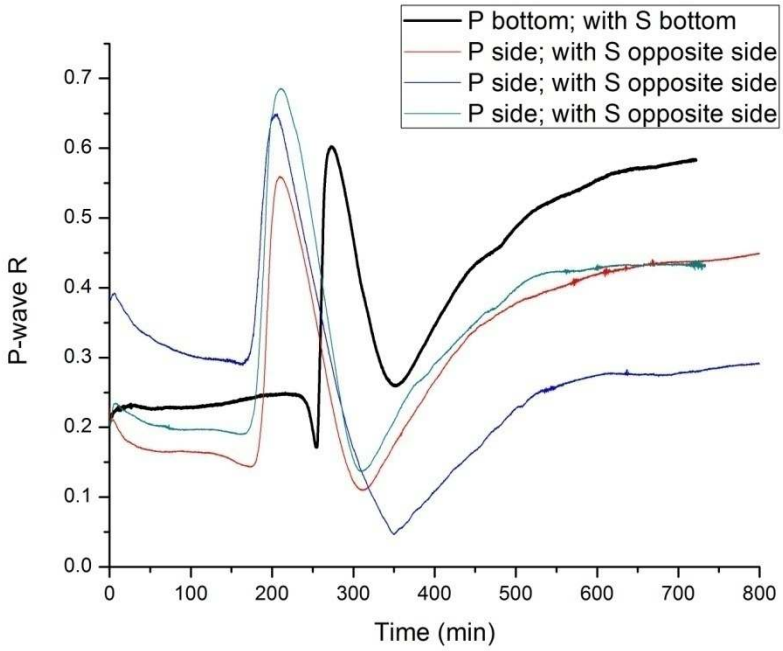

Figure 7.10. P-wave R-t curve with S-wave and P-wave transducers on the opposite side.

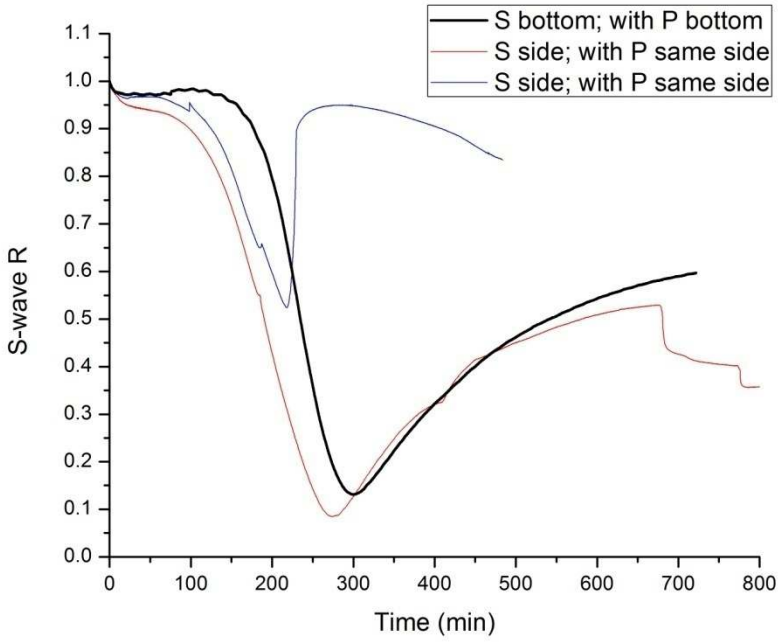

Figure 7.11. S-wave R-t curve with S-wave and P-wave transducers on the same side.

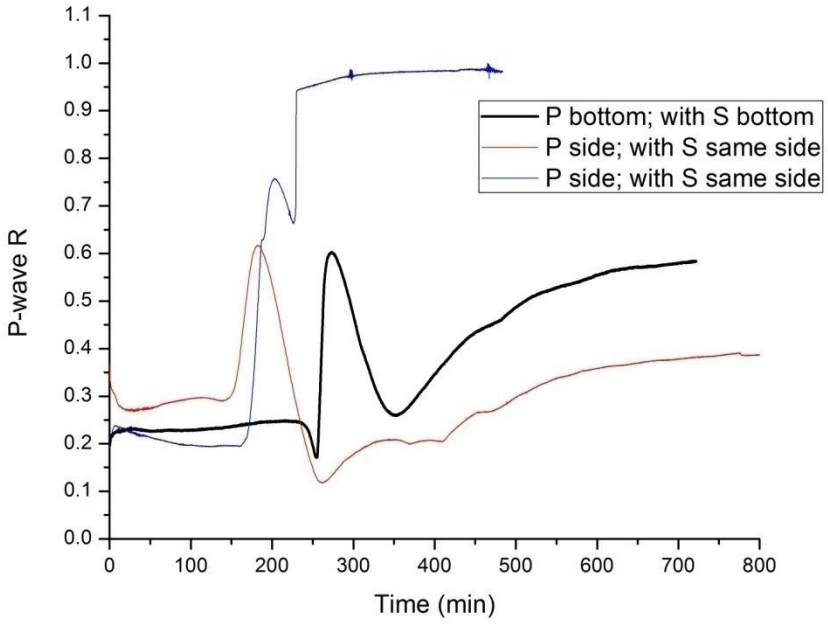

Figure 7.12. P-wave R-t curve with S-wave and P-wave transducers on the same side.

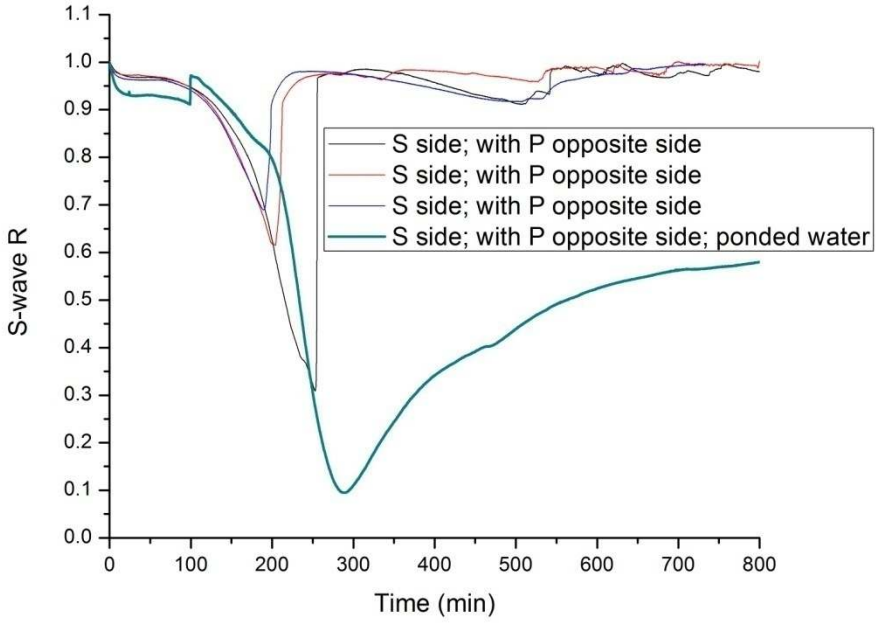

Figure 7.13. Effect of ponded water on side S-wave debonding.

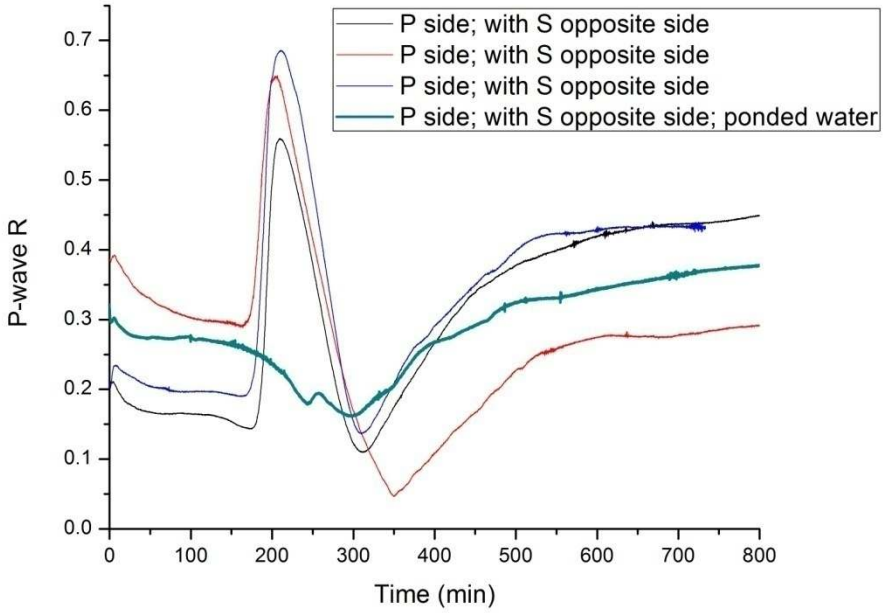

Figure 7.14. Effect of ponded water on side P-wave debonding.

7.2. Conclusions

The following conclusions were drawn from a study of instrument effects:

1. The pulser-receiver unit settings affected the response of the paste. Inversion occurred at higher R value for lower power setting; and P-wave debonding and recovery changed at lower power setting. The UWR response was a ‘real’ response of the cement paste.
2. The extent of debonding was higher on the side than on bottom.
3. The S-wave reflection was more prone to full debonding than the P-wave reflection. This supports the hypothesis that recovery was caused at least partially by movement of water into the air gap.
4. The S-wave transducer seemed to promote debonding in the P-wave reflection, and the P-wave transducer seemed to reduce debonding in the S-wave reflection.
5. Ponded water limited debonding in both P-wave and S-wave reflection, with transducers placed either on the side or on the bottom.

8. FORMWORK PRESSURE

Self-compacting concretes can potentially exert substantial pressure on formwork, and hence, study of formwork pressures is important. The pressure exerted by concrete decreases with time, as the concrete gradually stiffens. Since the stiffening process is detected by UWR, formwork pressure and wave reflection tests were done on the same concretes in this study in order to compare the two properties. Since the UWR uses much lesser concrete than the formwork pressure testing, any correlation, if found, would help in easily checking formwork pressure results, and also help in gaining a fundamental understanding of the pressure response.

In the present work, formwork pressure results with different fill heights of the formwork pressure container are given. Simultaneous S-wave and P-wave reflection were done on the concretes and the UWR and formwork pressure responses compared. The results of changing formwork pressure testing parameters such as the height of sensor and the effect of the film placed on the sensor are studied. Formwork pressure and UWR were done on concrete in the same container using a modified test apparatus, and the responses are directly compared. The effect of a large amount of concrete exerting pressure on the UWR transducers is studied.

8.1. Results

8.1.1. Fill height 0.3 m

The formwork pressure column is a cylinder 1 m high and 0.25 m in diameter. Filling the column completely with concrete uses a substantial amount of concrete, and hence initial tests were done with a column fill height of only 0.3 m. The pressure sensor was mounted at a height of 0.15 m. The UWR testing was done in the concrete UWR container. The concrete was mixed in a pan mixer and then poured into both the formwork pressure column and the UWR container. Three trials were tested with the same concrete mix (Concrete 3). Pressure results are shown in

Figure 8.1. S-wave R-t curves are shown in Figure 8.2 and P-wave R-t curves shown in Figure 8.3. The initial pressure value was very low, less than 0.4 psi. The pressure reduced with time, and dropped quickly to 0 psi in less than 100 minutes. The pressure continued to reduce, and an extend period of negative pressure was seen, for around 300 to 400 minutes. The pressure then suddenly increased to a slightly positive value. The S-wave R-t curve shows a continuous drop with time in R till inversion after which R changes direction. The P-wave R-t curve shows an initial stable period, followed by partial debonding and recovery. The UWR responses have been explained in detail in earlier chapters.

Prior studies had showed that pressure decreased steadily with time [24]. Negative pressures were also observed, but not explored. Abrupt increases in pressure were also not reported before. Negative pressures were attributed to shrinkage, which could potentially pull the concrete away from the face of the sensor, and create a vacuum which could suck the sensor towards it. Shrinkage was previously attributed to be the cause of partial debonding in the P-wave, and hence, the times of increase in pressure and times of partial debonding were compared. The pressure increases happened between 400 to 480 minutes for the tested concretes; however, the partial debonding occurred much earlier, 250 to 300 minutes. P-wave recovery for the three trials occurred between 300 to 350 minutes. The concretes tested were well into the recovery stage at around 400 to 480 minutes. Therefore, no clear correlation was found between the time of pressure increase and P-wave partial debonding. The only other salient feature on the formwork pressure curve was the time for the pressure to reach 0 psi, which occurred within the first 100 minutes of testing. The time taken for the pressure to reach 0 psi did not correlate with any changes in the UWR; initial setting time as determined by S-wave reflection was much later, 180 to 230 minutes. The time for the pressure to reach 0 psi also depends primarily on the filling

height. Since tests with a low filling height did not give much information, tests were done with the formwork pressure column completely filled (1 m filling height).

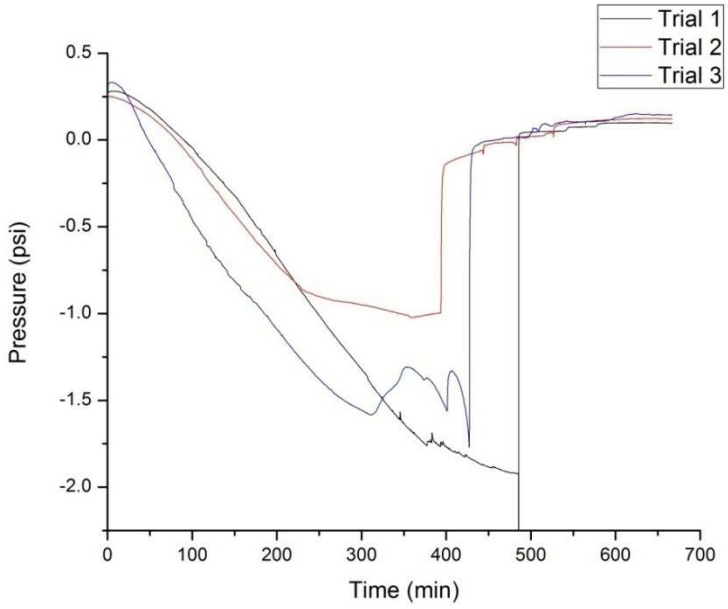

Figure 8.1. Variation of formwork pressure with time for three trials of a concrete mix, filling height 0.3 m, sensor 0.15 m (Concrete 3).

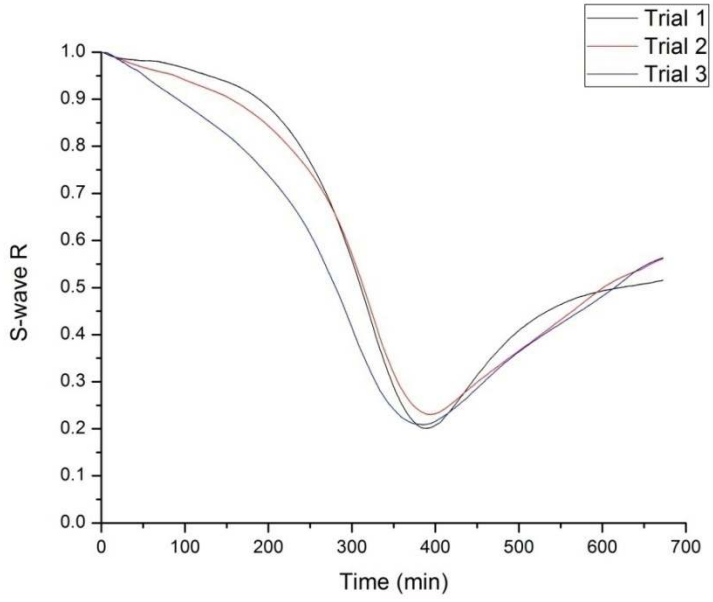

Figure 8.2. S-wave R-t curves for three trials of a concrete mix (Concrete 3).

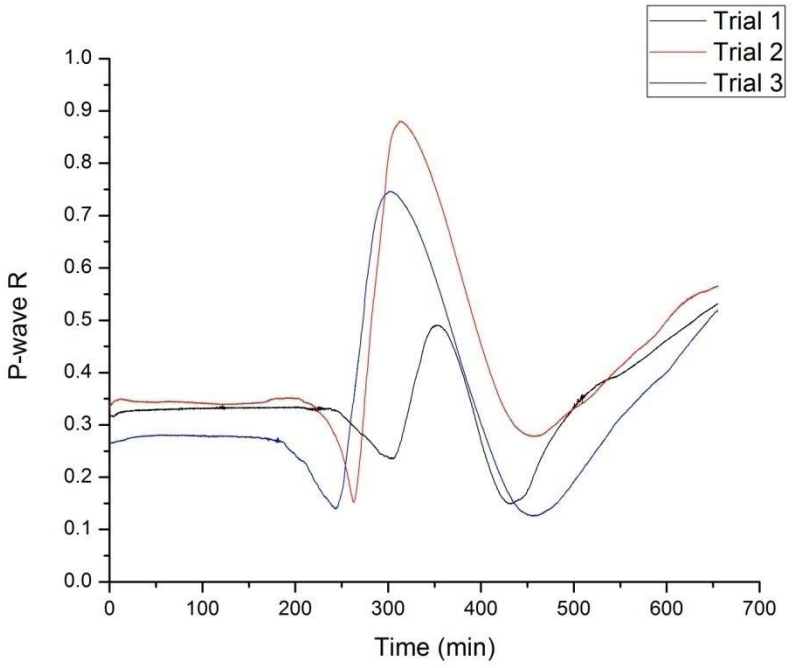

Figure 8.3. P-wave R-t curves for three trials of a concrete mix (Concrete 3).

8.1.2. Fill height 1 m

Tests were done with the formwork pressure column completely filled (1 m high). The sensor was mounted at 0.15 m, and hence, had a much higher head pressure than in previous tests. The UWR testing was done in the concrete UWR containers. Pressure results are shown in Figure 8.4. S-wave R-t curves are shown in Figure 8.5 and P-wave R-t curves shown in Figure 8.6. The concrete mix (Concrete 4) was slightly modified from the mix used for lower fill height, since that mix had slightly low flow. The formwork pressure decreased rapidly for the first 100 minutes, and then a change in slope occurred. The pressure subsequently decreased, but at a slower rate. Both the initial and the subsequent decrease were approximately linear. The pressure became 0 psi at around 250 minutes. One of the trials showed a sudden jump in pressure at around 650 minutes. Prior testing in UIUC [24] showed very similar initial response; however those tests were truncated at around 250 to 300 minutes, when pressure reached 0 psi. Initial and

final set times from S-wave reflection were around 230 to 260 minutes and around 400 minutes, respectively. Final set from P-wave reflection was between 350 to 400 minutes. P-wave recovery was around 450 minutes. As before, the time of the sudden jump in formwork pressure was much after P-wave recovery. The time for the change in slope in the formwork pressure was much before initial set. Initial set roughly corresponded to the time when formwork pressure became 0 psi, however, as pointed out before, this depended largely on the filling height, and was thus of no fundamental significance.

The reason for the sudden increase in the pressure was unclear. Cling film had been placed over the sensors prior to mounting in all tests to reduce suction due to shrinkage of the concrete. To determine whether the sudden increase in pressures was due to the film rupturing, tests were done with and without the film at the same sensor height. The results are shown in Figure 8.7. The sudden jump in pressure was seen without the film as well. Similar tests showed that the jump occurred irrespective of the film. The responses with and without the film were very similar, with the only difference being higher pressures shown with the film. Since testing the concrete without a film caused direct exposure of the sensor to the concrete, which could potentially cause damage to the sensor, further tests were done with the film.

The effect of sensor height on the pressure response was also tested with sensors at 0.15 and 0.45 mm. The responses were parallel to each other for the most part, but offset vertically, with the 0.15 m sensor showing more pressure, an expected response. It was observed that the time for the pressure to reach 0 psi clearly depended on the height of the sensor (and thus on the head pressure).

These tests did not reveal any similarities in the formwork pressure and wave reflection response. Since these tests were done on different containers, it was possible that the different

responses reflected that. Hence, both tests were simultaneously run in one container to compare formwork pressure and wave reflection.

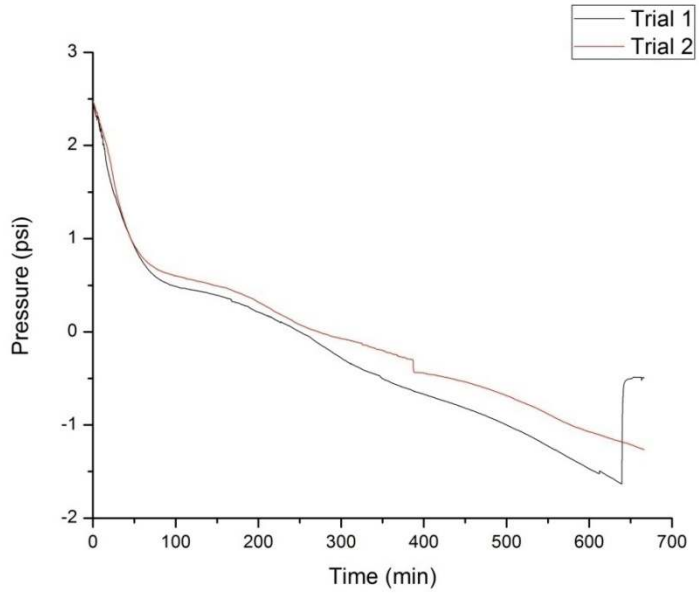

Figure 8.4. Variation of formwork pressure with time for two trials of a concrete mix, filling height 1 m, sensor 0.15 m (Concrete 4).

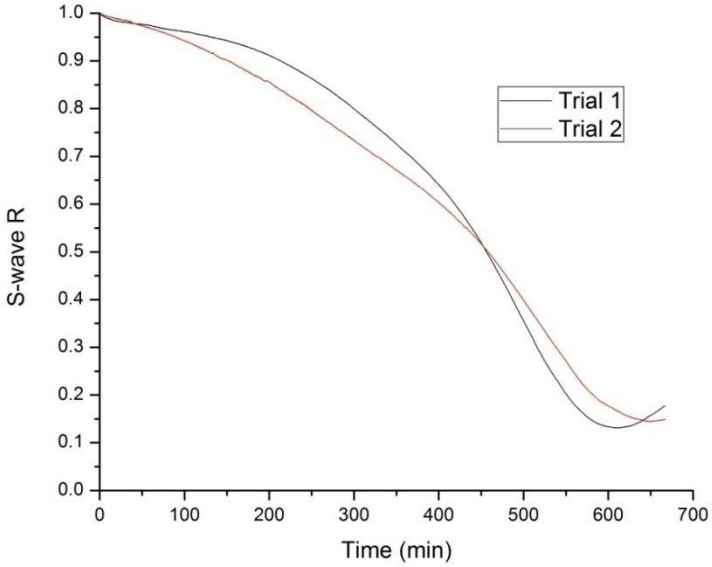

Figure 8.5. S-wave R-t curves for two trials of a concrete mix (Concrete 4).

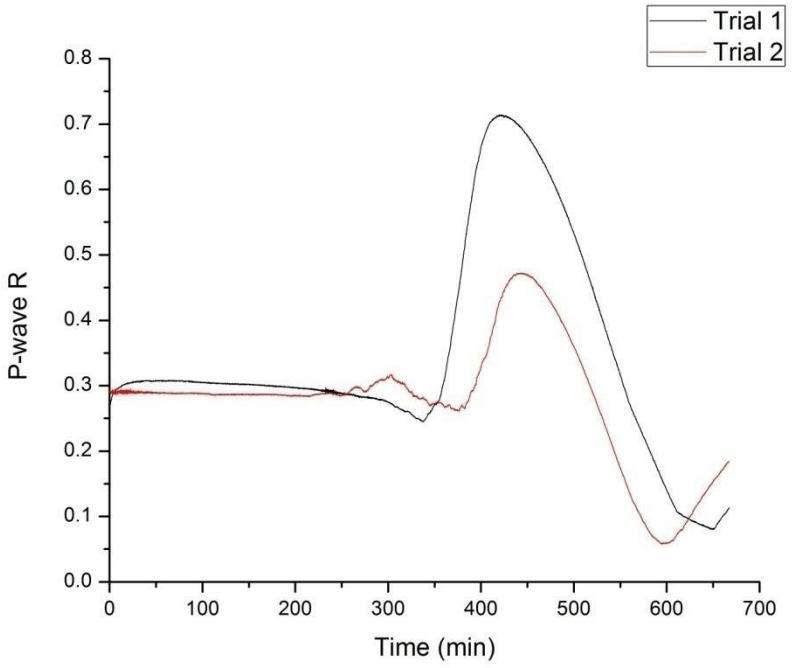

Figure 8.6. P-wave R-t curves for two trials of a concrete mix (Concrete 4).

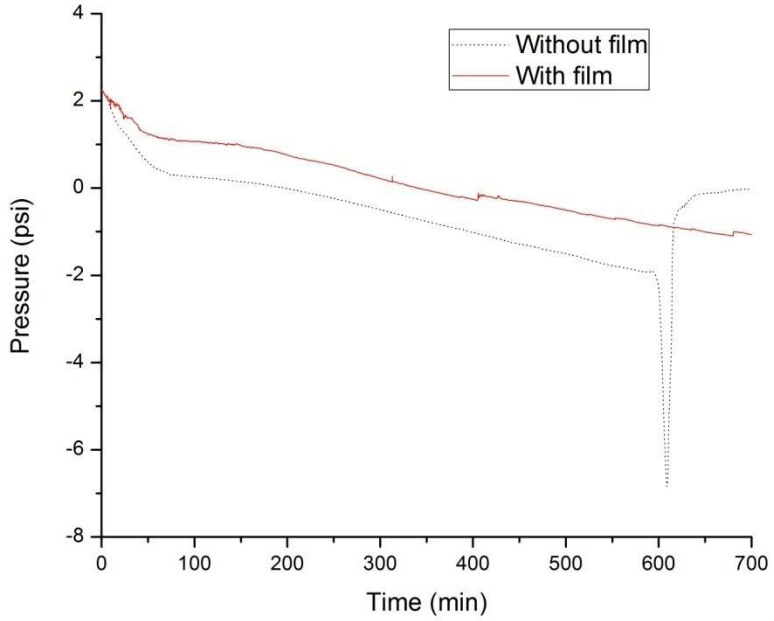

Figure 8.7. Effect of film on formwork pressure, filling height 1 m, sensor 0.15 m (Concrete 4).

8.1.3. Simultaneous formwork pressure and UWR in the same container

The formwork pressure container was modified so that formwork pressure and UWR could be simultaneously tested. The holes in the container where the pressure sensors were placed were filled with a piece of HIPS. S-wave and P-wave transducers were then mounted on the HIPS piece. The concrete was filled in the column, and UWR and formwork pressure were monitored as a function of time. The concrete used (Concrete 1) was slightly modified from the previous mix, which showed slight segregation.

To study the effect of pressure on the wave reflection response, the responses of the same concrete mix in the UWR container and the formwork pressure container were compared. S-wave reflection results are shown in Figure 8.8 and P-wave reflection results in Figure 8.9. The S-wave response in the formwork pressure container showed full debonding, and this was because the transducer was mounted on the side. The responses were similar initially, though the later response was different. The concrete in the formwork pressure container showed earlier setting. The P-wave responses were also similar initially, with the responses for the first 200 minutes being roughly parallel. However, the P-wave R was much lower in the formwork pressure container; and this lower R may be an effect of the pressure. Final set times were around 280 minutes, which was rather early. Recovery started at around 400 minutes; however, the nature of recovery was very different in the formwork pressure container. The extent of partial debonding extent was also much lower in the formwork pressure container, and both of these differences could possibly be due to the effect of pressure, however, it was noted that concrete UWR response was rather variable.

Two trials of the formwork pressure were done, and the responses are presented in Figure 8.10. The responses in the two trials were similar, there was a rapid linear decrease in pressure

for around 100 minutes, and the pressure went to 0 psi between 280 and 320 minutes. The sudden increase in pressure was not seen. The pressure remained roughly constant from around 100 to 150 minutes. After 150 minutes, the pressure started dropping linearly, though with a different slope from the initial linear drop. Initial set from S-wave reflection was around 200 minutes, which did not correspond to any change in the pressure response. Final set from UWR was around 280 minutes, which corresponded to the time the pressure reached 0 psi, but this point does not have any fundamental significance. Since the sudden increase in pressure was not seen, it could not be compared to partial debonding or recovery in P-wave UWR. Therefore, we were unable to identify a clear connection between formwork pressure and UWR responses.

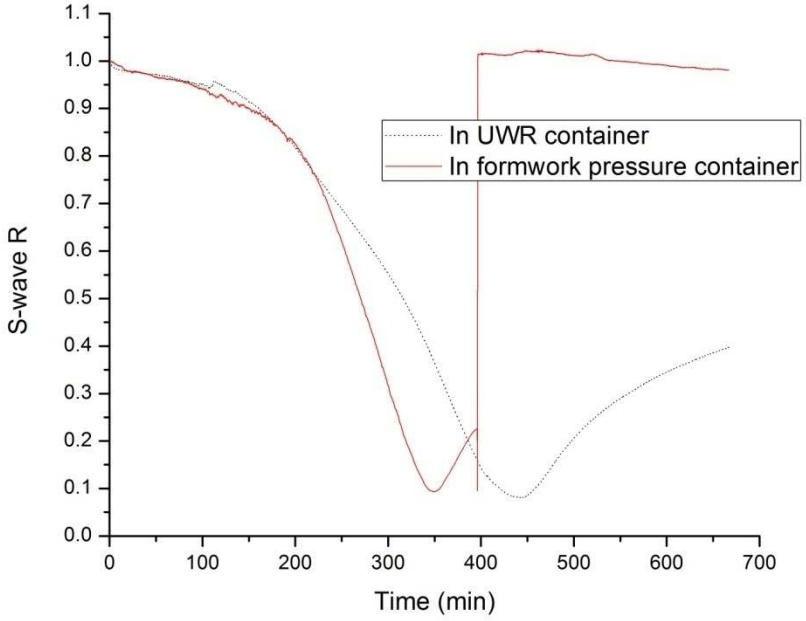

Figure 8.8. Effect of pressure on S-wave response (Concrete 1).

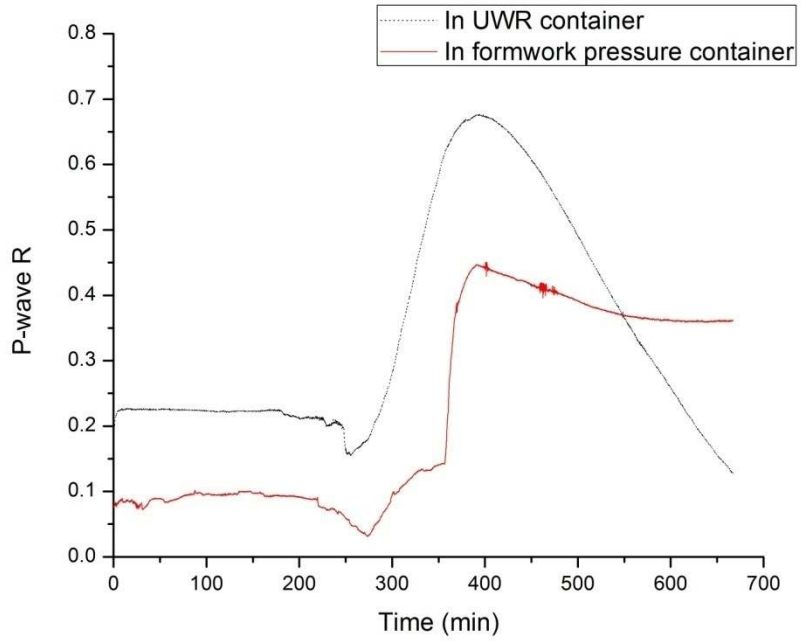

Figure 8.9. Effect of pressure on P-wave response (Concrete 1).

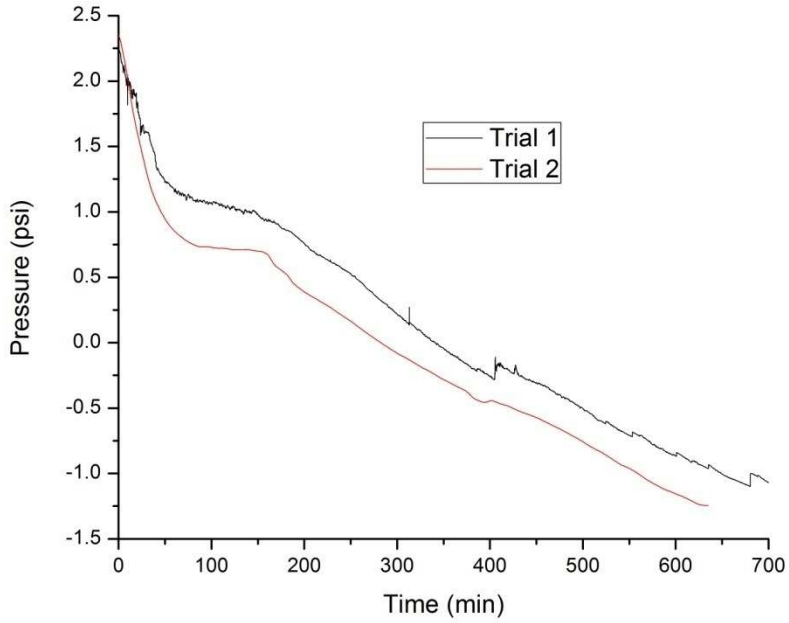

Figure 8.10. Variation of formwork pressure with time for two trials of a concrete mix, filling height 1 m, sensor 0.15 m (Concrete 1).

8.2. Conclusions

The following conclusions were drawn from formwork pressure testing:

1. The formwork pressure response depended on the pressure head.
2. The value of the initial pressure depended on the height of fill. The pressure rapidly dropped in a linear manner. Then, there was a change in slope, and the pressure further decreased linearly below 0 psi. Significant negative pressures were seen. Sometimes the pressure suddenly shot up to a small positive value.
3. Wave reflection was affected by the pressure exerted by a large amount of concrete.
4. There did not seem to be any clear correlation between formwork pressure and UWR responses.

9. SUMMARY AND KEY CONCLUSIONS

The objective of this research was to explore the use of ultrasonic wave reflection (UWR) for self-compacting pastes and concretes. A secondary objective was to interpret the UWR responses of various modified cement pastes. Changes in reflected ultrasonic wave energy with time were monitored by UWR and these changes were correlated with changes in the hydrating cement paste. Combined shear and longitudinal wave reflection was employed to obtain more information, and a sensitive high impact polystyrene buffer was used.

A modified version of the ASTM C403 penetration resistance test was used to obtain reference values for initial and final set. The setting times of various w/c pastes could easily be found using the method, and the effect of fly ash, superplasticizer, viscosity modifying agent, and temperature on the setting time could be explored. Setting times varied linearly with w/c.

The S-wave reflection response of normal and self-compacting pastes was explained and initial and final set times were found. For all pastes tested, set times from S-wave reflection and penetration resistance were linearly related, though correlation was only moderate and different set times were obtained from the two methods. S-wave reflection could distinguish small changes in w/cm, fa/cm, and sp/cm in self-compacting pastes. Curves were fit to the S-wave reflection response. S-wave R-t curves for concretes were shown to be broadly the same as that of the corresponding pastes, and paste and concrete set times were similar. Concrete set times could be determined accurately using S-wave reflection. The S-wave reflection response for mixes with various mineral and chemical admixtures was explained. Observations and conclusions were made as to the effect of these admixtures on stiffening. Rapid stiffening was detected by the method in fly ash pastes and geopolymers.

The P-wave R-t curve shape was interpreted, and partial debonding response was explained in detail. It was shown that this response was due to autogenous shrinkage, which causes an underpressure which draws water into the structure. It was shown that the partial debonding response was controlled primarily by the presence of free water in the pastes. Time domain data were used to further explain the partial debonding response. P-wave reflection could distinguish small changes in w/cm, fa/cm, and sp/cm. Final set times using P-wave reflection were found as the onset of partial debonding. This time was roughly the same as the time of final set from S-wave reflection for normal pastes, self-compacting pastes, and concretes. Changes in stiffening due to mineral and chemical admixtures were detected using the method, especially with an air entraining agent.

The effect of pulser-receiver unit settings was explained, and the effect of the unit power on the response analyzed. The pulser-receiver unit settings had an effect on the response, especially on the partial debonding and inversion levels. The effect of transducer position on the response was studied. The extent of partial debonding is higher with the transducers on the side than on the bottom. The S-wave transducer seemed to increase P-wave debonding, whereas the P-wave transducer seemed to decrease S-wave debonding. The S-wave reflection was more prone to full debonding than the P-wave reflection, supporting the hypothesis that recovery is caused at least partially by movement of water into the air. Ponded water limits debonding in both P-wave and S-wave reflection, with transducers placed either on the side or on the bottom.

Combined formwork pressure and UWR tests were performed. The variation of formwork pressure with time was obtained, and there seemed to be some effect of the pressure of a large amount of concrete on the UWR response. However, the formwork pressure and UWR results could not be correlated.

10. REFERENCES

1. Chung, C-W., Ultrasonic wave reflection measurements on stiffening and setting of cement paste, Ph.D. Dissertation, University of Illinois at Urbana-Champaign, 2010.
2. Taylor, H. F. W., Cement Chemistry, Academic Press, Harcourt Brace Jovanovich, 1997.
3. Mindess, S., Young, J. F., and Darwin, D., Concrete, Prentice Hall, 2003.
4. Okamura, H., and Ouchi, M., Self Compacting Concrete, *Journal of Advanced Concrete Technology*, Vol. 1, No.1, 2003, pp. 5-15.
5. ASTM Test Method for Time of Setting of Concrete Mixtures by Penetration Resistance (C 403), *Annual Book of ASTM Standards*, Vol. 04. 02, ASTM International, West Conshohocken, PA, 2003.
6. ASTM Test Method for Time of Setting of Hydraulic Cement by Vicat Needle (C 191), *Annual Book of ASTM Standards*, Vol. 04. 01, ASTM International, West Conshohocken, PA, 2003.
7. Guneyisi, E., Gesoglu, M., and Ozbay, E., Evaluating and forecasting the initial and final setting times of self-compacting concretes containing mineral admixtures by neural network, *Materials and Structures*, Vol. 42, 2009, pp. 469-484.
8. Pinto, C. A. R., and C. K., Effect of Silica Fume and Superplasticizer Addition on Setting Behavior of High-Strength Mixtures, *Journal of the Transportation Research Board*, Vol. 1574, 2007, pp. 56-65.
9. Chung, C-W., Mroczek, M., Park, I., and Struble L. J., On the Evaluation of Setting Time of Cement Paste Based on ASTM C403 Penetration Resistance Test, *Journal of Testing and Evaluation*, Vol. 38, No.5, 2010, pp. 61-68.

10. Voigt, T., and Shah, S. P., Properties of early age Portland cement mortar monitored with shear wave reflection method, *ACI Materials Journal*, Vol. 101, 2004, pp. 473-482.
11. Voigt, T., Akkaya, Y., and Shah, S. P., Determination of early age mortar and concrete strength by ultrasonic wave reflections, *ASCE Journal of Materials in Civil Engineering*, Vol. 15, 2003, pp. 247-254.
12. Voigt, T., Sun, Z., and Shah, S. P., Comparison of ultrasonic wave reflection method and maturity method in evaluating early-age compressive strength of mortar, *Cement & Concrete Composites*, Vol. 26, 2006, pp. 307-316.
13. Sun, Z., Voigt, T., and Shah, S. P., Rheometric and ultrasonic investigations of viscoelastic properties of fresh Portland cement pastes, *Cement and Concrete Research*, Vol. 36, 2006, pp. 278-287.
14. Valic, M. I., Hydration of cementitious materials by pulse echo USWR Method, apparatus and application examples, Cement and Concrete Research, Vol. 30, 2000, pp. 1633-1640.
15. Voigt, T., Ye, G., Sun, Z., Shah, S. P., and Breugel, K. V., Early age microstructure of portland cement mortar investigated by ultrasonic shear waves and numerical simulation, *Cement and Concrete Research*, Vol. 35, 2005, pp. 858-866.
16. Subramaniam, K. V., Lee, J., and Christensen, B. J., Monitoring the setting behavior of cementitious materials using one-sided ultrasonic measurements, *Cement and Concrete Research*, Vol. 35, 2005, pp. 850-857.
17. Rapport, J., Popovics, J. S., Kolluru, S. V., and Shah, S. P. Using ultrasound to monitor stiffening process of concrete with admixtures, *ACI Materials Journal*, Vol. 97, No. 6, 2000, pp. 675-683.

18. Öztürk, T., Rapport, J., Popovics, J. S., and Shah, S. P., Monitoring the setting and hardening of cement-based materials with ultrasound, *Concrete Science and Engineering*, Vol. 1, No.2, 1999, pp. 83-91.
19. Ozturk, T., Kroggel, O., Grubl, P., and Popovics, J. S., Improved ultrasonic wave reflection technique to monitor the setting of cement-based materials, *NDT & E International*, Vol. 39, 2006, pp. 258-263.
20. Guide to formwork for concrete (ACI 347-04), *American Concrete Institute*, 2004.
21. Tejeda-Dominguez, F., and Lange, D. A., Formwork Pressure of SCC for Tall Wall Field Applications, J *Journal of the Transportation Research Board*, Vol. 1914, 2005, pp. 1 -7.
22. Tejeda-Dominguez, F., Laboratory and Field Study of Self-Consolidating Concrete (SCC) Formwork Pressure, M.S. Thesis, University of Illinois at Urbana-Champaign, 2005.
23. Assaad, J., and Khayat, K., Effect of Coarse Aggregate characteristics on Lateral Pressure Exerted by Self-Consolidating Concrete, *ACI Materials Journal*, Vol. 102, No.3, 2005, pp 145-153.
24. Birch, F. B., Formwork pressure exerted by self consolidating concrete, M.S. Thesis, University of Illinois at Urbana-Champaign, 2006.
25. Shen, L., Role of aggregate packing in segregation resistance and flow behavior of self-consolidating concrete, Ph.D. Dissertation, University of Illinois at Urbana-Champaign, 2007.
26. Sant, G., Dehadrai, M., Bentz, P., Lura, P., Ferraris, C. F., Bullard, J. W., and Weiss, J., "Detecting the Fluid-to-Solid Transition in Cement Pastes", *Concrete International*, Vol. 31, 2009, pp. 53-58.